EXPERIMENTAL AND NUMERICAL INVESTIGATIONS ON FINNED PILE FOUNDATIONS SUBJECTED TO LATERAL LOADS

Thesis

Submitted in partial fulfilment of the requirements for the degree of

DOCTOR OF PHILOSOPHY

by

PANKAJ BARIKER

DEPARTMENT OF CIVIL ENGINEERING
NATIONAL INSTITUTE OF TECHNOLOGY KARNATAKA
SURATHKAL, MANGALORE – 575025

SEPTEMBER, 2023

DECLARATION

I hereby *declare* that the Research Thesis entitled **Experimental and Numerical Investigations on Finned Pile Foundations Subjected to Lateral Load** which is being submitted to the **National Institute of Technology Karnataka, Surathkal** in partial fulfilment of the requirements for the award of the Degree of **Doctor of Philosophy** in **Civil Engineering** is a *bonafide report of the research work carried out by me.* The material contained in this Research Thesis has not been submitted to any University or Institution for the award of any degree.

PANKAJ BARIKER
(197128CV020)
Research Scholar
Department of Civil Engineering

Place: Surathkal - 575025.

Date: 14/09/2023

CERTIFICATE

This is to *certify* that the Research Thesis entitled **Experimental and Numerical Investigations on Finned Pile Foundations Subjected to Lateral Loads** submitted by **Pankaj Bariker** (Register Number: **197128CV020**) as the record of the research work carried out by him, is *accepted as the Research Thesis submission* in partial fulfillment of the requirements for the award of degree of **Doctor of Philosophy**.

14/09/23

Research Supervisor

Dr. Sreevalsa Kolathayar M.Tech.(IITK), PhD(IISc).
Assistant Professor Grade-I
Department of Civil Engineering
National Institute of Technology Karnataka
Surathkal, Mangalore-575025, Karnataka, INDIA.
Mob: +91-9471192250, Email: sreevalsa@nitk.edu.in

NATIONAL INSTITUTE OF TECHNOLOGY KARNATAKA, SURATHKAL
DEPT. OF CIVIL ENGG.

Prof. Subhash C Yaragal

Chairman-DRPC

Chairman (DRPC)
Department of Civil Engineering
National Institute of Technology Karnataka
Surathkal, Mangalore - 575 025, Karnataka, INDIA

Dedicated to My Parents

ACKNOWLEDGEMENTS

I would like to thank the Almighty for giving me the strength, knowledge, ability, and opportunity to undertake this research study and to persevere and complete it satisfactorily.

First and foremost, I would like to express my deep sense of profound gratitude to my research supervisor **Dr. Sreevalsa Kolathayar**, *Assistant Professor, Department of Civil Engineering*, *NITK Surathkal* for his constant guidance, support, and motivation during my research work. His systematic and planned approach had consistently motivated me towards all activities including the completion of the research work in time. His valuable suggestions and comments at appropriate times during this investigation have contributed a lot in smooth conduct of the research work. Motivation, appreciation, moral support, and flexibility permitted during the course have helped me to complete my research successfully.

I am also thankful to RPAC Panel members **Prof. Sitaram Nayak**, *Professor, Department of Civil Engineering*, **NITK Surathkal** and **Dr. Basavaraj Talawar**, *Assistant Professor, Department of Computer Science and Engineering*, **NITK Surathkal** for their valuable guidance and suggestion throughout my work.

I am also thankful to Chairman-DRPC **Prof. Shubash C. Yaragal** and DRPC-Secretary **Dr. Mithun Mohan**, *Department of Civil Engineering*, **NITK Surathkal**, for their support and guidance throughout my work.

I would like to thank the **Ministry of Human Resource Development (MHRD)**, *Government of India*, for granting the financial support during the Ph.D. program and **DST/SERB** for providing the funding for setting up the necessary experimental setup and computation facility required for the research. I would also like to thank the Director: **Prof. B Ravi**, Dean (Academic): **Prof. Vidya Shetty** of *NITK Surathkal* for providing their extended support towards smooth conduct of the research work at the institute.

I must also thank the former HoDs: **Prof. K. Swaminathan**, and **Prof. B. R. Jayalekshmi**, faculty members, and staffs of the *Department of Civil Engineering*, *NITK Surathkal* for their kind help and support.

I must acknowledge the extended support of my fellow Ph.D. scholars and friends: **Dr. Srikar G, Mr. Varun Menon O, Ms. Dani Jose, Mr. Sandeepkumar N, Mr. Priyajit Kundu, Mr. Avinash R, Mrs. Sushma , Mrs. Niveditha M, Mr. Pruthviraj, S**, and **Mr. Chethan L**.

I must acknowledge the extended support of my fellow B.Tech. friends: **Mr. Piyush T, Mr. L. Chethan Kumar, Mr. Dhrubo N**, B.Tech., Civil Engineering (2022 Batch), and all other B.Tech. students associated with GT Lab. I must acknowledge the extended support of my B.Tech. batchmates: **Mr. Prashant Kammar**, and **Ms. Deepali Dani**.

I owe my utmost gratitude to my parents **Shri Muttappa Bariker** and **Smt. Ratna Bariker** for their love and support throughout my life. I thank both for giving me strength, guidance, and freedom to chase my dreams. I must thank my brother **Mr. Pritam Bariker** for being a constant pillar of support. I would also like to thank my paternal grandparents: **Late Shri Basappa Bariker** and **Smt. Laxmavva Bariker**, and my late maternal grandparents: **Shri Hanumantappa Guledagudda** and **Smt. Shantavva Guledagudda** for their prayers to achieve this glorious mark. I am grateful to my uncles, aunts, brothers, sisters, and all my relatives for their wishes and support. Finally, I cannot forget thanking the mother **Nature** for providing everything.

There are few more uncredited good hearts behind this success. I would like to thank every one of them.

Again, I am very grateful to my supervisor and my parents, who believed and encouraged me for making this mission possible.

PANKAJ BARIKER

ABSTRACT

This thesis presents an innovative finned pile foundation system as an alternative to regular pile foundations to resist larger lateral loads and improve pile group efficiency. The work presented in the thesis is an effort toward achieving the global targets set through Sustainable Development Goals (SDGs), particularly SDG#9 (Industry Innovation and Infrastructure) and SDG#11 (Sustainable Cities and Communities) by reducing the carbon footprints through the reduction in usage of carbon-intensive materials for infrastructure. It is proposed to make an innovative alteration to the regular piles to meet the infrastructure requirements with less usage of concrete and steel. This work evaluates the lateral load resistance of finned piles for onshore foundation applications. It compares their performance under seismic excitation with regular pile mats for high-rise buildings and wind turbines. In addition to physical model experiments, the numerical studies were performed in a FEM framework. Physical model experiments for individual long piles embedded in c–ϕ soil were conducted on scaled-down models, and the load-displacement behaviour was studied. The study presented the influence of fin factors such as fin position, width, length, orientation, embedment in pile cap, and eccentric loading and suggested the optimum fin parameters to increase the lateral resistance to the maximum.The findings demonstrated that finned piles, which had fins embedded in pile caps, exhibited superior performance compared to regular piles lacking fin embedment. The cost-benefit study supported the construction economy with finned piles, using only 55% of the material used by regular piles.

In an effort to enhance the lateral resistance of pile groups, this study explored the implementation of innovative finned piles. The research examined the influence of multiple factors, such as fins, the quantity of piles (n), pile spacings (s), and their behavior when subjected to eccentric loading. The results showed that FP-groups have a higher lateral resistance than RP-groups, resulting in improved pile group efficiency of up to 185%. The study found that pile spacing is more influential than the number of piles. A cost-benefit analysis compared the finned pile groups to regular pile groups. Additionally, regression analyses were performed to establish a correlation that enables

the calculation of the lateral resistance of finned pile groups based on different fin parameters.

Furthermore, this study places emphasis on mitigating the adverse effects of earthquakes, wind forces, dredging activities, and machine vibrations on multi-story buildings that are supported by piled mats. The study aims to minimize vibrations within the structure by using an innovative finned-pile foundation system, which can withstand 65% to 80% higher lateral load than conventional pile systems. The seismic responses of a 25–story building resting on a finned-pile mat were studied in the FEM framework through time–history analysis for varying fin lengths. The findings indicated that incorporating finned–pile mats had a notable impact in reducing vibrations and seismic effects on the building. It was suggested that an optimal fin length of $0.6L_p$ would effectively balance both seismic performance and construction efficiency for finned–pile mats.

Furthermore, the study investigated the potential of utilizing finned-pile mats (FP-Mat) as a foundation system to enhance the performance of wind turbines when subjected to seismic excitation. The study used finite element method (FEM) modelling to perform time–history analyses on wind turbines resting on piled mats under different earthquake excitations, considering soil–structure interaction. The results showed that FP–Mat with a fin length of 0.5m reduced the vibration by 27% compared to regular–pile mat (RP–Mat) and reduced the wind turbine's segmental drift within acceptable limits. The FP–Mat was also found to reduce the tower's tilting by 30%–40% under seismic excitation, reducing the risk of collision between the tower and blades, leading to a more sustainable design strategy. Overall, the study emphasized the need for careful assessment of the seismic performance of wind energy harvesting devices in an earthquake–prone regions and the potential benefits of using Finned Pile–Mat as a sustainable and alternative foundation system.

***Keywords*:** Finned–Pile, Lateral–load, Finned–pile group, Pile–group efficiency, Finned–pile Mat, High–rise Building, Wind–Turbine, Seismic Excitation.

TABLE OF CONTENTS

LIST OF TABLES

LIST OF FIGURES

NOMENCLATURE

$(D_p)_{eq}$	Equivalent pile diameter
$(L_p)_{eq}$	Equivalent pile length
$(\eta_g)_{FP}$	Pile group efficiency for the finned pile-group
$(\eta_g)_{RP}$	Pile group efficiency for the regular pile-group
A_{peak}	Peak acceleration
BM	Bending Moment
C_c	Coefficienct of curvature of soil
C_u	Coefficienct of uniformity of soil
D_p	Pile-diameter
D_r	Relative density of sand
D_{50}	Average particle size of soil
E	Young's modulus
E_pI_p	Flexural stiffness of Pile
G	Specific gravity of soil
I	Second moment of inertia
L_f	Fin-length
L_p	Pile-length
L_u	Ultimate lateral resistance of individual pile
$M35$	Concrete with f_{ck} of 35 MPa
M_w	Magnitude of earthquake
P_4 *and* P_5	Pile group with four and pile piles
R_{inter}	Interface reduction factor
SF	Shear force
U_{peak}	Peak displacement
W_f	Fin-width
$[(L_u)_g]_{FP}$	Ultimate lateral resistance of finned pile-group
$[(L_u)_g]_{RP}$	Ultimate lateral resistance of regular pile-group
Δ_{allow}	Allowable displacement

β	Characteristic length
βL_p	Dimensionless length
η	Fin-Efficiency
η_g	Pile group efficiency
γ_b	Bulk unit-weight of soil
γ_d	Dry unit-weight of soil
ν	Poisson's ratio
ϕ	Angle of internal friction
ψ	Dilation angle of soil
σ	Normal stress on soil
τ	Shear stress of soil
θ	Angle between fins and lateral load
c	Cohesion of soil
c_u	Undrained shear strength of soil
e	Eccentricity of the applied lateral load
f_y	Yield strength of steel
f_{ck}	Characteristic strength of concrete
h	Segmental height
n	Pile-numbers in the pile-group
p	Pressure on pile
s	Pile-spacing in the pile-group
t	duration of earthquake
t_f	Fin-thickness
t_p	Pile-thickness
u_w	Pore water pressure
w	Water or moisture content
w_L	Liquid limit of soil
w_P	Plastic limit of soil
$y\ or\ \Delta$	Displacement of pile head

ABBREVIATION

2D	**T**wo **D**imensional
3D	**T**hree **D**imensional
API	**A**merican **P**etroleum **I**institute
CPT	**C**one **P**enetration **T**est
FDM	**F**inite **D**ifference **M**ethod
FEM	**F**inite **E**lement **M**ethod
FP	**F**inned **P**ile
FP-FEPC	**F**inned **P**ile - with **F**ins **E**mbedded in **P**ile **C**ap
FP-WFE	**F**inned **P**ile - **W**ithout **F**in **E**mbedment
GCR	**G**roup **C**apacity **R**atio
GRF	**G**roup **R**eduction **F**actor
GSD	**G**rain **S**ize **D**istribution
LVDT	**L**inearly **V**arying **D**isplacement **T**ransducer
MCF	**M**angalore **C**hemicals and **F**ertilizers
MDD	**M**aximum **D**ry **D**ensity
MRPL	**M**angalore **R**efinery and **P**etrochemicals **L**imited
MSEZ	**M**angalore **S**pecial **E**conomic **Z**one
OMC	**O**ptimum **M**oisture **C**ontent
RNA	**R**otor **N**acelle **A**ssembly
RP	**R**egular **P**ile
SDG	**S**ustainable **D**evelopment **G**oals
SSI	**S**oil **S**tructure **I**nteraction
UPCL	**U**dupi **P**ower **C**orporation **L**imited
USCS	**U**nified **S**oil **C**lassification **S**ystem

CHAPTER 1

INTRODUCTION

1.1 GENERAL

A finned pile has multiple fin-forming plates welded at the top of a traditional regular pile along its perimeter. Finned piles have many synonyms, such as rocket, winged, and fin piles. The pile foundation transforms from a standard pile to a finned pile by reinforcing pile head with fin-forming plates, as depicted in Figure 1.1. Thereby, the lateral capacity of the foundation system is enhanced. (Nasr, 2014).

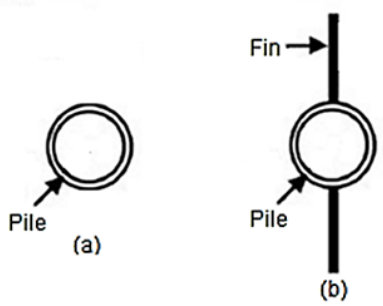

Figure 1.1 Cross-sectional views at pile-head for (a) Regular pile and (b) Finned pile.

Deep foundations are employed to sustain the larger lateral loads due to wind, machine operation loads, earthquake loads, and the effect of eccentricity due to vertical loads. The regular pile foundations must be appraised to carry the applied lateral loads without excessive displacement.In most cases, the foundations encounter lateral loads concentrated at the pile-head location, surpassing the capacity of the pile-shaft alone to withstand these loads due to insufficient stiffness. Hence, it is imperative to enhance the cross-section of the pile, particularly at the pile-head position (Peng, 2005). While pile foundations can offer some resistance against lateral loads, they may not effectively support larger loads using shorter lengths and smaller diameters. This situation calls for the implementation of an innovative pile foundation that can economically withstand lateral loads using smaller diameter and shorter length piles.

Figure 1.2 illustrates that the lateral resistance (L_u) of finned piles is influenced by multiple factors. By effectively considering those, L_u of finned-pile foundations can be enhanced, leading to an improved structural response during seismic excitation.

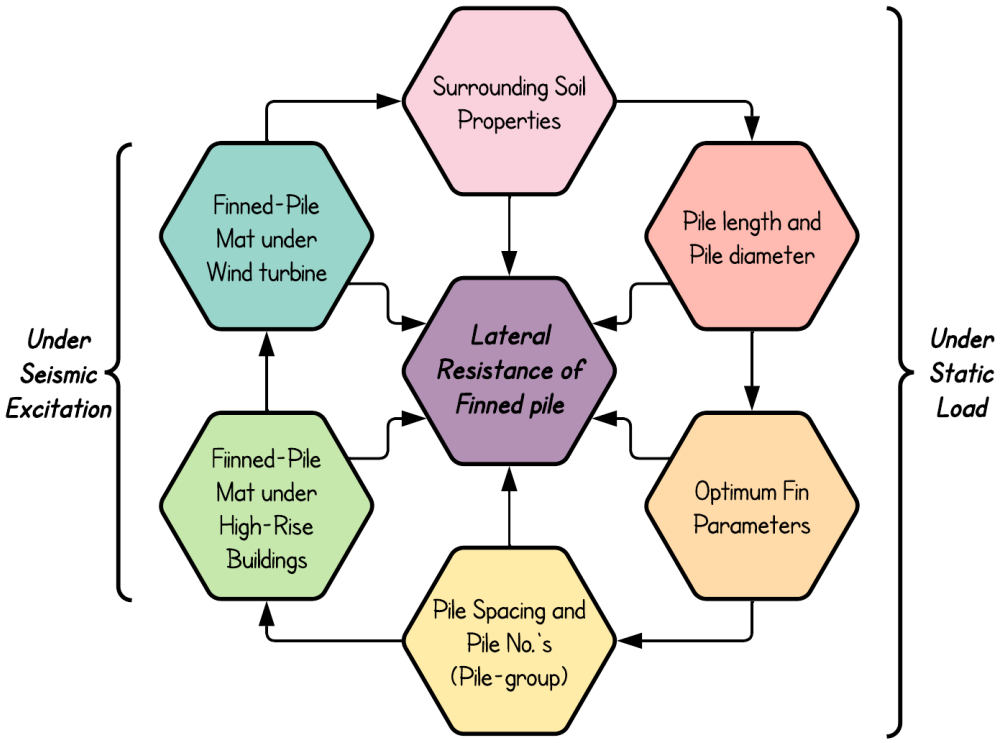

Figure 1.2 Factors influencing the lateral resistance of finned piles

1.2 FINNED PILE AS AN ALTERNATIVE

The work presented in the thesis is an effort toward achieving the global targets set through Sustainable Development Goals (SDGs), particularly SDG#9 (Industry Innovation and Infrastructure) and SDG#11 (Sustainable Cities and Communities) by reducing the carbon footprints through the reduction in usage of carbon-intensive materials for infrastructure. It is proposed to make an innovative alteration to the regular piles to meet the infrastructure requirements with less usage of materials. This work evaluates L_u of finned piles for onshore foundation applications. It compares their performance under dynamic loading with regular pile mats for high-rise buildings and wind turbines.

Recent studies have made efforts to enhance the stiffness of the pile-soil system by affixing fin-forming plates to the pile (Albusoda and Alsaddi, 2017; Babu and Viswanadham, 2018, 2019; Bariker et al., 2020; Peng, 2005). By incorporating fins, the pile's capacity to bear lateral loads is enhanced, ensuring compliance with strength criteria by minimizing lateral displacement within acceptable limits. Consequently, the serviceability criteria are met (Bariker et al., 2020). Thus, finned piles can be an alternative innovative foundation system to the regular pile foundation system subjected to considerable lateral loads.

Utilizing the finned-pile technique, i.e., intrusion of the fin forming plates adjoining to the pile-shaft, the project is economical because of lesser pile length and lower maintenance during its lifetime. Additionally, due to reduced lateral deformation at the pile-head (Peng, 2005), the utilization of finned piles enhances the activation of a larger soil volume. This, in turn, leads to improved passive resistance against lateral loads in the vicinity of the pile (Bariker et al., 2020). Several studies adopted finned piles as an alternative to larger dimensions monopile in the case of offshore foundations (Ambi et al., 2019, 2020; Bariker et al., 2020; Bienen et al., 2012; Gandhi and Selvam, 1997; Germanischer and Hamburg, 2005; Murphy et al., 2016; Peng, 2005; Peng et al., 2010).

1.3 BACKGROUND AND SIGNIFICANCE OF THE STUDY

There is a vital need to adopt an innovative and economic approach for resisting larger lateral loads with considerably small lateral displacement using piles of smaller diameters and lengths; this can be achieved by adopting finned piles. Limited literature exists on foundation systems involving groups of finned piles exposed to static lateral loads and seismic excitation. Consequently, this study aims to comprehend the behaviour of finned-pile foundations under these loads and offers valuable insights into the collective performance of FP-Groups.

Previous literature has commonly treated the base of buildings as rigid when conducting seismic response studies. However, the amplification or de-amplification of vibrations is influenced by factors like structure type and the characteristics of underlying soil. Neglecting the amplification effects may result in underestimating the extent of vibrations in seismic-response analyses of rigid base high-rise buildings. Thus, it is advisable to consider the interaction between the soil, pile, and structure while examining the seismic response of structures (Fatahi et al., 2011; Kramer, 1996). Additionally, soil damping plays a crucial role in reducing the stresses that contribute to vibration (Wolf and Obernhuber, 1985) and alters the input excitation across the system (Anand and Satish Kumar, 2018).

There is an increasing demand for comprehensive assessment of the seismic performance of wind turbines in earthquake-prone regions worldwide (Katsanos et al., 2016). In 2021, the wind turbines contributed about 6.6% of the world's electricity, which rose from 3.5% in 2015 and is aimed to increase the contribution to 20% by 2030 (Zieliński et al., 2022). Even though the turbines resting on piled mats are safe enough to resist the wind load, they proved critical during the earthquake. Hence, there is a need to reduce the earthquake effects on wind turbines by using innovative foundation

techniques. Lateral resistance of the soil is of prime concern while dealing with the wind turbine, as wind or earthquakes indirectly induce lateral deformation, leading to severe damages. Therefore, the foundation must withstand these detrimental effects due to earthquakes.

The current study examines the efficacy of finned piles as foundation systems in withstanding lateral loads. In addition, this study concentrates on the economic concern of overcoming the use of larger length piles and reducing the lateral displacements in foundation systems. This study also quantifies the performance of finned pile mats under seismic excitation in reducing the vibrations caused due to seismic excitation.

1.4 RESEARCH OBJECTIVES

The objective of this study is to explore the behaviour of finned piles under various geotechnical conditions. By conducting experimental and numerical investigations, the study aims to gain insights into the unique characteristics of finned-pile groups as onshore foundations for resisting lateral loads. Additionally, the study aims to conceptualize the utilization of finned piles as foundation systems under seismic excitation.

The objectives of the present research work are as follows:

1. To conduct parametric studies and determine the optimal fin parameters for laterally loaded finned piles installed in c-ϕ soil.
2. To analyze and compare the group efficiency of laterally loaded finned pile groups with that of regular pile groups
3. To investigate the effect of finned pile mats under high–rise buildings under seismic excitation.
4. To examine the impact of a finned pile mat under a wind turbine subjected to seismic excitation.

1.5 NEED OF THE PRESENT STUDY

Significant research efforts have been dedicated to investigating the lateral behaviour of both regular and finned piles. However, the majority of these studies have primarily concentrated on improving the L_u of larger offshore finned piles, typically with a diameter of approximately 4 meters. Nevertheless, there are limited studies examining the lateral behaviour of onshore finned piles with smaller dimensions (ranging from approximately 0.5 to 1 meter in diameter) installed in either purely cohesion-less or cohesive soils. Moreover, there is a lack of studies on the behaviour of finned piles in c-ϕ soils. It is worth noting that the presence of fines in the soil exhibits contrasting

behaviour compared to sandy soils (Rahman and Lo, 2014), suggesting that finned piles may exhibit improved performance in c-ϕ soils compared to sandy soils. Furthermore, there is a notable absence of research in the literature regarding finned pile groups subjected to lateral loads and their group efficiency.

1.6 ORGANIZATION OF THE THESIS

Chapter 2: This chapter deals with the literature review for the present work.
Chapter 3: This chapter deals with the materials and methodology adopted in the experimental work.
Chapter 4: This chapter deals with the results and discussions on the experimental and numerical analysis of finned piles compared to regular piles under lateral load.
Chapter 5: This chapter deals with the results and discussions on the experimental and numerical analysis in investigating the pile-group efficiency and regression analysis of finned pile groups subjected to lateral loads.
Chapter 6: This chapter deals with the effect of soil structure interaction on a high-rise building resting over a finned pile mat under seismic excitation.
Chapter 7: This chapter deals with the effect of soil structure interaction on the wind turbine resting over a finned pile mat under seismic excitation.

CHAPTER 2

LITERATURE REVIEW

2.1 INTRODUCTION

Under lateral loads, piles act as transversely loaded beams, transferring the load from the pile to the surrounding soil through the lateral resistance offered by the soil. This displacement of the pile against the soil in front of it leads to the development of stress and strain in the soil, resulting in resistance against the pile's movement. The upper shallow soil layers primarily bear the majority of the load, providing the primary support. Therefore, it is crucial to enhance the flexural stiffness (E_pI_p) of the pile, particularly in this specific region of the soil-pile system.

In search of innovative foundations in resisting lateral loads, performed extensive studies over the years. Innovative piles represent smaller diameters and lengths (compared with regular piles) that can resist larger lateral loads with smaller lateral displacement, i.e., within permissible limits. Also, by adopting innovative piles, the seismic response of the infrastructures can be mitigated economically.

Hence, when considering the adoption of a finned pile as an innovative foundation solution, it becomes crucial to conduct a comprehensive examination of various factors such as fin parameters, pile length, soil properties, pile spacing, and the number of piles in pile groups. Therefore, conducting a fin-parametric study holds significant importance in the selection of a suitable finned pile, even when considering the project's economic aspects. Understanding the optimal pile spacing within pile groups is essential for the implementation of a finned pile as an innovative foundation. This perspective has motivated numerous experimental and numerical investigations aiming to assess the impact of piles on enhancing the L_u of both regular and finned pile foundation systems. The findings of these investigations are presented in the subsequent sections.

2.2 LATERAL RESISTANCE OF REGULAR PILES

The early studies on lateral resistance of piles primarily relied on conventional methods that overlooked the contribution of soil resistance surrounding the pile, rendering the

proposed theories unrealistic. However, subsequent advancements in theories have emerged that consider the bending behavior of piles, providing a more realistic approach for analyzing laterally loaded piles using elastic and plastic theories.

The first elastic theory, proposed by Matlock and Reese (1960), introduced the concept of treating the soil surrounding the pile as a series of closely spaced independent elastic springs. This theory incorporated the use of subgrade modulus and relied on known values of elastic constants E and μ. By solving the prescribed differential equations under various conditions, the theory enabled the determination of deflection, bending moment, shear force, and soil reactions along the length of the pile.

In the case of a laterally loaded pile, even a relatively smaller working load can result in significant lateral deformation, setting it apart from an axially loaded pile. The determination of the pile's lateral resistance under lateral loads can be achieved by either calculating the ultimate lateral load (based on strength criteria) or evaluating the permissible deflection under working load (based on serviceability criteria) (Shamsher and Sharma, 1990). It is important to note that laterally loaded piles often exhibit substantial lateral deformation prior to failure, potentially exceeding the permissible lateral deformation limits (Tomlinson and Woodward, 2008). Therefore, when designing a laterally loaded pile, particular attention should be given to the allowable lateral deformation (Δ) of the pile in comparison to its ultimate lateral resistance (L_u).

Therefore, this section focuses on reviewing previous research studies that have investigated the two criteria mentioned earlier, namely the L_u and Δ of piles, as well as other relevant factors, to assess the L_u of laterally loaded piles.

2.2.1 Ultimate Lateral Resistance of Piles

Hansen (1961) proposed a trial-and-error method based on earth pressure theory for a pile system under lateral load for locating the rotation point shown in Figure 2.1. The lateral resistance of the pile at any depth was calculated by applying equilibrium equations. This theory is valid only for short-rigid piles embedded in c-ϕ soils.

Broms (1964a,b) expanded upon the aforementioned study by introducing simplified assumptions regarding the distribution of soil resistance along the pile length. This theory is applicable to both rigid and flexible piles on purely cohesion-less soil, as described in Broms (1964a), or on cohesive soils, as discussed in Broms (1964b). The authors provided criteria for selecting piles (both short and long piles) based on a dimensionless embedment factor (η or β), taking into account the influence of the

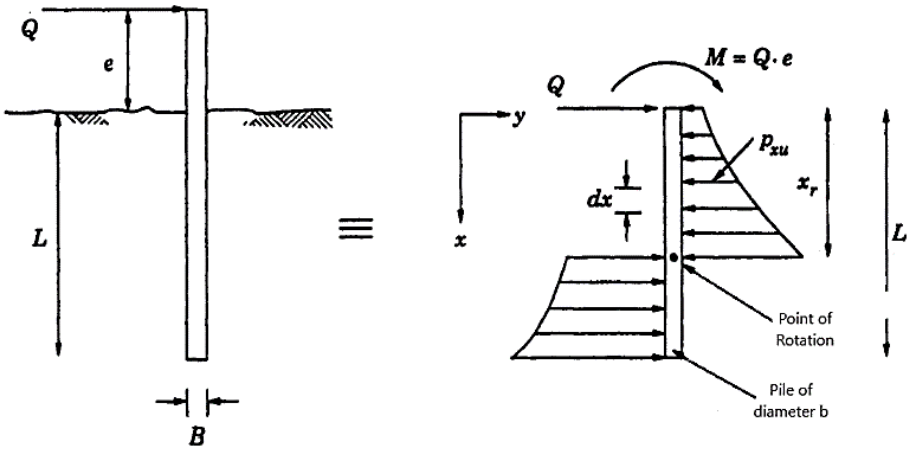

Figure 2.1 Pressure distribution for laterally loaded short-rigid pile (Hansen, 1961)

pile's stiffness (E, I) and the soil's embedment factor (η_h), as outlined in Table 2.1. According to the theory, short piles are assumed to behave as rigid piles when subjected to lateral loads, rotating about a fixed point. On the other hand, long piles are considered flexible and exhibit significant passive resistance throughout their length, with bending dominating the pile's rotation. Consequently, the analysis methods differ for short-rigid piles and long-flexible piles.

Table 2.1 Recommendations' by Broms (1964a,b) for pile selection criteria

Observations	**Cohesionless soil**	**Cohesive soil**
Embedment factor, (η or β)	$\eta = \sqrt[5]{\frac{EI}{\eta_h}}$	$\beta = \sqrt[4]{\frac{EI}{K_h}}$
For, Short pile	L/$\eta \leq 2$	L/$\beta \leq 2$
For, Long pile	L/$\eta \geq 4$	L/$\beta \geq 3.5$

2.2.2 Permissible Lateral Deformation of Piles

According to various design codes, the lateral design of piles often relies on the permissible lateral deformation rather than the load capacity of the piles. Typically, the permissible lateral deformations are estimated using either the modulus of subgrade reaction approach introduced by Matlock and Reese (1956) or the elastic continuum approach proposed by Poulos (1971a,b).

The non-dimensional approach by Matlock and Reese (1956) for piles subjected to lateral force and moment, assuming the pile as beam resting on elastic foundation,

with $k_h = \eta_{hx}$. Matlock and Reese (1960) developed a series of formulae for calculating deflection, slope, moment, shear, and soil reactions as illustrated in Figure 2.2.

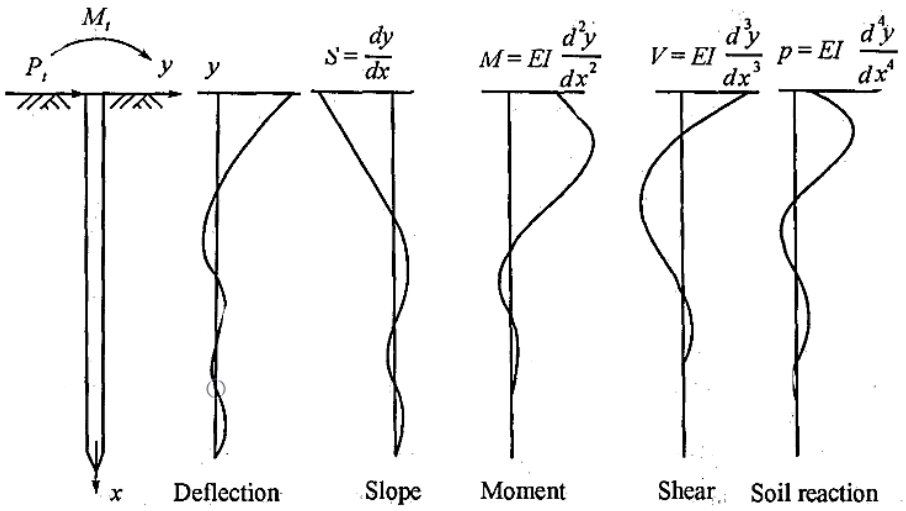

Figure 2.2 A complete solution of the laterally loaded pile (Matlock and Reese, 1956)

Xu et al. (2020) studied the field behaviour of offshore monopiles under lateral loading conditions. i.e., for monotonic and cyclic lateral loading. From gathered strain results bending moment, lateral deflections were derived from API and hyperbolic methods and later analyzed to get p-y curves with various available methods. The maximum lateral displacement at an ultimate load of 800kN was 369mm and 351mm, respectively. They have achieved the maximum moment at 6.5m and 5.5m depth (i.e., corresponding depths of $11.95D_p$ and $12.15D_p$) below the seabed level. Out of the API and hyperbolic methods of predicting lateral displacement and bending moment, the hyperbolic method predicts more significant errors than the API method. They proposed a modified p-y curve for predicting the field behaviour more reliably.

2.2.3 p-y Curve Method

The modulus of subgrade reaction approach proposed by Matlock and Reese (1956) is capable of estimating the lateral load carrying capacity within the elastic range. However, its applicability can be extended beyond the elastic range, even into the plastic range, by employing the p-y curve methods (Matlock, 1970; Reese et al., 1974; Reese and Welch, 1975; Bhushan et al., 1979). These non-linear p-y curve methods enable the prediction of the load at various loading stages.

A comprehensive methodology for developing p-y curves was presented by Reese et al. (1974), who conducted an analysis of full-scale field piles subjected to static and cyclic loading in sandy soils. The study encompassed pile-head deflection, pile-head rotation, bending moment (BM), and pile length to generate the p-y curves. It was observed that the p-y curves typically consist of three straight lines and a parabolic segment, as illustrated in Figure 2.3 below. The key findings of the study include guidelines for constructing the remaining portions of the p-y curves (i.e., $\alpha = 0.5\phi$, $\beta = 45 + 0.5\phi$). The deflection values between the parabolic segment and the intermediate straight lines were determined to be b/60 and 3b/80, respectively.

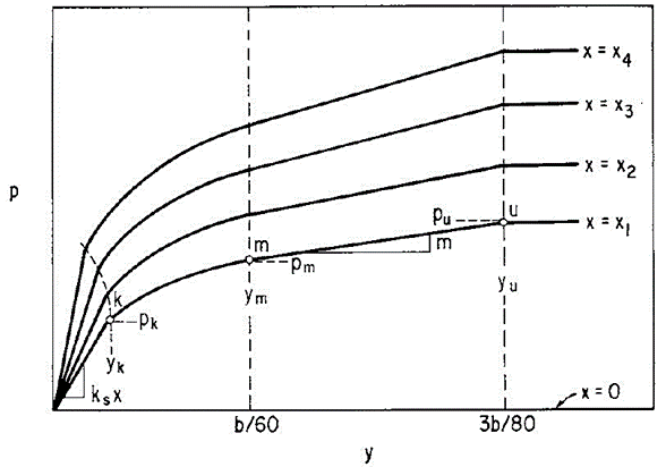

Figure 2.3 The typical family of p-y curves recommended by (Reese et al., 1974)

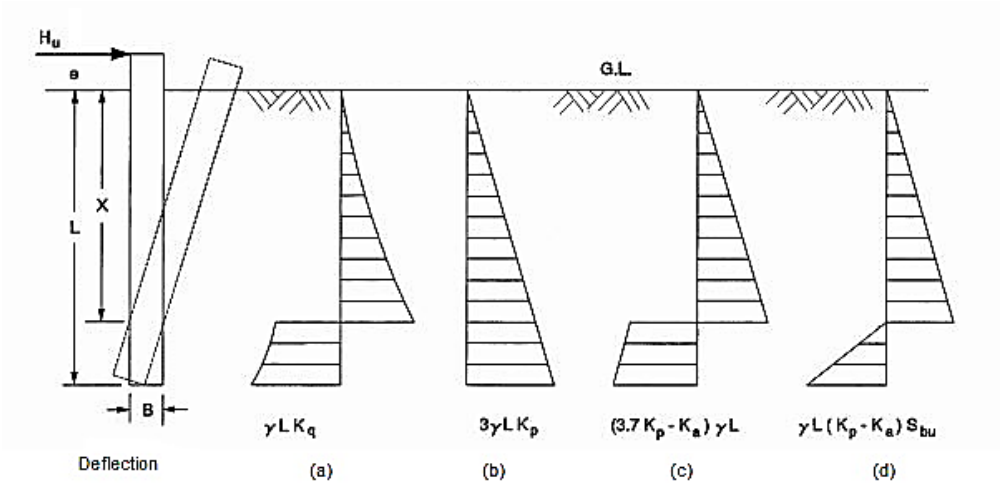

Figure 2.4 Lateral pressure distribution profile by (a) Hansen (1961), (b) Broms (1964a), (c) Christos and Michael (1993), and (d) Meyerhof et al. (1981)

The determination of the L_u of a pile relies on the distribution of soil pressure along its length, as depicted in Figure 2.4. To estimate this pressure distribution and

the lateral capacity of rigid piles, Prasad and Chari (1999) introduced a simplified approach. The authors conducted a comparison of the soil pressure distribution with relevant previous studies, including those by Hansen (1961); Broms (1964a); Christos and Michael (1993); Meyerhof et al. (1981), and found the comparison to be satisfactory in terms of agreement.

Zhang et al. (2005) analysed the distribution of lateral resistance around the pile cross-section experimentally. They proposed a theory by separating the total lateral resistance into the resistance provided by soil in front of the applied load front of the pile (i.e., frontal resistance) and resistance developed along to sides of the pile (i.e., side resistance) as shown in Figure 2.5 below, for long-flexible piles.

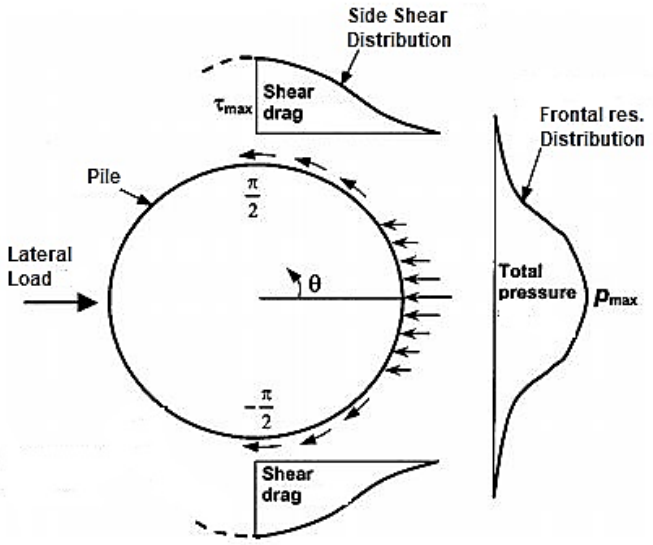

Figure 2.5 Distribution of frontal and side shear resistances. (Zhang et al., 2005)

The influence of pile position relative to the slope crest and loading direction on laterally loaded piles embedded in sandy soil was investigated by Muthukkumaran (2014). The study revealed that the lateral displacement corresponding to L_u of the pile reached 8% and 16% for loose and dense sand, respectively. In subsequent research, Deendayal et al. (2016); Rathod et al. (2018) conducted a series of model tests on laterally loaded piles embedded in clayey soil. They examined the response of these piles when placed on slopes and compared it with the findings of 3D numerical analyses. The results shown that L_u of the piles decreased when installed on slopes due to a reduction in the passive resistance in front of the soil.

2.2.4 Numerical Studies on Laterally Loaded Piles

The finite difference method (FDM) was employed by Howe (1955); Matlock and Reese (1960); Bowles (1974) in their attempts to analyze piles under lateral loads. Initially, Bowles (1974) utilized the FDM for analysis purposes. However, the finite element method (FEM) has proven to be a substantial improvement, as FDM-based solutions overlook the contribution arising from pile rotation.

In their work, Kok and Bujang (2008) introduced a 2D finite element program to simulate the lateral behavior of individual piles in two scenarios: one near an excavation and the other for slope stabilization. Nevertheless, in this 2D analysis, the pile was modeled with plain strain model, which resulted in the neglect of shear resistance developed along the sides of the pile. Consequently, this led to an underestimation of the bending moment (BM) along the length of the pile.

By explicitly addressing a set of dominating factors, Jayantha et al. (2010) provided an alternative theoretical technique for predicting p-y curves for single piles subjected to horizontal loads in undrained clay. This approach is based on finite difference analysis, providing the lateral displacement utilizing the suggested closed-form solutions. The results of the tensile failure condition are substantially closer to those obtained by Matlock (1970) experimental approach.

In their study, Kim and Jeong (2011) conducted numerical investigations using 3D non-linear finite element modeling to analyze the p-y curve variations along the length of the pile. They performed parametric analyses and observed a linear increase in the L_u with increasing pile diameter. Furthermore, the accuracy of the finite element models was verified through lateral field load tests conducted on steel piles in the field. The comparison between the numerical study and field measurements showed good agreement, confirming the reliability of the findings and their consistency with observed trends in practice.

The field test results of horizontally loaded bored cast-in-situ piles placed in residual soil using M35 grade concrete were published by Naveen et al. (2012). To replicate these lateral stress tests on larger diameter piles in residual soil, Naveen and Denise Penelope (2016) employed a 2D FE model. The simulations were conducted using ALP OASYS software and compared with the previous studies conducted by Naveen et al. (2012). The comparison demonstrated good agreement, including a favorable correlation with field data, as presented in Table 2.2.

Table 2.2 Comparison between field test and FEM analyses

Study type	Displacement (mm)
Field testing	4.12
Plaxis 2D analysis (Naveen et al., 2012)	5.51
ALP OASYS analysis (Naveen and Denise Penelope, 2016)	5.83

A series of numerical analyses was conducted by Kranthikumar and Jakka (2020) to investigate the impact of the pile's edge distance from the crest of a slope on its L_u. The findings indicated that an increased edge distance of the pile on the slope resulted in higher L_u, while a steeper slope inclination led to a decrease in L_u.

2.3 LATERAL RESISTANCE OF FINNED PILES

Over time, several studies have been conducted on the lateral resistance of individual finned piles, considering both static and cyclic loads (Albusoda and Alsaddi, 2017; Ambi et al., 2019, 2020; Bienen et al., 2012; Babu and Viswanadham, 2018, 2019; Bariker et al., 2020; Gandhi and Selvam, 1997; Germanischer and Hamburg, 2005; Murphy et al., 2016; Nasr, 2014; Peng et al., 2004; Peng, 2005; Sakr et al., 2020; Yaghobi et al., 2019). Additionally, Peng et al. (2011); Rudolph and Grabe (2013); Albusoda et al. (2018) investigated the behavior of finned piles under cyclic loading conditions. Furthermore, some studies have focused on numerical validation of the findings..

2.3.1 Experimental Studies

A study conducted by Peng (2005) investigated the lateral resistance of monopiles by incorporating fin-forming plates into the pile structure. The researchers performed static loading analyses on finned piles to simulate p-y curves and validated their findings using LPILE and LUSAS software. The effectiveness of fins in enhancing the static loading capacity was evaluated based on the ultimate lateral loads and the lateral displacement of the pile head. The relationship between L_u and Δ, derived from the p-y curves (Figure 2.6), emphasized the significance of fins in improving the lateral resistance. The study also proposed optimal dimensions for the fins, suggesting an ideal fin-width (W_f) of $0.5D_p$ and a fin-length (L_f) of $0.5L_p$.

Ambi et al. (2019, 2020) conducted a series of model tests on regular and finned piles in loose sand to investigate the impact of fin shape on L_u under combined loading

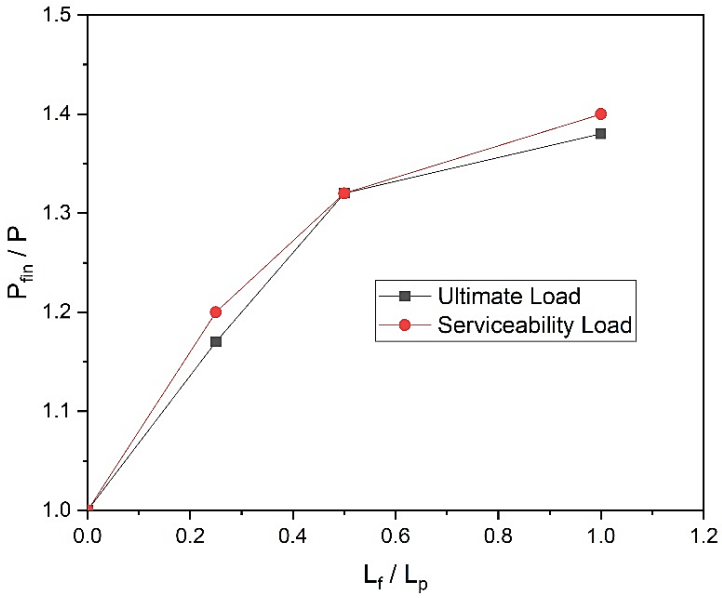

Figure 2.6 Variation of fin efficiency with fin-length (Peng, 2005)

conditions. The study focused on analyzing the impact of fin length, fin width, aspect ratio, and surface area in resisting lateral loads under combined loading conditions. The researchers quantified the enhancement in L_u by using an efficiency factor based on Load-displacement curves of the finned piles. In their findings, Ambi et al. (2019) observed that the ultimate lateral loads were higher for combined loading conditions compared to lateral load alone for both regular and finned piles. They also found that the finned piles exhibited greater effectiveness under combined loading than under lateral loading alone, particularly when studying the effect of L_f and W_f. Multiple length factors (L_f/L_p) were considered, and it was observed that a higher L_u was achieved for a W_f of D_p under combined loading and lateral loading conditions.

Albusoda and Alsaddi (2017) conducted model tests on individual piles as well as pile groups with configurations of 4 and 5 piles, with pile spacings of 4d and 6d. The four pile group configurations, namely G4S4, G5S4, G4S6, and G5S6, are illustrated in Figure 2.7. The tests revealed that individual finned piles exhibited a 76% increase in L_u compared to regular piles. The study aimed to investigate the effect of finned pile groups by analyzing three main categories of influencing factors: fin effect, pile spacing, and pile group pattern. The failure load corresponding to a Δ of $0.2D_p$ (20%) was considered, which differs from the 10% used by Peng (2005). The finned pile groups, G4S4, G5S4, G4S6, and G5S6, demonstrated increases in L_u by 75%, 59%, 60%, and 82%, respectively, compared to regular pile groups, using an optimal W_f/D_p equal to 1.0 as suggested by Nasr (2014). The effect of pile spacing was also analyzed, and it

was found that pile groups with larger spacing of 6d exhibited a 15% and 26% increase in L_u, respectively, compared to configurations with a pile spacing of 4d. Furthermore, the results indicated that the G5 configuration showed a 27% and 39% increase in L_u for pile spacings of 4d and 6d, respectively, compared to the G4 configuration.

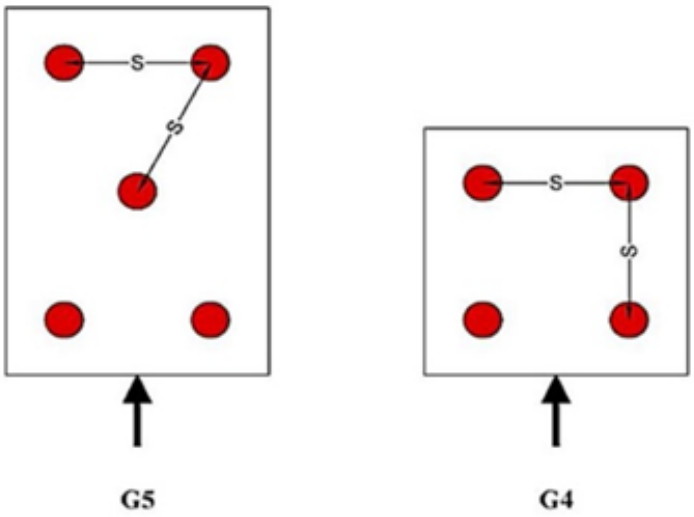

Figure 2.7 Pile group configuration (Albusoda and Alsaddi, 2017)

Murphy et al. (2016) attempted to investigate the field behaviour of winged-monopile, formed by attaching the steel plates to regular piles near the ground line to increase the pile stiffness and lateral resistance. The author performed experimental tests of instrumented regular and winged monopolies at two sandy sites, drawing conclusions from the lateral load-displacement curves and BM profiles. Tests were carried out for two fin geometries with fin-lengths of $0.14L_p$ and $0.28L_p$, respectively, with fin-widths being $0.75D_p$ forming two fin geometries WP1 and WP2. At site-1 (Blessington), when tested with the ultimate load as the criteria (i.e., load at the lateral displacement of about $0.1D_p$), L_u increased by 16% and 36% for WP1 and WP2, respectively. Tests were conducted as per Germanischer and Hamburg (2005), taking service limit state (SLS) into account the displacement of L/500 (i.e., Lateral displacement nearly equal to 1.2% of D_p). It was reported that Site-1 required applied loads of 111% and 130% more than regular piles for WP1 and WP2. In contrast, Site-2 required applied loads as high as 117% and 129% more than regular piles obtained from lateral load-displacement curves shown in Figure 2.8. The lateral loads corresponding to serviceability and ULS displacements increased significantly with wings to monopiles. The addition of wings reduced lateral displacement by 45% and 60% more than the reference pile.

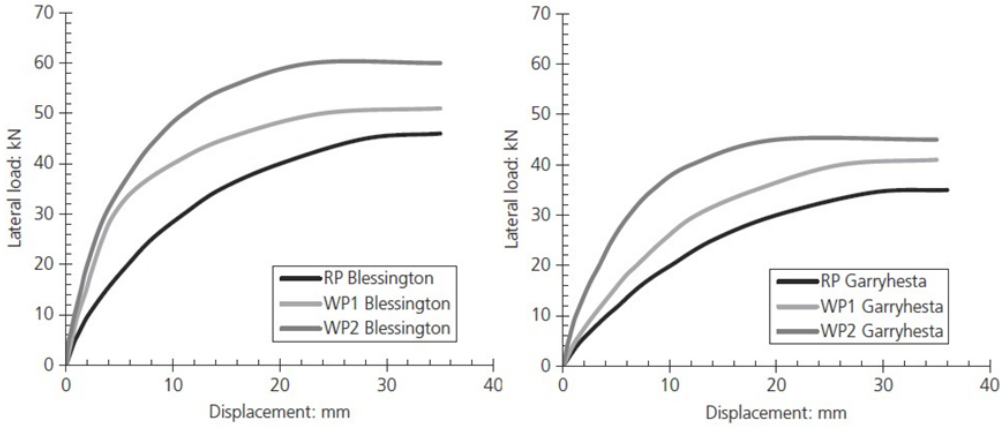

Figure 2.8 Lateral load-displacement curves for two sites (Murphy et al., 2016)

Sakr et al. (2020) performed model tests to enhance L_u of piles in clayey soils by incorporating a fin system at the pile head. The study examined the impacts of various parameters, like geometric fin dimensions, pile type, fin shape, fin number, and inclination angle, on the lateral resistance. The tests were conducted on smooth-surfaced steel piles installed in kaolin-based artificial deposits with two different shear strengths of 11kPa and 15kPa. The influence of the slenderness ratio was investigated by conducting tests for two L_p/D_p ratios of 10 and 22. The L_u was obtained at a Δ of $0.1D_p$. To analyze the effect of geometric fin dimensions, separate tests were performed for the L_f and W_f. For L_f of $0.4L_p$, the L_u increased by 36% and 54% for slenderness ratios of 10 and 22, respectively, in clay with a shear strength of C_u = 15kPa. Similarly, the lateral capacity increased by 67% and 29% for L/D values of 10 and 22, respectively, in clay with a shear strength of C_u = 11kPa. The study also investigated the effect of W_f/D_p for different values 0.5, 0.75, and 1.0, while keeping the fin length constant at $0.4L_p$. It was observed that the fin with a width equal to D_p exhibited the highest L_u.

Rudolph and Grabe (2013) investigated the impact of changing loading directions and the effectiveness of finned piles in reducing accumulated displacements under high-cyclic loads. Field tests were conducted on two tubular steel piles, one of which was a finned pile, as depicted in Figure 2.9. The loading direction (ψ) was varied incrementally up to 90°, and cyclic loading tests were performed for 100,000 cycles, with the initial cycles exhibiting non-linear behavior. Therefore, the results were extracted from the subsequent 75,000 cycles of each test, focusing on the corresponding start and end of the elastic range (y_{el}^{start} and y_{el}^{end}). The pile head displacements during cyclic lateral loading were recorded and presented in Table 2.3.

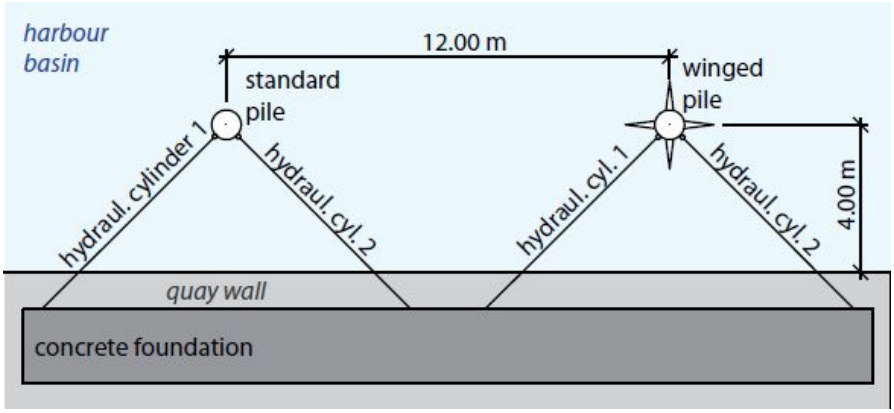

Figure 2.9 Field test setup employed (Rudolph and Grabe, 2013)

Table 2.3 Overview of test results by Rudolph and Grabe (2013)

Angle, ψ (°)	**Standard Pile**			**Winged Pile**		
	y_{el}^{start} (mm)	y_{el}^{end} (mm)	$y_{acc}^{(N=75000)}$ (mm)	y_{el}^{start} (mm)	y_{el}^{end} (mm)	$y_{acc}^{(N=75000)}$ (mm)
30	45.0	54.0	7.0	60.0	50.0	18.0
0	40.5	37.0	2.0	49.5	46.0	7.0
60	41.0	39.5	5.0	48.5	49.0	6.5
90	41.5	39.6	4.0	51.0	49.0	7.0

Comparing the finned pile to the standard pile, it was observed that the finned pile resulted in larger pile head displacements but mitigated the influence of change in loading directions. The increased accumulation behavior in the finned pile could potentially be attributed to disturbances caused during the pile installation.

Bienen et al. (2012) conducted centrifuge model tests to investigate the impact of attaching wings at pile head on the L_u of the pile under monotonic and cyclic loading. The study focused on the behavior of finned piles under different loading conditions, considering two slenderness ratios (L/D) of 4 and 12.5, which represented fixed-head-short piles and free-headed-long piles, respectively. The tests were conducted for two loading directions: wings perpendicular to the load and wings at a 45° angle to the load. The study also examined the effect of wings on both rigid and flexible piles. The tests were conducted in two series. In the initial test series, monotonic loads were applied until a Δ of $0.2D_p$, and the load at Δ of $0.1D_p$ was considered the L_u. The results showed that L_u of the pile increased with an increase in the pile's embedment depth. Overall, the centrifuge model tests demonstrated that the presence of wings at the pile head had a significant impact on the L_u of pile, resulting in a stiffer initial response. The study provided valuable insights into the behavior of finned piles under both monotonic and cyclic loading conditions, considering different slenderness ratios and loading directions.

2.3.2 Numerical Studies

Haldar and Babu (2008) investigated the impact of spatial variability in c_u on the behavior of large-scale piles subjected to transverse loads in clayey soil. The study focused on understanding the propagation of failure in the soil near the pile by analyzing the accumulated shear strain. They found that the failure behavior can be described by considering the accumulated shear strain in the soil. In a subsequent study, Haldar and Sivakumar Babu (2009) developed a reliability-based design method for the piles under transverse load. This method took into account the influence of various soil properties, including those correlated with Cone Penetration Test (CPT) results. The objective was to enhance the design process by considering the uncertainties associated with soil properties and their effects on the L_u of pile.

Peng et al. (2010) conducted a comprehensive study on the performance of finned piles subjected to lateral loads using 3D non-linear analysis. The main objective was to investigate the impact of fins on pile-soil interaction, stress distribution, and deformation of the fins. The findings from this analysis provided evidence supporting

the use of fins to enhance the L_u of piles. The study considered various parameters related to the fins, such as fin length and loading directions, to assess their influence on the lateral resistance. The failure load or L_u was defined as the load at a Δ of $0.1D_p$ (10%). Additionally, the authors examined the effect of loading direction on the L_u of finned piles, comparing loads applied in line with the fins and loads applied at a 45° angle with the fins. It was noted that applying the load at a 45° angle with the fins resulted in a slight increase in the L_u compared to loading in line with the fins.

Albusoda et al. (2018) conducted a comprehensive study to investigate the behaviour of regular and finned piles installed in multi-layered sand subjected to lateral loading. The study included comparisons between single piles and pile groups consisting of four and five piles with spacing ratios (s/d) of 3 and 6, forming the groups G4S3, G5S3, G4S6, and G5S6. Small-scale model tests were performed using aluminum piles with a slenderness ratio (L/D) of 45. The failure load was defined as the load at Δ of $0.2D_p$ (20%). To further analyze the behavior of single piles and pile-group systems, a 3D FE program was employed to obtain numerical results for comparison with the experimental findings. The results showed a close agreement between the experimental and numerical results for single piles, as well as for the four and five-pile groups. The inclusion of fins at the pile head resulted in an increase in L_u by 76% and 81% for single piles and pile groups, respectively, as compared to regular piles.

Nasr (2014) employed numerical analyses to investigate the effects of fin length, fin width, and fin shape on increasing the L_u of piles in loose and medium sands. The study analyzed the effect of L_f on the L_u by considering various fin lengths represented as a ratio of fin length to pile length (L_f/L_p). L_u of finned pile increased as L_f/L_p increased up to 0.4, beyond this threshold, the increase in L_u became marginal, indicating that the contribution of the fin diminishes after L_f/L_p exceeded 0.4. Similarly, the effect of fin width (W_f/D_p) was investigated for different values such as 0.5, 1.0, 1.5, and 2.0, while keeping the fin length constant at 0.4. The study found that the lateral load increment was higher when W_f equals D_p. The findings provided insights into the optimal dimensions and configurations of fins to enhance the L_u of piles.

Numerical investigations of the finned piles' under lateral loads were conducted by Yaghobi et al. (2019) using the ABAQUS software. The study aimed to comprehensively analyze the influence of fin dimensions while maintaining a constant aspect ratio, in order to assess the effectiveness of fins in enhancing lateral resistance. To facilitate mesh generation, a 3D FE mesh in the form of a cylindrical model

with a diameter and height of 1m was constructed. Modelled the soil as a 3D continuum eight-noded (C3D8R) element assigned with the Mohr-Coulomb model. Pile as four-noded (S4R) shell element assigned with steel material as the linear-elastic model with interaction between soil and pile as Coulomb-friction model with a strength reduction factor of 0.67. Performed mesh sensitivity analysis to use lesser computation time by considering four mesh types large, medium, small, and uniform mesh, with mesh sizes finer near pile and coarser near boundaries.

Comparisons between ABAQUS models and small-scale experimental studies were conducted for finned piles subjected to lateral load. The results, depicted in Figure 2.10, considered the L_u as the load at Δ of $0.4D_p$ (40%). Parametric studies were also performed, focusing on finned piles with rectangular fins fixed at the pile head. In these studies, the pile length (L_p), pile thickness (t_p), and fin thickness (t_f) were kept constant. However, other parameters such as fin length, fin width, and pile diameter were varied to investigate their impact on increasing the lateral load. It is worth noting that the fin thickness was slightly higher than the pile thickness, as the pile is responsible for bearing most of the applied load when it is stiffer than the fins. The study aimed to explore the potential of utilizing fins at the pile head and smaller diameter piles as a means to achieve higher L_u while optimizing material usage.

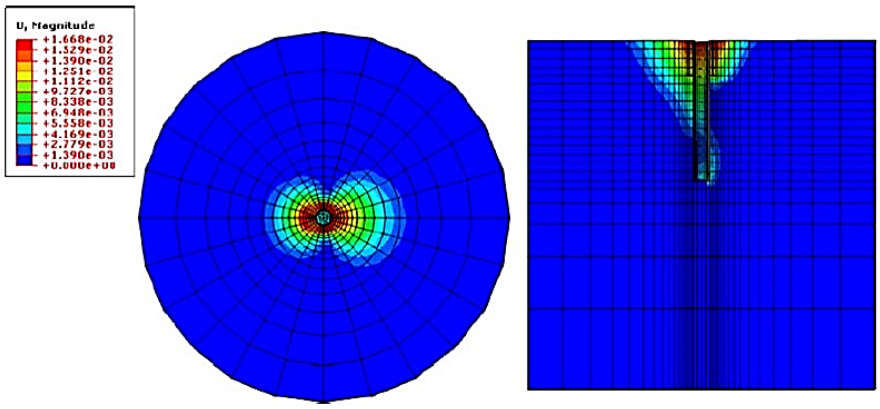

Figure 2.10 Displacement contours for the finned pile model (Yaghobi et al., 2019)

The improvement in L_u of monopiles through the addition of fins at the pile head, resulting in finned piles, was investigated by Babu and Viswanadham (2018, 2019). This study focused on the impact of various factors, like relative density (D_r) of the sand, fin length, fin orientation, and fin position. A 3D model was developed using ABAQUS, The model followed the rectangular configuration proposed by Karthigeyan et al. (2007), with plan dimensions equal to $23D_p$ and a height of $L_p + 13.5D_p$. The analysis included finned piles with various ratios of L_f/L_p ranging from 0.25 to 1.0. The study revealed that there was an increase in L_u up to a fin length of $0.5L_p$. However,

for fin lengths greater than $0.5L_p$, the increase in L_u was marginal. The efficiency of the fins showed higher variation for finned piles with L_f/L_p of 0.5 in loose sand with a D_r of 40%, suggesting that the fins are more effective in loose sands compared to dense sands. The effect of fin position was evaluated for three positions: pile top, middle, and bottom. The results indicated that fins positioned at the pile top were more suitable than other two positions.

2.4 EFFECTS OF SOIL STRUCTURE INTERACTION

Three systems, namely structure, foundation, and soil, are interrelated throughout the structural response to an earthquake. When seismic pressures substantially influence base movement relative to free activity in the soil, studying the soil-structure interaction is critical. Two essential techniques, direct method and sub-structure, are applied to handle soil-structure interaction (SSI) problems, are applied (Wolf and Song, 2002). Many recent studies like Makris and Chang (2000) have used this approach for SSI analysis of complicated structures by utilising powerful computational resources on contemporary computers.

To model and analyse the soil and structure in a single phase, the direct SSI approach is used. The soil-structure system is separated into two substructures in the substructure approach: the soil medium and the structures. This strategy is based on the superposition principle. The direct route to the sub-structure technique has the benefit of considering non-linear material behaviour (Majumder and Ghosh, 2016; Santoni et al., 2001). In this study, for the SSI analyses, both soil and structure are selected together.

The response of a high-rise framed structure was investigated by Fatahi et al. (2011) using nonlinear FDM formulations under two different boundary conditions: with and without soil-structure interaction (SSI). The study aimed to compare the inelastic behavior of the structure under various seismic excitations. The results showed that when soft soils were considered, the inter story drifts increased, and the structural performance shifted towards a collapse state when SSI was considered in the analyses. This finding highlighted that neglecting SSI in the inelastic design of the structure is insufficient to ensure its safety.

The behavior of different structures under the influence of soil-structure interaction (SSI) was described by Kramer (1996). The study found that SSI has a greater impact on heavier structures situated on soft soils compared to lighter structures on stiff soils. When considering SSI, the natural frequency of the soil, foundation, structure system is reduced more than that of the structure alone. However, due to

the significant vibration-induced degradation of soil stiffness, the displacement of the structure system may be higher. The study also concluded that inertial interactions have a greater influence on the response of the structure compared to kinematic interactions.

A series of non-linear SSI analyses were performed by Wolf and Obernhuber (1985), utilizing dynamic stiffness or soil flexibility. The study revealed that a significant portion of the internally generated stresses in the system are redistributed due to the degradation of soil stiffness during seismic excitation. Additionally, a portion of the supplied energy is dissipated through soil damping. The study emphasized the importance of considering interaction effects in SSI studies and determined that kinematic interactions dominate at lower levels of seismic excitation, while inertial interactions become more significant at higher levels.

The impact of inelastic SSI on the performance of buildings was investigated by Sáez et al. (2013) using FE formulations. The study focused on two regular reinforced concrete buildings of different sizes, considering their foundation on both dry and saturated sand, to examine the influence of the soil in dynamic SSI. The findings revealed that in the case of buildings situated on saturated sand, the inelastic SSI effects were consistently negligible. This can be attributed to the increased pore water pressure (u_w), which results in larger soil displacements compared to the dry soil conditions.

A hybrid numerical method was developed by Kucukarslan et al. (2003) to analyze the inelastic SSI of a structure supported by a pile foundation. In this method, finite linear elements were used to model the piles and structural elements, while infinite elements were employed to represent the soil boundaries. The non-linear behavior of the soil was simulated using non-linear springs along the pile length. The validity of the model was confirmed by comparing its results with available static load experiments.

Givens et al. (2012) performed SSI analyses on two instrumented buildings of a 13-story building with two basement floors and 10-story shear-wall buildings without embedment. Both the buildings were analysed with four simplified and alternative models, namely, (a) with fixed base, (b) subterranean model fixed as a base, (c) embedded portion of the structure with fixed-end springs, and (d) bathtub model. It was concluded that the fixed base building model produces poor results where as the bathtub model provides agreeable results.

2.5 SUMMARY

2.5.1 Lateral Resistance of Regular and Finned Pile Foundations

In general, piles serve as foundations for critical structures built on soft soil layers with varying soil conditions. They are designed to withstand significant lateral and axial loads, especially for structures such as transmission towers, wind turbines, and chimneys. The magnitude of lateral load is typically around 10% to 15% of the axial loads for onshore structures and 25% to 30% for offshore structures (Narasimha Rao et al., 1998)). The evaluation of lateral resistance can be determined either by estimating the L_u based on strength criteria or by assessing the allowable deflection (Δ_{allow}) under working loads based on serviceability criteria (Shamsher and Sharma, 1990). It is worth noting that laterally loaded piles exhibit significant lateral deformation prior to failure, often surpassing the permissible lateral deformation (Tomlinson and Woodward, 2008).

Early studies on pile behavior introduced the concept of closely spaced independent elastic springs representing the soil around the pile, along with the sub-grade modulus concept (Matlock and Reese, 1960). Broms (1964a,b) further developed the theory and proposed simplified assumptions for distributing the L_u along the pile length. This wedge theory is applicable to both short and long piles in cohesive and cohesionless soils. Reese et al. (1974) introduced pressure-deflection (p-y) curves, which describe the L_U based on static and cyclic load tests on full-scale field piles. Subsequent studies (Reese and Welch, 1975; Bhushan et al., 1979) aimed to improve the efficiency of the p-y curve method. Zhang et al. (2005) developed a method that divided the lateral resistance into frontal and side shear resistance, suitable for flexible piles.

Several studies have focused on investigating the L_u of individual fin-piles under static loading, emphasizing their effectiveness in increasing the lateral resistance of the foundation system (Albusoda and Alsaddi, 2017; Ambi et al., 2019; Bienen et al., 2012; Babu and Viswanadham, 2018, 2019; Bariker et al., 2020; Gandhi and Selvam, 1997; Germanischer and Hamburg, 2005; Murphy et al., 2016; Nasr, 2014; Peng et al., 2004; Peng, 2005; Sakr et al., 2020; Yaghobi et al., 2019). These studies have considered the Δ of $0.1D_p$ (10%) as the limit state criterion. The presence of fins in the pile activates a larger soil volume, resulting in increased passive resistance against applied lateral load in front of the pile (Bariker et al., 2020).

Furthermore, several investigations have explored the use of finned piles as an alternative to larger diameter monopiles for offshore foundations (Bienen et al., 2012; Bariker et al., 2020; Germanischer and Hamburg, 2005; Peng, 2005; Peng et al., 2010).

Studies by Albusoda et al. (2018) and Peng et al. (2011) have focused on the behavior of finned piles under cyclic loads, which have shown reduced lateral displacement (Δ) and increased lateral capacity (L_u). Peng et al. (2010) conducted a 3D FE analysis of finned piles subjected to lateral loads, considering the size of the soil model. To mitigate stress concentration and the influence of model box sides during loading, a cube with boundary dimensions of $22.5D_p$ and $2.5L_p$ was utilized.

2.5.2 Soil Structure Interaction of Piled-Mat

Previous research in the field has typically treated the base of buildings as rigid when conducting seismic response studies. However, the amplification or de-amplification of vibrations depends on the characteristics of the structure and the properties of the soil on which it is built. When analyzing the seismic response of a rigid base high-rise building, neglecting the amplification effects can lead to an underestimation of the actual vibrations experienced. Therefore, it is beneficial to consider the SSI while studying the seismic response of multi-story buildings (Fatahi et al., 2011; Kramer, 1996). The exchange of internal stresses within the system is largely influenced by the degradation of soil stiffness caused by seismic excitation, resulting in the dissipation of energy due to soil damping (Wolf and Obernhuber, 1985). Additionally, changes in the excitation across the system can also have an impact (Anand and Satish Kumar, 2018).

Numerous literature explored the SSI experimentally to analyse the influence of SSI on different structures. Gazetas and Stokoe (1991); Gazetas (1991) performed shake table tests and established the reliability impedance functions. Boulanger et al. (1999) investigated the dynamic p-y analyses by performing centrifuge model tests for various seismic excitations and shaking intensities.

SSI involves the transfer of internal stresses between the soil and structure within the system during an earthquake, leading to changes in the seismic response of the soil structure system as the soil stiffness degrades. It is a reliable technique for predicting the actual response of structures. The majority of previously published studies (Arboleda-Monsalve et al., 2020; Bagheri et al., 2018; Bilotta et al., 2015; Galal and Naimi, 2008; Han, 2002; Scarfone et al., 2020) have reached a consensus that the pile-raft technique, which takes into account SSI, offers an alternative approach to mitigate the adverse effects on buildings. It is important to note that post-earthquake effects on buildings cannot be completely eliminated by any remedial foundation technique; however, incorporating SSI can significantly reduce the detrimental impact of earthquakes on high-rise structures. Therefore, SSI is crucial for conducting seismic-response analyses and assessing seismic disturbances.

Piled-mat systems typically support the safety of high-rise structures. The passive earth pressure resists the lateral loads subjected to piles due to the soil surrounding the pile (Bariker et al., 2020; Bariker and Kolathayar, 2021; Nasr, 2014) and the interaction between soil-pile (Rollins and Sparks, 2002), which is dependent on the soil type and pile, geometry and material of pile, and soil. Also, the effect of vertical loads is not so significant on lateral loads when both are applied simultaneously (Suits et al., 2011). The seismic behavior of high rise buildings is of great significance and differs from buildings without shear walls (Zhang and Far, 2022). Therefore, it is crucial to implement appropriate measures aimed at mitigating the adverse effects of earthquakes on high rise structures.

2.6 RESEARCH GAPS

Considerable research has been conducted to investigate the behaviour of regular and finned piles loaded laterally, with a focus on increasing the L_u of larger offshore finned piles, typically characterized by a diameter of around 4 meters. However, only a limited number of studies have been reported on the behaviour of onshore finned piles, which have smaller dimensions ranging from approximately 0.5 to 1 meter in diameter. Moreover, these studies have mainly focused on either purely cohesive or cohesion-less soils, with no research available specifically on c-ϕ soils. Furthermore, there is a lack of studies addressing the lateral behaviour of finned pile groups subjected to lateral loads and assessing their overall effectiveness in resisting such loads as a group. Interestingly, the presence of fines in the soil can result in reverse behavior compared to sandy soils, as highlighted by Rahman (2014). Hence, it is possible that finned piles may exhibit efficient performance in c-ϕ soils, demonstrating their potential effectiveness beyond sandy soil conditions.

Pile-mat systems are commonly employed to support high-rise buildings and wind turbines on weaker soil strata. These structures need to be robust enough to withstand various external forces, including lateral loads from earthquakes, wind, and axial loads. Existing literature indicates that conventional pile systems can experience increased displacement due to SSI. Hence, there is a need for an innovative piled-mat foundation system to mitigate these effects, as conventional pile foundations often have limited lateral capacities relative to their axial capacities. Remarkably, there is currently a scarcity of research examining SSI analyses specifically for high-rise buildings or wind turbines supported by finned pile mats.

CHAPTER 3

METHODOLOGY AND MATERIALS

3.1 DESCRIPTION OF PROBLEM

3.1.1 Lateral Resistance of Finned Pile Foundations

Finned pile foundations are a type of deep foundation commonly used to support structures in areas with soft or weak soil conditions. The finned pile consists of a cylindrical shaft with longitudinal fins or plates that extend outward from the shaft. These fins or plates increase the surface area of the pile, thereby improving its resistance to lateral loads.

The conventional pile foundations face a challenge in effectively resisting these lateral loads, particularly when the magnitude and direction of the lateral load surpass the capacity of the piles. This limitation has the potential to cause structural failure, which in turn can have serious implications including the loss of lives and damage to properties. Therefore, there is a need for an innovative foundation system that can effectively withstand and counteract lateral loads.

3.1.2 Response of Finned Pile Mat under Seismic Excitation

Regular pile mat foundations represent a form of deep foundation that combines the benefits of both pile foundations and mat foundations. Finned piles efficiently transfer the loads exerted by the superstructure to the underlying soil, while the mat foundation offers supplementary support and facilitates even distribution of the loads across the underlying soil. However, the performance of piled mat foundations can be significantly affected by seismic excitations, leading to structural damage and collapse.

The challenge with conventional pile mat foundations during seismic events is to ensure their resilience against ground motions caused by earthquakes, preventing excessive damage or collapse. That requires a comprehensive understanding of the foundation's response to the ground motions.

The seismic response of finned pile mat foundations is influenced by various factors such as foundation geometry, stiffness, soil properties, ground motion

characteristics, and interaction with the superstructure. Thus, the analysis of finned pile mat foundations under seismic excitations involves assessing their performance under different scenarios and identifying key factors that impact their response. Ensuring that the foundation provides safe and reliable support for the superstructure under seismic loads

To tackle these challenges, it is necessary to employ sophisticated analytical and computational tools like FE analysis and SSI modeling. These tools enable a comprehensive understanding of the behavior and response of finned pile mat foundations. Additionally, the foundation design should adhere to the guidelines and regulations outlined in local building codes and standards. These codes stipulate the minimum performance criteria that structures must meet when subjected to seismic loads. By incorporating these requirements, the foundation design can ensure compliance with safety and performance standards.

3.2 METHODOLOGY

Figure 3.1 illustrates the comprehensive methodology employed in this study, providing a detailed overview of the research process. Additionally, Table 3.1 outlines the specific action plan adopted for conducting the study, delineating the planned steps and procedures.

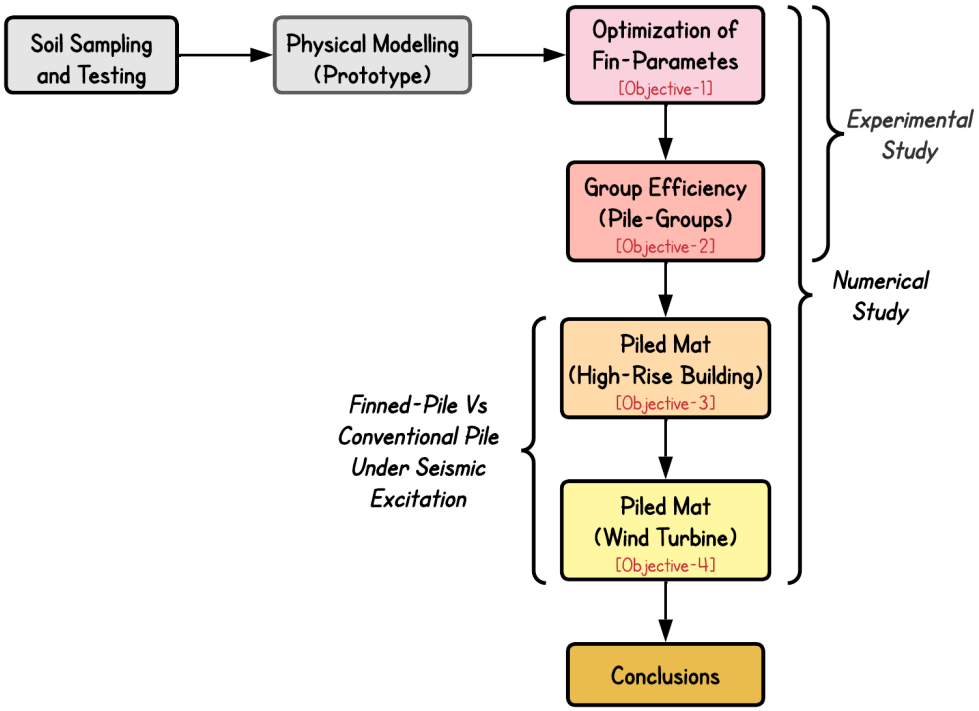

Figure 3.1 Schematic flow chart of the project methodology

Table 3.1 Detailed action plan adopted in the study

No.	Objective	Action Plan
1	To conduct parametric studies and determine the optimal fin parameters for laterally loaded finned piles installed in c-ϕ soil. (Experimental and Numerical)	• The impact of fin parameters like fin-position, fin-width, fin-length, fin-orientation, and fin-embedment on L_u of onshore finned-pile, are studied. • Finally, optimum fin parameters are finalised that resist maximum lateral load and are responsible for making the study economical.
2	To analyze and compare the group efficiency of laterally loaded finned pile groups with that of regular pile groups. (Experimental and Numerical)	• The group efficiency, (η_g), typically decreases as the number of regular piles increases. The influence of the finned pile group on η_g is examined. • The study focuses on examining the influence of spacing between pile (s) and the pile numbers (n) in a group on $(L_u)_g$.
3	To investigate the effect of finned pile mats under high-rise buildings under seismic excitation. (Numerical)	• The primary objective of this study is to mitigate the detrimental seismic effects on high-rise buildings and wind turbines supported by piled mats, with a specific focus on minimizing structural vibrations.
4	To examine the impact of a finned pile mat under a wind turbine subjected to seismic excitation. (Numerical)	• Time-history analyses were performed on FP-mat with varying fin lengths and compared with regular piled mat (RP-Mat). • The seismic behaviour was analyzed by examining parameters such as peak acceleration (A_{peak}), peak displacement (U_{peak}), and inter segmental or story drifts.

3.3 MATERIALS

For this investigation, soil samples were obtained from the Mangalore Special Economic Zone (MSEZ) site. Basic geotechnical soil tests were conducted as per SP 36 (Part1) (1987), and the resulting soil properties are presented in Table 3.2. The GSD curve of the soil is illustrated in Figure 3.2, and classified as low compressible silt-sandy silt (ML-SM) ASTM D-2487-17e1 (2017). The shear strength parameters and Young's soil modulus (E) were estimated by performing the consolidated undrained triaxial test. The hollow mild-steel pile (E = 210 GPa) of 2mm thick (t_p) with a diameter of 21mm (D_p) was used. The schematic diagram of the finned and regular piles is shown in Figure 3.3.

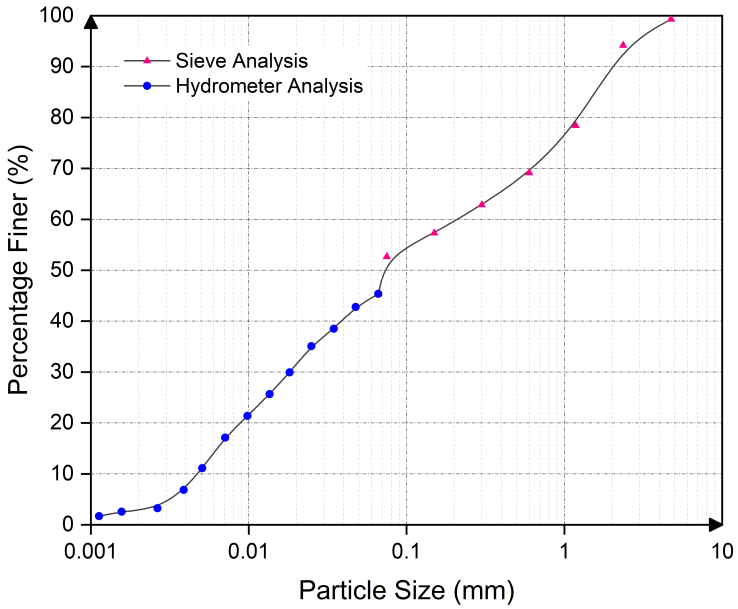

Figure 3.2 Particle size distribution (GSD) curve of the soil

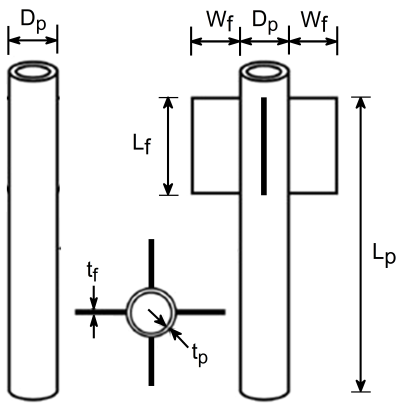

Figure 3.3 Schematic diagram illustrating the model piles utilized in the study

Table 3.2 Properties of the soil used in the study

Properties	Details
Specific Gravity (G)	2.59
Natural bulk unit-weight, γ (kN/m^3)	13.54
Natural moisture content, w (%)	17.3
Sand (%)	46.7
Silt (%)	50.6
Clay (%)	2.7
Coefficient of Uniformity, C_u	46
Coefficient of Curvature , C_c	0.35
Liquid Limit, w_L (%)	48.3
Plastic Limit, w_P (%)	34.0
Soil Classification (USCS Classification)	ML - SM
Maximum Dry Density (MDD), (kN/m^3)	15.42
Optimum Moisture Content, OMC (%)	20.0
Friction angle, ϕ ($^\circ$)	23.5
Cohesion, c (kPa)	32.0

3.4 PILE DIMENSIONING

Long-flexible piles were modelled according to Poulos et al. (1980), defining the relative stiffness factor (K_{rc}) that is dependent on both soil and pile parameters, as shown in (3.1).

$$K_{rc} = \frac{E_p\, I_p}{E_s\, L_p^4}. \tag{3.1}$$

Here, E_p represents the pile's modulus of elasticity (210 GPa), and I_p denotes the M.I. of the pile ($5.45 \times 10^{-9} m^4$). The parameter E_s represents the secant modulus of the soil (6.6 MPa), and L_p indicates the embedded length of the pile (665 mm). Consequently, the values of K_{rc} are calculated as 8.86×10^{-4} and 1.63×10^{-3} for regular and finned piles, respectively. As per the criteria established by Poulos et al. (1980), a pile is considered long and flexible when $K_{rc} < 10^{-2}$.

The experimental and numerical investigations included both regular and finned piles with a length of 665 mm. To simulate the behavior of actual piles, a small-scale pile was utilized in this study. The pile dimensions were increased by a scaling factor of 24, while maintaining the same soil and pile materials as the experimental model described by Nasr (2014). The outer and inner diameters of the steel pile (D_p) were 21 mm and 17 mm, respectively. Pile and fins of 2 mm (t_p) and 2.9 mm (t_f) thick steel

material (E=210 GPa) were adopted. Figure 3.4 illustrates the model piles employed in this study.

Figure 3.4 Small-scale model piles used in the study

3.5 EXPERIMENTAL SETUP

For research purposes, conducting manual testing on full-scale piles in the field requires a significant amount of testing time, materials, construction, and data acquisition setup. Therefore, in this study, small-scale model tests were utilized to address the research objectives. It is essential to minimize the influence of scaling effects to ensure comparable behavior between the prototype and full-scale investigations (Wood, 2004). The scaling effect can be influenced by factors such as soil particle size and boundary conditions of the test tank in small-scale studies. However, if $D_p/D_{50} \geq 30$, the scaling effect becomes negligible (Franke and Muth, 1985). In the present study, the ratio D_p/D_{50} is 308.8, indicating that the particle size effect is minimal. The walls of the testing tank must be smooth and wide enough so that sidewalls' friction and boundary conditions will not influence the small-scale analysis (Bransby and Smith, 1975). Hence, the testing tank dimensions were fixed as per the recommendations of (Karthigeyan et al., 2006) with a tank length of $57D_p$ and depth of $32D_p$ and the distance between the tank base, and pile-tip is $16D_p$.

The model experiments were conducted within a steel test tank with dimensions of 1.2m$\times$1.2m$\times$1.0m, as depicted in Figure 3.5. The soil was blended with natural water content before being deposited in the tank and compacted in layers to attain density. The soil density was compared at different parts of the tank and was found within 5% of each other. The pile was installed in the model box, as per specifications provided by Karthigeyan et al. (2006, 2007); Phillips and Valsangkar (1987), such that

sides of the model box do not influence the resistance developed by soil against applied lateral loading. After placing the steel pile of the desired length in the model box, a hydraulic jack was employed to apply the lateral load, and the magnitude of the applied lateral load was measured using a load cell. To measure the lateral-displacement (Δ), two LVDTs were connected to the pile-head, as depicted in Figure 3.6. All the equipment, including load cells and LVDTs, were connected to a data logger that recorded the testing data.

Figure 3.5 Experimental setup adopted in the small-scale model testing

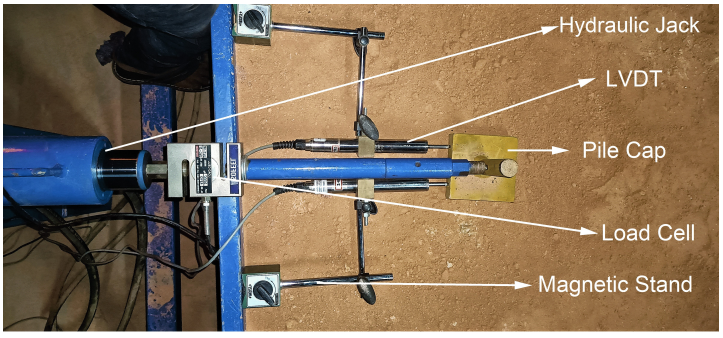

(a)

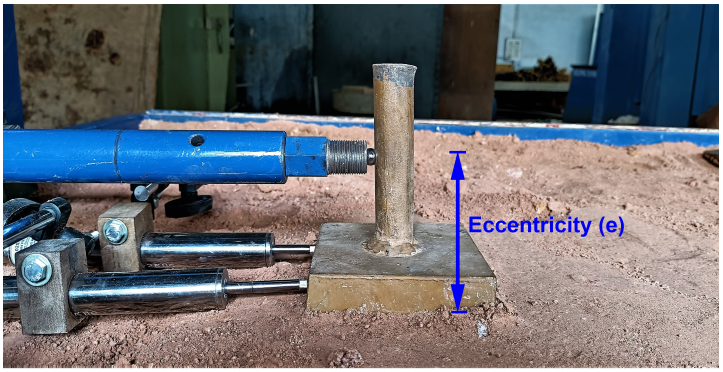

(b)

Figure 3.6 Model setup showing (a) All equipment; and (b) Eccentricity of loading

3.6 NUMERICAL ANALYSIS

Few research studies Nasr (2014); Yaghobi et al. (2019) are available in the literature on 3D FE analysis simulating laterally loaded piles. Previous studies efficiently considered soil continuity, non-linearity, soil-pile interface, and boundary conditions. This study used ABAQUS to simulate the model tests through analyses over laterally loaded small-scale individual finned piles.

The c-ϕ soil was represented using the Mohr-Coulomb model, while the pile by a steel material utilizing the linearly-elastic model. Soil and piles were modelled as 3D deformable parts in this study. ABAQUS offers a suitable platform for defining the tangential interface friction formulation, with penalty options available to account for the interaction between soil and pile. The friction coefficient between the soil and the steel hollow pile is typically between $0.5\times\tan(\phi)$ and $\tan(\phi)$ (Hsu et al., 2001). In this study, a friction coefficient value of $0.67\times\tan(\phi)$ is considered. Table 3.3 displays the material properties.

Table 3.3 Material properties adopted in numerical study

Characteristic Properties	**c-ϕ soil**	**Steel pile and fins**
Material model	Mohr-Coulomb model	Linear-Elastic model
Unit-weight, γ (kN/m^3)	13.54	78
Poisson's ratio, ν	0.33	0.30
Young's Modulus, E (MPa)	6.3	210 x 10^3
Cohesion, c (kPa)	32	–
Friction angle, ϕ (°)	23.5	–
Dilation angle, ψ (°)	1.0	–

To reduce computation time, the analysis was performed on only the symmetrical half of the 3D model, as it exhibited symmetry about the x-axis, which corresponds to the direction of the applied load. Each part was discretized with 8-node linear brick for defining the mesh, reduced integration (C3D8R) element and mesh refining was performed to get accurate results. The model employed a graded element size approach, with smaller-sized elements near the pile surface and larger-sized elements towards the edges of the soil cube. The interaction between the soil and pile was simulated using a surface-to-surface contact formulation, utilizing a penalty friction model for tangential contact and a hard-contact behavior for normal contact. Figure 3.7 illustrates the 3D geometry of the finned pile within the soil model.

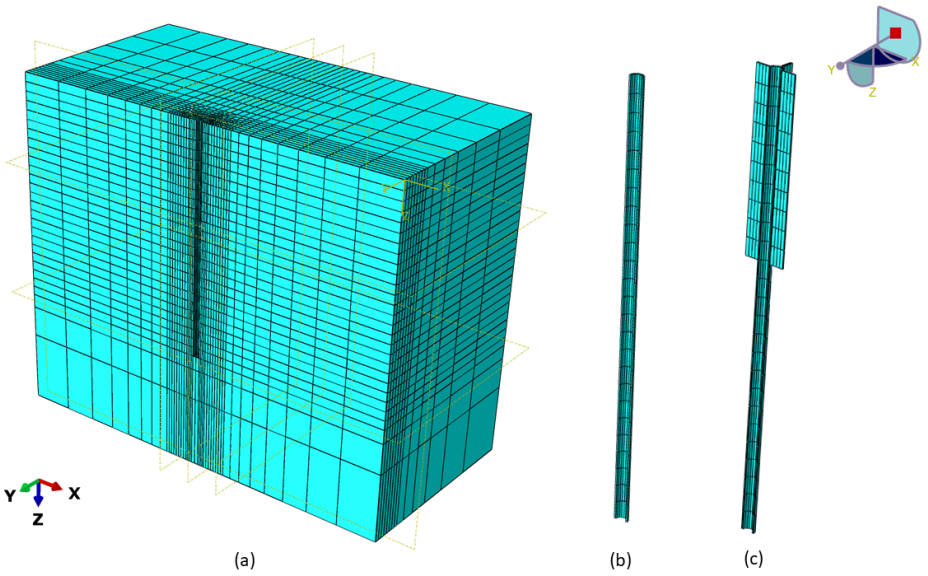

Figure 3.7 3D geometry of FEM Symmetrical model used for the study. (a) Soil model; (b) Regular pile; and (c) Finned pile

3.7 SUMMARY

This chapter presented the methodology adopted to achieve all the research objectives. Numerical analyses were performed on finned pile foundations for the first two objectives, validated with small-scale 1g model tests. For the latter two, using the ABAQUS software, numerical analysis was performed to study the seismic response of the high rise building and wind turbine supported by the FP-Mat system as reported in the subsequent chapters.

CHAPTER 4

OPTIMIZATION OF FIN PARAMETERS

4.1 INTRODUCTION

Deep foundations are employed to sustain the larger lateral loads due to wind, machine operation loads, earthquake loads, and the effect of eccentricity due to vertical loads. The regular pile foundations must be appraised to carry the applied lateral loads without excessive displacement. Generally, the lateral loads on the foundations act over the pile-head position. The pile cross-section lacks the required stiffness, resulting in undue pile displacement (Δ) (Peng, 2005).

L_u of a laterally loaded pile in a sandy medium increased with an increase in L_f for small-scale model pile and the full-scale pile after 3D non-linear analysis (Peng et al., 2010). With optimum fin dimensions, rectangular fins resist larger lateral loads than triangular fins in sands (Nasr, 2014). According to Yaghobi et al. (2019), when dealing with offshore scenarios and resisting higher lateral loads, using fins with a smaller cross-section pile is more economical than using larger piles. Beyond optimum fin-length, the increase in L_u for finned pile is marginal (Babu and Viswanadham, 2019). Hence, achieving economic optimization of fin-length is recommended.

In the south Canara region of India's west coast, sandy-silty soil is abundant. Most significant buildings there, including many skyscrapers and high-head chimneys of major organizations like the Thermal Power Plant of UPCL, Mangalore Refinery and Petrochemicals Limited (MRPL), Mangalore Chemicals and Fertilizers Limited (MCF), are built on pile foundations of larger length. Therefore, there is a need for innovative foundations that are both cost-effective to build and effective at withstanding higher lateral loads.

The objective of this study is to assess and quantify the behavior of finned pile foundations as an alternative to regular piles of the same dimensions, particularly under increased lateral load conditions. Additionally, this chapter aims to evaluate the impact of various fin parameters like fin-position, fin-length, fin-width, fin-orientation, fin-embedment and loading eccentricity (e) by performing both small-scale 1g model tests and numerical analyses. The findings of these investigations will contribute to optimizing the selection of fin parameters.

4.2 MESH SENSITIVITY ANALYSIS

Prior to conducting the parametric study, mesh sensitivity analysis was performed on the 3D FE model of the regular and finned pile systems. Hence, various mesh refinements were performed, such that the effect of mesh size on the results is reduced to the maximum extent for increased accuracy.

For mesh sensitivity analysis, coarse, medium, refined, and fine element distributions were considered for the study. Mesh-sensitivity effects were investigated for both the regular and finned pile systems, yielding 1296, 8333, 18784, and 26680 elements for the regular pile and 1304, 8409, 18986, and 27195 elements for the finned pile system. The results of refined meshing have shown a marginal variation with fine meshing in resisting lateral load. It indicates that the refined element distribution accurately predicts the lateral load within a reasonable computation time, as shown in Figure 4.1.

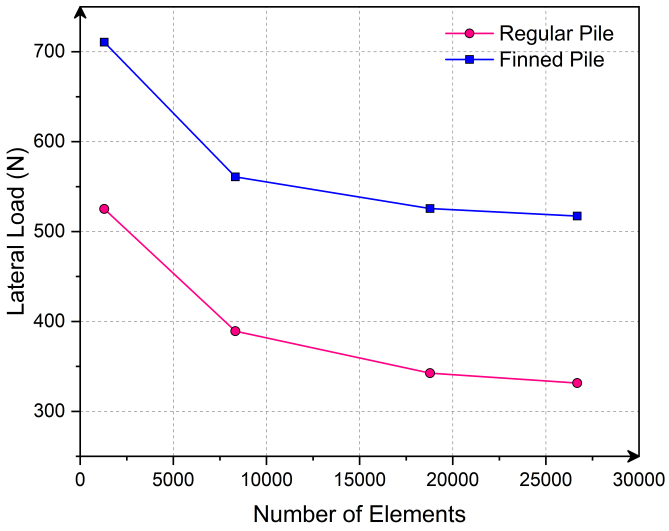

Figure 4.1 Mesh sensitivity analysis for regular pile and finned pile model

Since the refined meshing adopted is well validated with the previous experimental and numerical researches by Peng et al. (2010); Babu and Viswanadham (2018, 2019) as shown in Figure 4.2. The same meshing method is adopted for all parametric studies performed in this chapter.

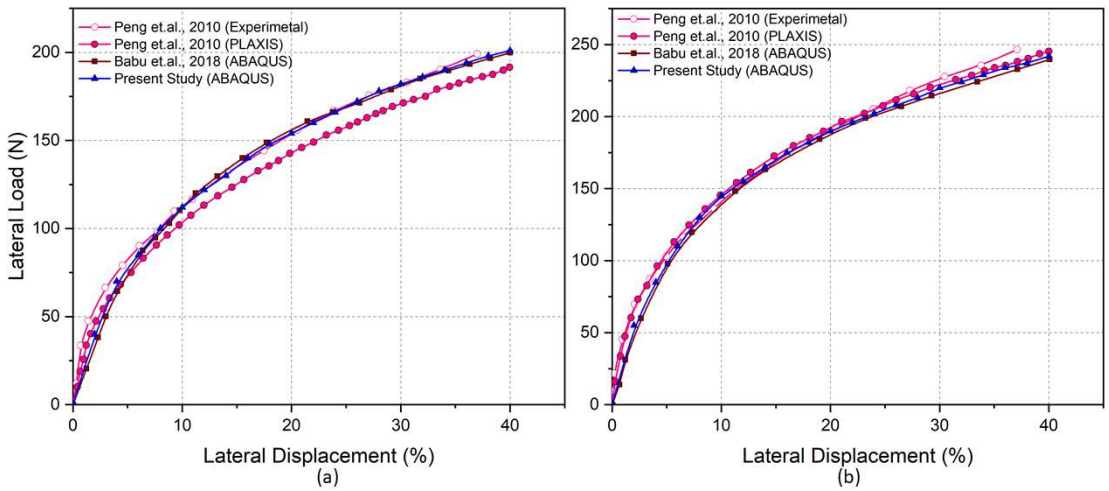

Figure 4.2 Validation of the present study with the previous researches on (a) Regular Pile; and (b) Finned-pile

4.3 RESULTS AND DISCUSSIONS

The findings from the experimental and numerical analyses are presented in terms of the curves depicting lateral load and displacement at the pile head. The lateral displacement at the pile (Δ) is represented by a dimensionless factor $\Delta/D_p(\%)$, representing the normalised lateral displacement. This study conducted experimental and numerical analyses until a normalised lateral displacement (Δ/D_p) of 40% was reached (Yaghobi et al., 2019). A graph plotted to depict the correlation between lateral load and normalized lateral displacement. The ultimate lateral load (L_u) was identified as the load at Δ/D_p of 10% (Babu and Viswanadham, 2019; Nasr, 2014; Peng et al., 2010; Uncuoğlu and Laman, 2011). As shown in (4.1), the effect of the fins in a finned pile is expressed in terms of fin-efficiency (η), a dimensionless factor. Since fin-efficiency remains the same for symmetrical and complete model analyses, symmetrical analysis results are considered.

$$Fin\text{-}Efficiency = \eta = \frac{L_{u(Finned-pile)}}{L_{u(Regular-pile)}} \tag{4.1}$$

4.4 PARAMETRIC STUDIES ON FINNED PILES

Generally, piles are adopted in groups. To study the finned pile groups, one has to study the parametric effects of the individual finned pile. Its utilization is most economical by considering the most suitable fin parameters. Therefore, several parametric studies were conducted to examine the influence of each individual finned pile in withstanding the lateral load, as outlined in Table 4.1. The pile of length 665 mm embedded in c-ϕ soil behaves as a long pile that can be used for the mechanical stabilization of weak strata. The parametric studies included long regular piles and finned piles with four fins positioned at 90° intervals around the pile. In Series I tests, the focus was on comparing the L_u of regular and finned piles and examining the influence of eccentricity (as shown in Table 4.1). Additionally, Series II tests investigated the effect of fin position, Series III tests examined the impact of fin length (L_f), Series IV tests explored the impact of fin width, Series V tests analyzed the influence of fin orientation, and Series VI tests investigated the impact of fin embedment.

Table 4.1 Experimental and FE analytical program for individual finned pile study

Series	Constant Parameters	Variable Parameters
I	Regular and Finned piles L_p = 665 mm,	e/D_p of 0 and 3.2
II	Finned pile, L_f/D_p = 12, and $W_f = D_p$	fin-positions, e/D_p
III	$W_f = D_p$; Rectangular-fin at Top-position	fin-length (L_f/D_p), e/D_p
IV	L_f/D_p = 12; Rectangular-fin at Top-position	fin-width (W_f/D_p), e/D_p
V	L_f/D_p = 12 W_f/D_p = 1.0; Fin at Top-position	fin orientation, e/D_p
VI	L_f/D_p = 12, $W_f = D_p$; Fin at Top-position	fin-embedment, e/D_p
All finned piles have four fin-forming plates Except fin-orientation of 45°, all studies have lateral load applied along fin.		

4.4.1 Effect of Fins and Loading Eccentricity

To study the effect of fins, tests and analyses were performed on regular and finned piles under lateral load and loading eccentricity (e/D_p). The analysis was performed over finned piles with the top-fin position for the soil of the desired unit-weight as shown in Series I of Table 4.1 and Figure 4.3.

The relationship between lateral load and lateral deformation for both regular and finned piles in the complete model is represented by the lateral load vs. lateral deformation curve, as depicted in Figure 4.4(a). The addition of fins to the pile leads

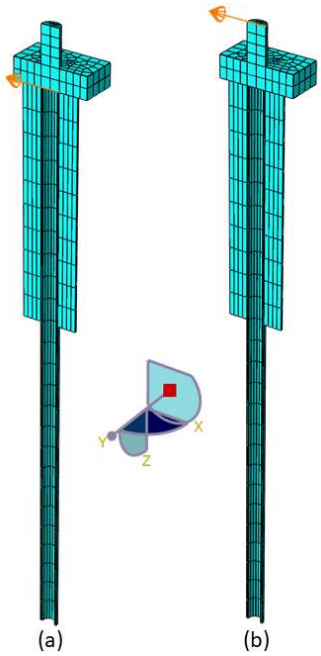

Figure 4.3 3D Symmetrical finned pile model for (a) e=0; and (b) e=3.2D_p

to an increase in L_u, however, the resistance decreases when subjected to an eccentric lateral load, which is a combination of the lateral load and the moment generated by the applied eccentric load. This observation is depicted in Figure 4.4(b). Greater pile length activates the larger depth of influence, developing greater passive resistance in the soil-pile system; hence long piles work better in weaker soil.

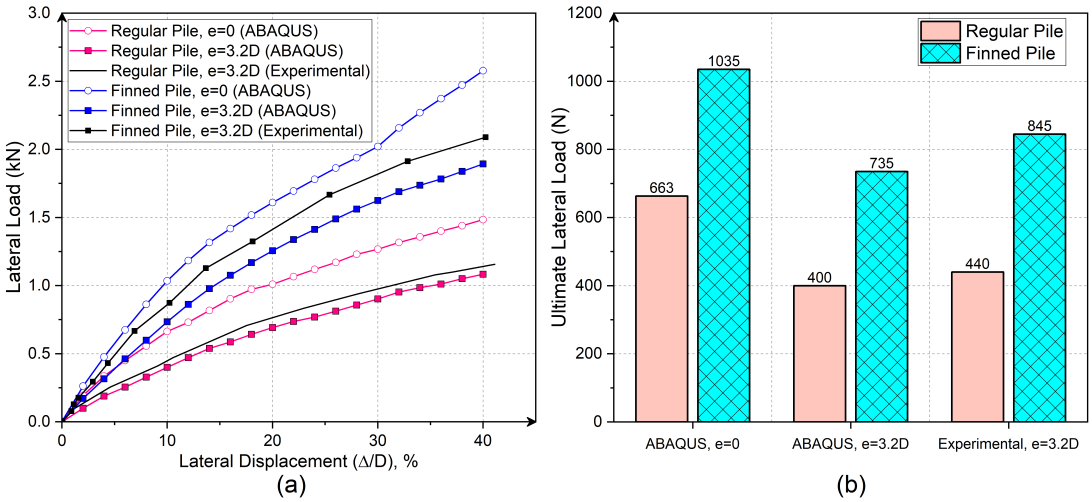

Figure 4.4 Variation of resistance for (a) varying analysis types; and (b) varying pile types

Finned piles exhibit greater lateral resistance compared to regular piles due to the presence of fins at the pile head. The addition of fins enhances the flexural stiffness

of the pile and expands the soil's zone of influence. As a result, a larger passive resistance is activated within the critical zone where the lateral load is applied to the pile. The results for the eccentric lateral load (e=3.2D$_p$) from ABAQUS match the experimental results for the regular pile and finned pile by 91% and 87%, respectively. The finned piles work better than regular piles even under eccentric lateral loads, as validated by experimental and numerical studies, as shown in Figure 4.4(b). The study reveals that the L_u of a finned pile decreases as the eccentricity (e/D_p) increases from 0 to 3.2. When an eccentric load is applied, the L_u decreases by 30% for finned piles and 40% for regular piles. This leads to the conclusion that finned piles demonstrate greater efficiency than regular piles against applied eccentric loads.

4.4.2 Effect of Fin-position

Experimental and numerical analyses were conducted on piles with fins positioned at different locations namely the top (relative to the bottom of the pile cap), mid-length, and bottom (pile tip) positions, as outlined in Series II of Table 4.1. The internal stresses developed in finned piles with different fin positions are shown in Figure 4.5. The pile with the fin in the mid-length position experiences more stress than the pile at the top, indicating that it withstands a lesser load.

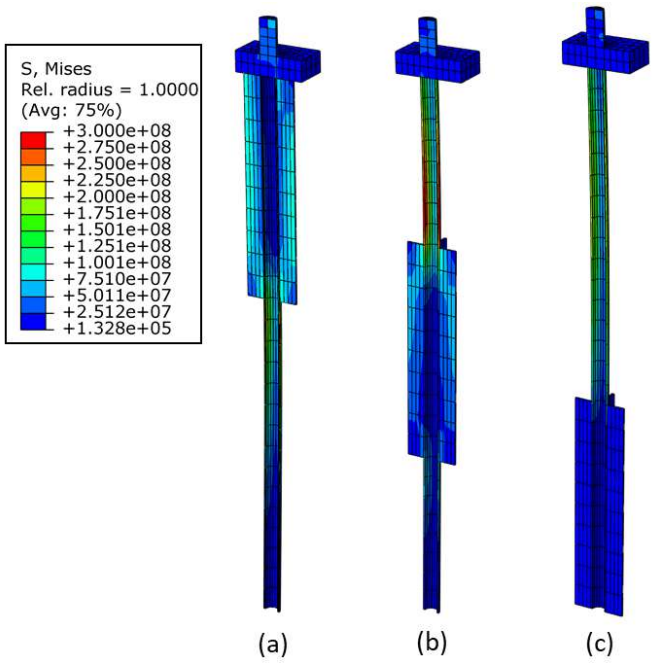

Figure 4.5 Internal stresses developed in finned piles for varying fin-positions in ABAQUS: (a) Top-fin position; (b) Mid-length position; and (c) Bottom position

L_u developed was greater for the top-fin position than the other two, as shown in Figure 4.6(a). Since fins were attached at the critical position on the pile where the lateral load is applied, the top-fin position results in higher L_u due to the enhancement of flexural rigidity by fin-forming plates, than the other two positions as shown in Figure 4.6(b).

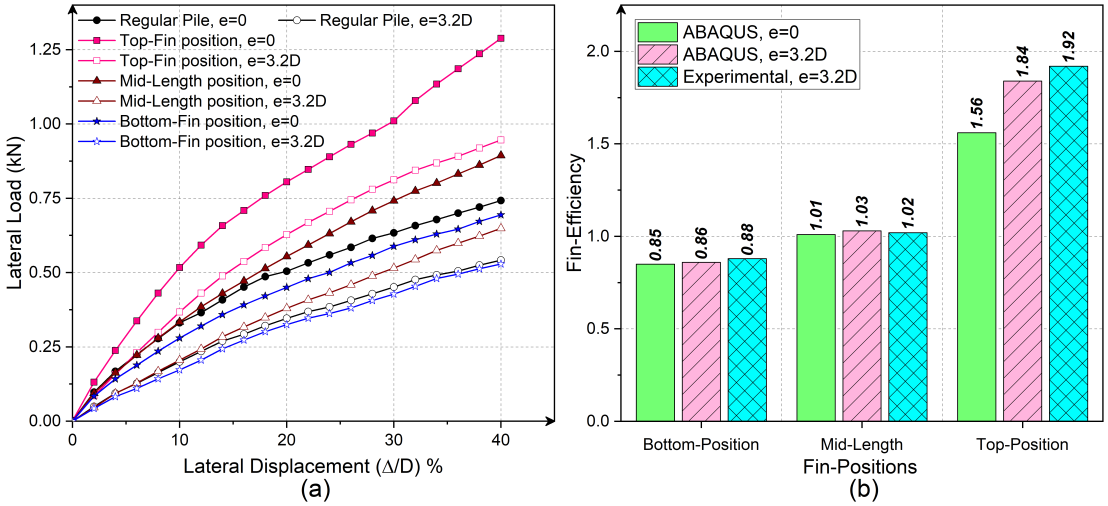

Figure 4.6 Variation of (a) Lateral Resistance; and (b) Fin-efficiency for varying fin-positions

Fins contribute higher flexural stiffness (E_pI_p) at the finned pile's fin portion than the pile's stem portion of the pile; hence, Finned piles provide more bending resistance than the regular pile. The variation of BM for FP: pile-shaft, fins in FP, complete finned pile (FP: pile-shaft + fins) and regular pile are plotted as shown in Figure 4.7. The provision of fins on piles reduces the bending resistance on the pile shaft alone by reducing the lateral displacement. To investigate the reduction in BM along the pile shaft caused by the presence of fins in the finned pile, the variation of BM along the pile length is plotted for all the parametric studies conducted. Also, the provision of fins over the pile alters the behaviour of the finned pile shaft at the fin location.

The variation of BM along the pile length for different fin positions is illustrated in Figure 4.8, based on numerical studies. The inclusion of fins in the pile results in a decrease in the BM on the pile shaft at the fin location, thereby enhancing the pile's capacity to resist larger lateral loads. The BM on the pile-shaft for the top-fin position is lesser than that of a regular pile for non-eccentric and eccentric loading, whereas for the other two fin positions bending resistance at fin-positions was lower than that of the finned pile with the top-fin position. Considering the installation of a pile in the field, the pile with fins at the top will be more convenient than the other two fin positions.

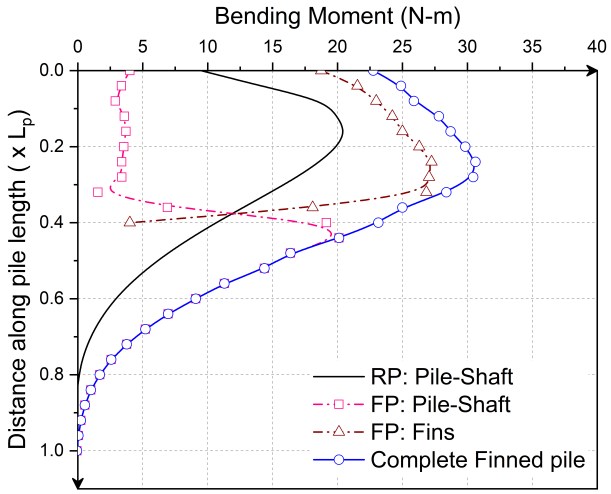

Figure 4.7 Variation of BM along pile length for pile-shaft and fins in the finned pile for eccentric lateral load (e=3.2D_p)

Considering all these advantages, the top-fin position is considered the optimum fin position for the foundation application. The pile above the point of fixity is active in resisting the lateral load. Hence, mid-length and bottom fin positions might help to enhance the stability of the slope if used as an anti-slide pile, as the potential failure surface will be at a deeper depth beneath the slope, requiring a greater resisting component against the driving one (Kourkoulis et al., 2011; Sawant and Shukla, 2012; Qin et al., 2016; Qin and Chian, 2017).

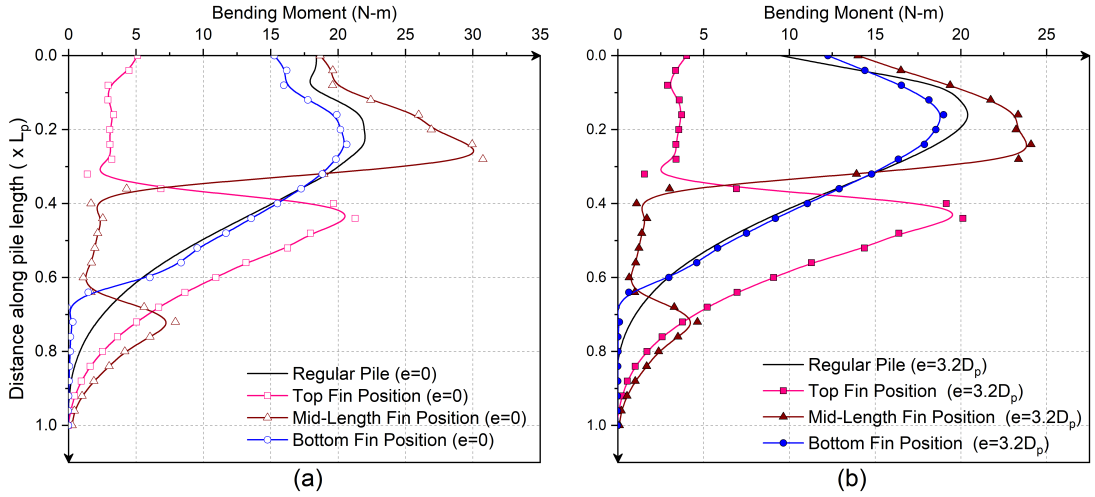

Figure 4.8 Variation of BM along the pile length for varying fin-positions under lateral load at (a) e=0, and (b) e=3.2D_p

4.4.3 Effect of Fin-Length

To investigate the effect of fin length on the L_u of finned piles, tests were conducted on finned piles with different fin lengths (L_f). The fin length was expressed as a dimensionless factor relative to the pile diameter, referred to as the fin-length ratio (L_f/D_p) (Sallam et al., 2023). The influence of fin length was quantified using L_f/D_p throughout the study. Analyses were carried out for L_f/D_p ratios of 6, 12, and 18, as presented in Series III of Table 4.1. The internal stresses developed within the pile are depicted in Figure 4.9.

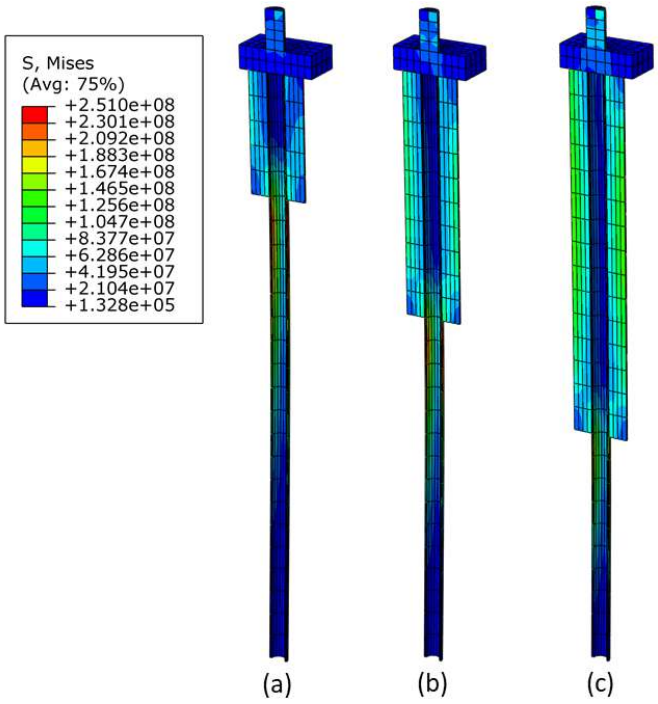

Figure 4.9 Internal stresses developed in the pile for varying fin-lengths in ABAQUS: (a) $L_f = 6D_p$; (b) $L_f = 12D_p$; and (c) $L_f = 18D_p$

For the finned pile with lesser fin length (i.e., $L_f = 6D_p$), the stresses developed in fins are lesser, and for larger fin length (i.e., $L_f = 18D_p$) stresses are larger, leading to deflection of fins. Hence, the usage of optimum fin length is suggested. The relationship between lateral resistance and fin-length ratios is illustrated in Figure 4.10(a). It is evident that the lateral resistance increases as the fin length ratio increases. A longer fin length enhances the flexural rigidity of the pile, particularly for longer pile lengths, resulting in improved fin efficiency, as demonstrated in Figure 4.10(b).

L_u of the finned pile exhibits a significant increase with a longer fin length, as depicted in Figure 4.11. This is attributed to the increased BM on the pile shaft in the fin zone. The presence of fins enhances the bending resistance of the finned piles, as the

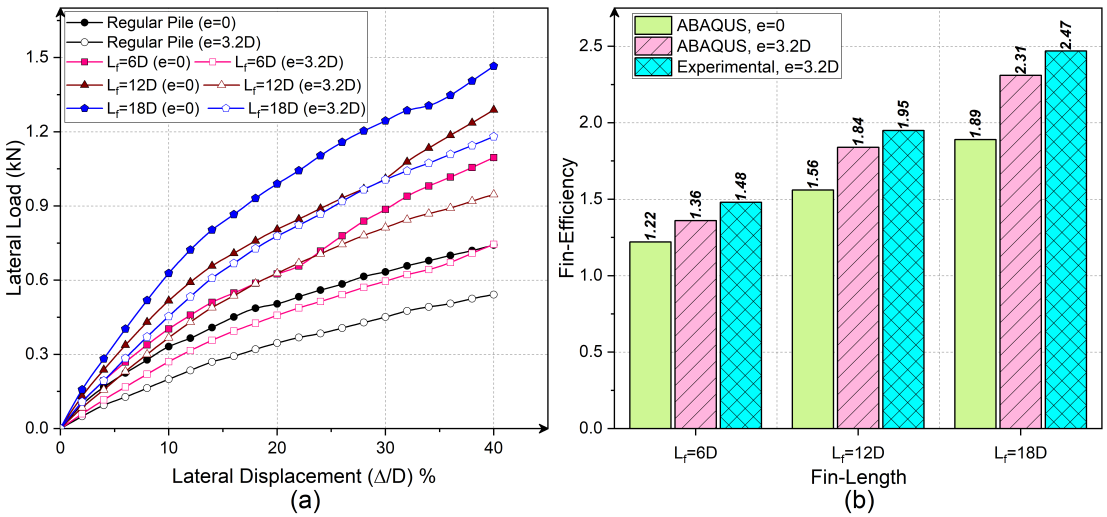

Figure 4.10 Variation of resistance of FP for (a) Varying fin-lengths and its (b) fin-efficiency

BM contribution from the fins complements that of the pile shaft. It was observed that larger fin lengths offer advantages in terms of bending resistance, but their installation in the field requires larger machinery. Therefore, to strike a balance between performance and construction economy, the optimum fin length was determined. The finned pile with a L_f/D_p of 12 exhibited significant BM, thus serving as the optimal choice.

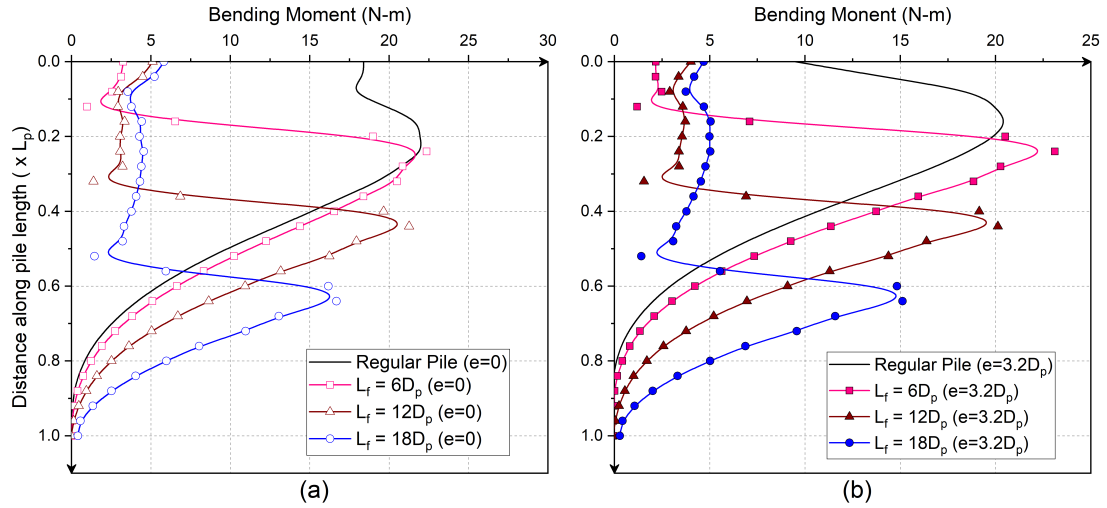

Figure 4.11 Variation of BM along the pile length for varying fin-lengths at (a) e=0, and (b) e=3.2D_p

4.4.4 Effect of Fin-Width

Experimental tests were conducted on the finned pile with different fin widths (W_f) to examine the impact of fin width on L_u of the finned pile. The fin-width dimensionless factor concerning pile diameter (W_f/D_p) is called the fin-width ratio. The W_f/D_p ratios of 0.5, 1.0, and 1.5 were studied, with fin-shaped rectangular fins at the pile-head position as described in Series IV of Table 4.1. The internal stresses developed in the finned piles for varying fin-widths are as shown in Figure 4.12. When the fin width of a finned pile is smaller ($W_f/D_p = 0.5$), the fins undergo higher stress due to the concentrated load, whereas for a pile with a larger fin width ($W_f/D_p = 1.5$), the pile shaft experiences higher bending stress due to the increased fin area. Therefore, it is essential to determine the optimal fin width to mitigate these undesirable effects.

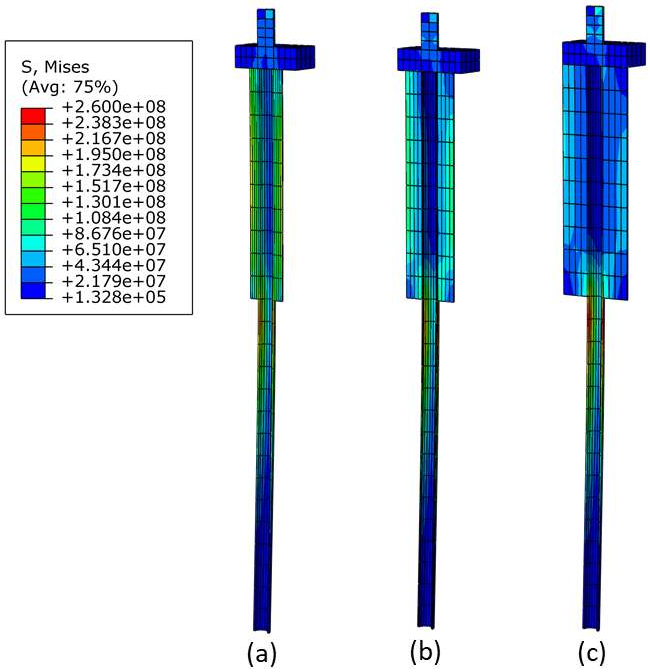

Figure 4.12 Lateral resistance developed for varying fin-widths in ABAQUS: (a) $W_f = 0.5D_p$; (b) $W_f = 1.0D_p$; and (c) $W_f = 1.5D_p$

Figure 4.13(a) shows that increasing the fin width increases the L_u of the pile. A larger zone of influence is activated around the pile, resulting in significant soil resistance. This increase in resistance is significant up to a W_f equals to D_p. However, the resistance was not significant for a fin width of 1.5, leading to a smaller increase in fin efficiency, as shown in Figure 4.13(b). Hence, the optimum fin-width (W_f/D_p) was considered 1.0 from the above considerations.

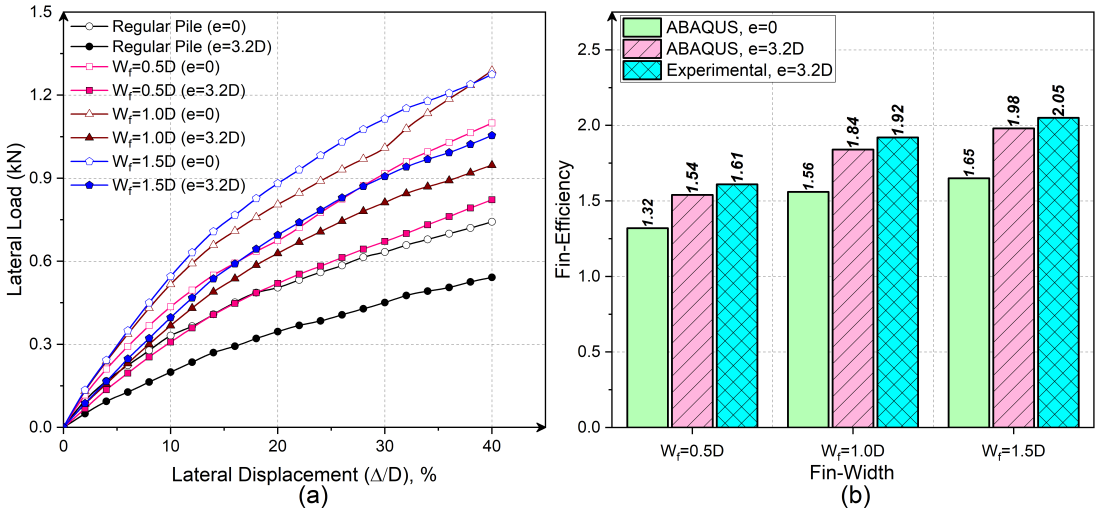

Figure 4.13 Variation of fin-efficiency for varying fin-widths: (a) Lateral load - displacement curves; and (b) Fin- efficiency

Even though the finned pile's L_u increases with an increase in W_f/D_p, the change in peak BM on the pile-shaft was marginal. The internal BM experienced by pile-shaft for various fin-widths is shown in Figure 4.14. The reduction in bending resistance at the fin-zone of the pile was considerable till W_f/D_p of 1.0 but diminished for fin-width of 1.5. Hence, unlike fin length, fin width is limited in increasing the pile's lateral resistance beyond optimum. Hence, considering material usage and economy, the optimum fin-width (W_f/D_p) is considered 1.0.

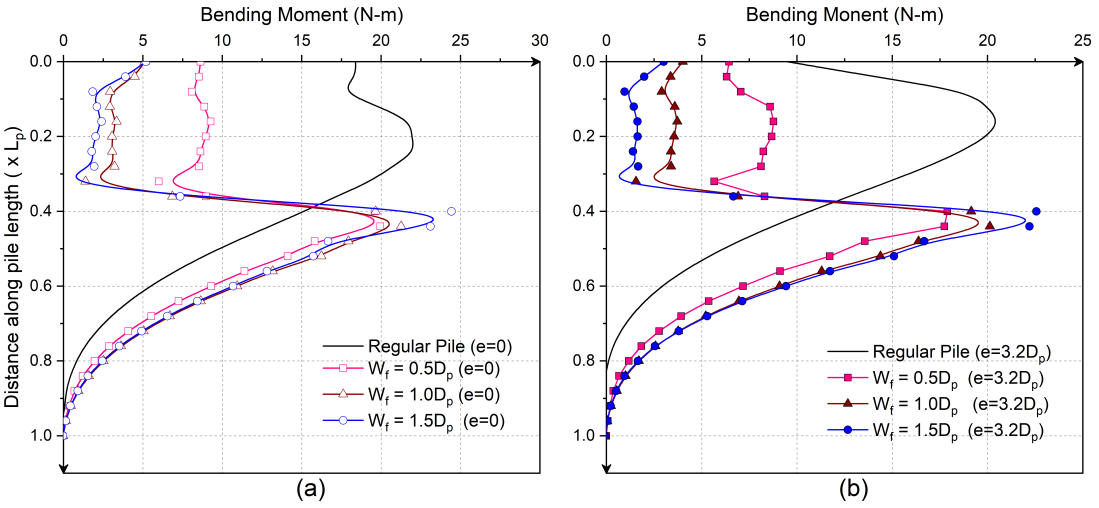

Figure 4.14 Variation of BM along the pile length for varying fin-widths at (a) e=0, and (b) e=3.2D_p

4.4.5 Effect of Fin-Orientation

As wind can cause lateral loads to be applied to the pile in any direction, we conducted a study to examine the effectiveness of fin orientations in resisting loads from different lateral directions. Experimental and numerical analyses were performed on different fin orientations (θ, i.e., the angle between fins and load), namely fins in line with & 90° with load (0° & 90°) and fins at 45° with the load, as shown in Figure 4.15. As listed in Series V of Table 4.1, optimum fin dimensions were adopted for analyses.

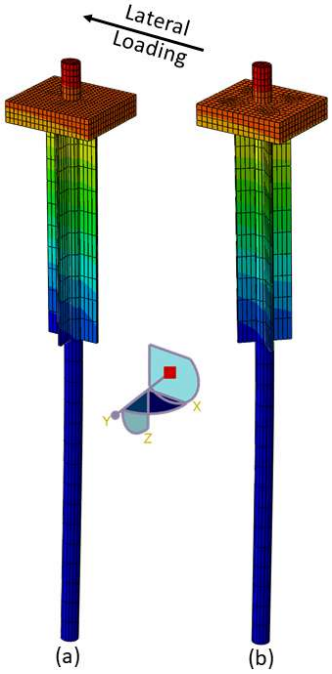

Figure 4.15 Complete finned pile 3D model used for fin-orientation analysis (a) Fins in line with and 90° with load (θ=0° & 90°); and (b) Fins at 45° to load (θ=45°)

It was found that piles with fins oriented at 45° to the load resisted nearly equal lateral loads as those with fins in line with the load. Therefore, fin orientation does not affect the L_u of finned piles under non-eccentric loading (e=0). However, it does have an impact under eccentric loading (e=3.2D_p); the finned pile with fins at 45° increases marginally with load, as shown in Figure 4.16(a), leading to a marginal increase in fin-efficiency, as illustrated in Figure 4.16(b). The L_u of the pile showed only a slight increase for a fin orientation (θ) of 45°, and correspondingly, the BM experienced by the pile shafts was also marginal, as depicted in Figure 4.17.

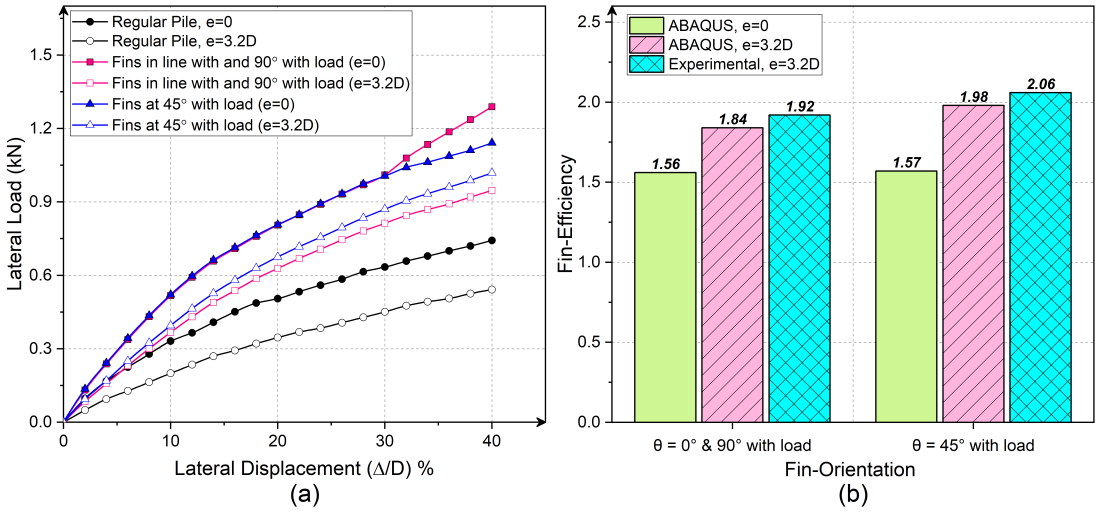

Figure 4.16 Variation of fin-orientation: (a) Lateral load - displacement curve; and (b) Fin-efficiency

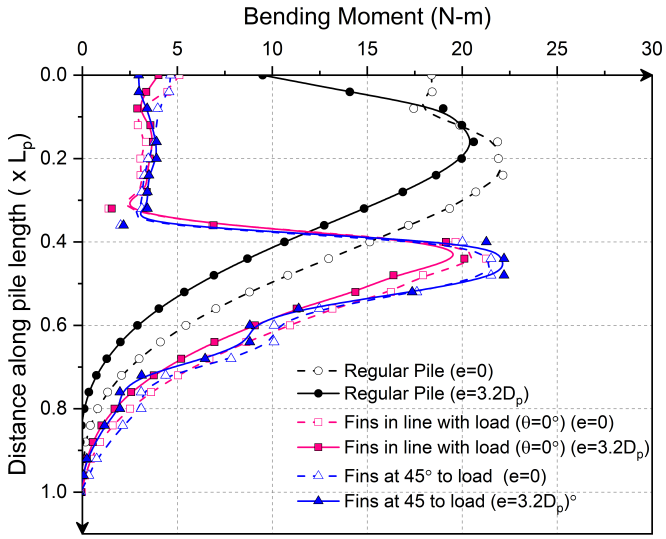

Figure 4.17 Variation of BM along pile length for varying fin-orientations

4.4.6 Effect of Fin Embedment in Pile-Cap

In foundation engineering practices, it is common to utilize piles in groups where they are integrated with a pile cap to form a monolithic structure. Thus, connectivity between the pile and pile cap at the pile head plays a significant role in the lateral resistance of finned pile. In the numerical analysis conducted in this study, the finned piles with fins embedded in the pile cap were modeled as monolithic structures. To investigate the effect of fin embedment on individual piles, fins were welded with pile-cap, and two conditions were examined: finned piles without fin embedment in the pile cap (FP-WFE) as described in the previous section, and finned piles with fins embedded in the pile cap (FP-FEPC). The internal stress experienced by the finned piles is illustrated in Figure 4.18 and is also presented in Series VI of Table 4.1.

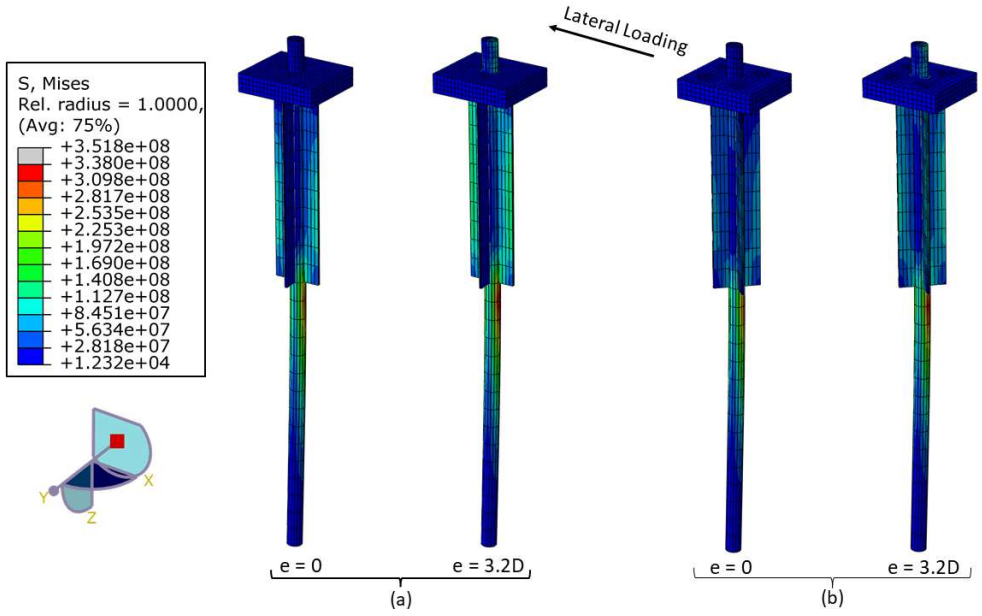

Figure 4.18 Finned pile models utilized in 3D analyses: (a) Fins embedded in the pile-cap, θ=0° & 90°; and (b) Fins embedded in the pile-cap, θ=45°

Compared to the finned pile without fin embedment in the pile cap (FP-WFE), more lateral resistance was found for the pile with fins embedded in the pile cap (FP-FEPC). Fin-embedment leads to increased fin-efficiency as shown in Figure 4.19(a). The increase in L_U can be attributed to the incorporation of fins in the pile cap, which enhances the pile's ability to withstand critical eccentric loads in a manner similar to non-eccentric loads, as depicted in Figure 4.19(b). This behaviour of the finned pile encourages the utilization of finned pile in groups.

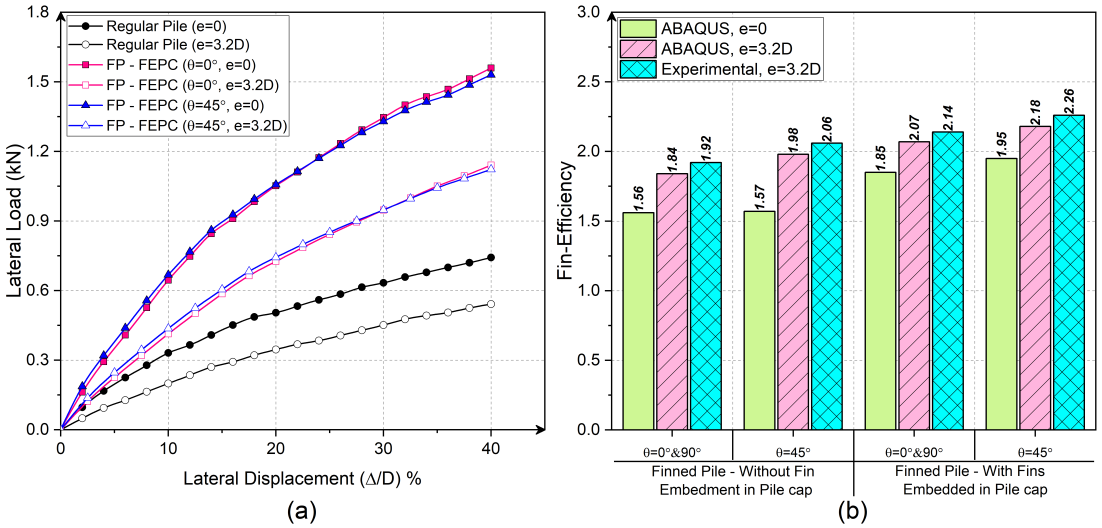

Figure 4.19 Variation of lateral resistance for varying fin-fixity: (a) Lateral load - displacement curves; and (b) Fin-efficiency

Figure 4.20 illustrates the internal BM encountered by the pile under the lateral load for both conditions. It is observed that the BM in the fin portion of the pile was marginally the same. The BM for both loading cases (e=0 and e=3.2D) is almost identical. However, from Figure 4.18, the FP-FEPC with θ=45° experiences larger internal stress when the load is applied at eccentricity (e=3.2D), and hence, greater BM is generated. Although the peak BM of the finned pile with fins embedded in the pile cap (FP-FEPC) was approximately 30% lower than that of the finned pile without fin embedment in the pile cap, it remained well within the permissible BM limit of 0.66 times the yield strength (f_y), i.e. indicates that the pile was safe from critical failure.

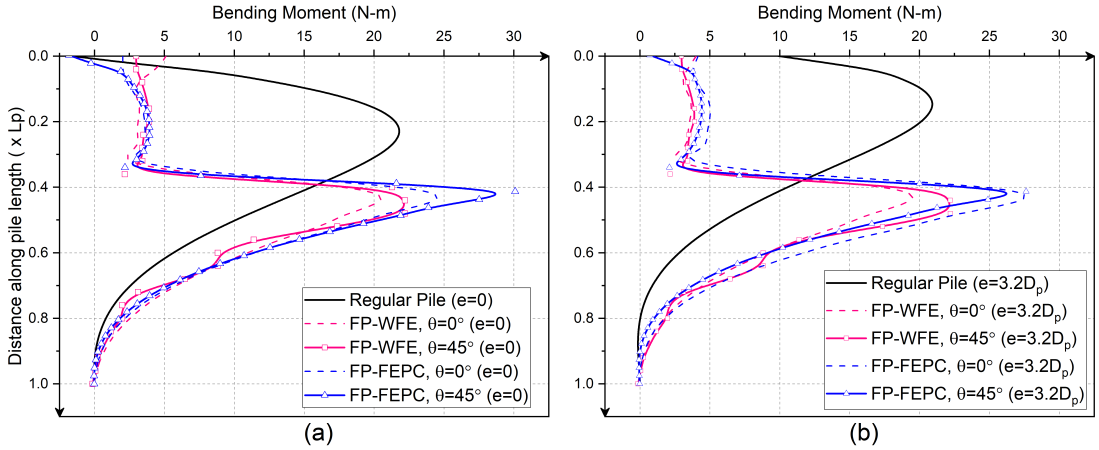

Figure 4.20 Variation of BM along the pile length for FP-WFE and FP-FEPC with varying fin orientations subjected to: (a) Non-eccentric load; e=0, and (b) Eccentric load; e=3.2D_p

As a result, fin-embedment in the pile cap influences the L_u, i.e., FP-FEPC resists 17.3% and 23.64% more load than the other case, for fin-orientation (θ) of 0° and 45° respectively. Material usage is the same for both orientations. Hence, the optimum fin-embedment case is FP-FEPC with 45° to load. The enhanced passive resistance of the finned pile is attributed to the enlarged cylindrical zone created by the presence of fins surrounding the pile. with the diameter of the cylinder being $3D_p$ (i.e., $D_p + 2W_f$). Hence, considering pile group interaction effects, minimum spacing (S_{min}) between piles in a finned pile group must be at least $5D_p$ (for, finned pile with fin width $W_f = D_p$), such that overlapping of stresses is avoided when applied with the lateral load.

The 3D analyses performed over the finned pile for varying fin parameters are listed in Table 4.1, such that the system resists enormous lateral load with lesser lateral displacement. From the above-discussed fin-parameter studies, the optimum fin-parameters arrived at are listed in Table 4.2. The finned pile provides higher L_u for the above-studied soil properties with following optimum parameters.

Table 4.2 Optimum fin parameters for the finned pile

Optimum fin parameters	**Description**
Fin-position	Top-position or pile-head position
Fin-length	L_f/D_p = 12
Fin-width	$W_f = D_p$
Fin-orientation	θ=0° & 90°
Fin-embedment	Fins embedded in pile-cap (θ=45°)

This study emphasized the noteworthy behavior of the finned pile in $c-\phi$ soil, and its uniqueness lies in the utilization of the soil abundantly present in practical field conditions. Previous research on finned piles with $L_f = 0.4L_p$, installed in sandy soils, improved the lateral resistance by 86% (Nasr, 2014) and by 73% (Albusoda and Alsaddi, 2017), whereas, for the case of clayey soil, improvement was 54% (Sakr et al., 2020). In this study, the improvement was observed to be 126%, indicating the enhanced efficiency of finned piles in $c-\phi$ soil compared to sandy or clayey soil. Notably, the optimum fin length remained consistent ($L_f = 0.4L_p$ or $12D_p$) regardless of the soil type.

4.5 MATERIAL COST BENEFIT ANALYSIS

A finned pile is advantageous in resisting larger lateral loads and addresses the economic concern of the construction. The construction economy can be studied in two ways: the dominance of lateral load against material usage or vice-versa. The economic assessment of the finned pile was performed using the optimal fin parameters outlined in Table 4.2. In checking the case of L_u dominance, analyses were performed for the regular pile of length (L_p) 665mm to assess the equivalent pile-diameter $(D_p)_{eq}$ providing the similar lateral resistance as the finned pile with optimum fin-parameters. The $(D_p)_{eq}$ for the regular pile was found to be 40mm (1.9 times D_p) as listed in Table 4.3, i.e., the regular pile needs 21.21% more material than the finned pile, increasing the cost of construction. Hence, the finned pile is an alternative to the large-dimension regular pile, even for an onshore application.

Table 4.3 Summary of results from equivalent pile diameter study

Description	**Pile diameter (D_p), mm**	**Lateral load (L_u), N**	
		e = 0	**e = 3.2D_p**
FP[a]-21mm	21	644.90	436.90
RP[b]-21mm	21	331.46	199.90
RP-25mm	25	401.62	244.34
RP-30mm	30	511.35	323.99
RP-35mm	35	560.10	374.16
RP-40mm	40	623.80	430.28

[a] FP - Finned Pile, (Reference load)

[b] RP - Regular Pile.

The variation of BM developed by regular piles of varying pile diameter (D_p) (as shown in Table 4.3) as compensation for resisting the L_u as that of the finned pile with D_p of 21mm is shown in Figure 4.21. For both the loading types, eccentric and non-eccentric loads, the peak BM of the compensatory regular pile with D_p of 40mm (RP-40mm) is almost 213%, and 232% higher for e=0 and e=3.2D_p respectively, than that of reference finned pile (FP-21mm).

Analyses were performed over 21mm diameter finned piles with varying pile lengths (L_p) and their corresponding optimum fin-length (L_f = 0.4L_p) to study the economic dominance. Equivalent pile length $(L_p)_{eq}$ is the finned pile length at which the lateral resistance is the same as the 665mm regular pile, and listed in Table 4.4. The $(L_p)_{eq}$ of the finned pile is about 30% of the regular pile length (0.3L_p), i.e., about

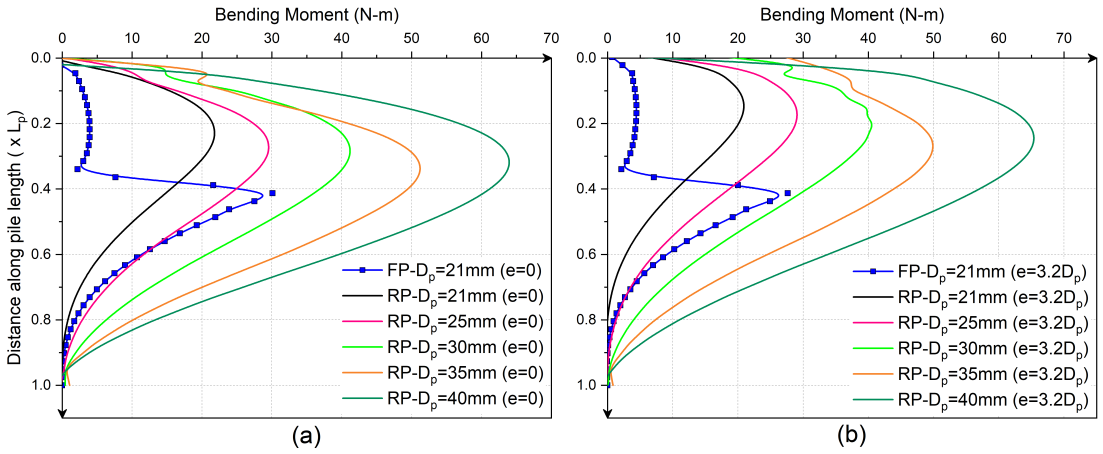

Figure 4.21 Variation of BM for regular piles of varying pile diameters under: (a) Non-eccentric loading; e=0, and (b) Eccentric loading; e=3.2D_p

199.5mm, leading to effective material usage. The finned pile with equivalent pile length needs only 54.5% of the material used by the regular pile supplemented by pile installation cost, reducing the overall cost and achieving the economy.

Table 4.4 Summary of results from equivalent pile-length study

Description	**Pile Length (L_p), mm**	**Lateral load (L_u), N**	
		e = 0	**e = 3.2D_p**
RP[a]-665mm	665	331.46	199.90
FP[b]-665mm	665	664.90	436.90
FP-598mm	598	641.60	415.44
FP-532mm	532	616.96	393.11
FP-466mm	466	591.83	370.03
FP-399mm	399	556.43	341.52
FP-333mm	333	510.28	304.24
FP-266mm	266	445.69	251.48
FP-199mm	199	370.19	187.30

[a] RP - Regular Pile, (Reference load)

[b] FP - Finned Pile

The variation of BM developed by finned piles of varying pile length (L_p) (as shown in Table 4.4) as compensation for resisting L_u as that of the regular pile with L_p of 665mm is shown in Figure 4.22. For both the loading types eccentric and non-eccentric loads, the peak BM of the compensatory finned pile with L_p of 199mm (FP-199mm) is just 43.2% for e=0 load and, and L_p of 266mm (FP-266mm) 76.2% for e=3.2D_p loading respectively, than that of reference regular pile (RP-665mm).

From Figure 4.21 and Figure 4.22, it is concluded that the finned pile is not only advantageous in resisting the larger lateral load but also in reducing the peak BM that a pile can experience under a considered load. Hence, it is more economical in construction than regular pile foundations.

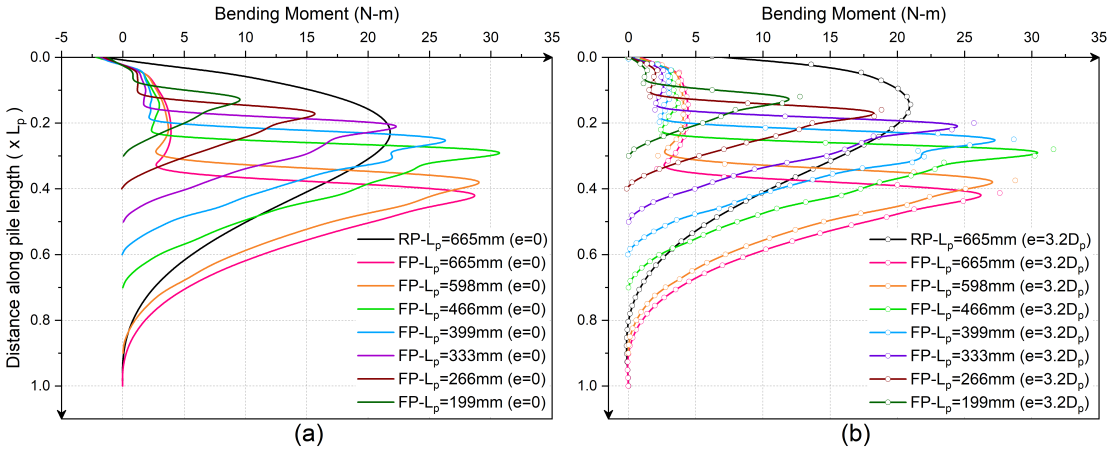

Figure 4.22 Variation of BM for finned piles of varying pile lengths subjected to: (a) Non-eccentric load; e=0, and (b) Eccentric load; e=3.2D_p

4.6 SCALING EFFECT ON ANALYSES

This part highlights the numerical analyses of full-scale piles by performing the analyses over full-scale finned piles for all the fin parameters studied above. A series of numerical analyses were performed for optimum fin-parameters listed in 4.2, Fin-Length (L_f), fin-orientation (θ), fin-embedment in the pile cap, and loading eccentricity. The fin-efficiency (η) results of full-scale analyses are compared with small-scale experimental and numerical studies (Table 4.5) to illustrate the benefit of finned piles as foundations at full scale.

The dimensions of the pile, fin, mesh seeding, distribution, and mesh boundaries were increased approximately by 24 times (D_p=0.504m, L_p=15.96m, W_f=0.504m, t_f=0.048m, soil-meshing depth = 24m) to generate the same number of elements as in the small-scale study to simulate large-scale behaviour. For numerical analysis of full-scale models in ABAQUS, the results for non-eccentric lateral loading vary

between 0.6% to 4.25% from small-scale numerical studies. For eccentric loading (e=3.2D_p), results vary between 0.5% to 3.5% of the small-scale studies.

Table 4.5 Summary of fin-efficiencies for various scaling parameters

Loading Type	**Fin-Parameter**	**Fin-Efficiency (η)**		
		Small-scale study		**Large scale**
		Experimental	**ABAQUS**	**ABAQUS**
e=0	Regular Pile	–	1.00	1.00
	L_f/D_p = 6	–	1.215	1.223
	L_f/D_p = 12	–	1.560	1.579
	L_f/D_p = 18	–	1.894	1.932
	FP-WFE, ($\theta = 0°$)	–	1.560	1.579
	FP-WFE, ($\theta = 45°$)	–	1.570	1.609
	FP-FEPC, ($\theta = 0°$)	–	1.946	2.014
	FP-FEPC, ($\theta = 45°$)	–	2.017	2.102
e=3.2D_p	Regular Pile	1.00	1.00	1.00
	L_f/D_p = 6	1.466	1.353	1.415
	L_f/D_p = 12	1.923	1.840	1.882
	L_f/D_p = 18	2.438	2.270	2.340
	FP-WFE, ($\theta = 0°$)	1.923	1.838	1.882
	FP-WFE, ($\theta = 45°$)	2.060	1.978	1.989
	FP-FEPC, ($\theta = 0°$)	2.143	2.070	2.102
	FP-FEPC, ($\theta = 45°$)	2.264	2.180	2.214

Based on the findings from both small-scale and large-scale studies, it can be concluded that finned piles offer advantages in resisting both non-eccentric and eccentric lateral loads. This enhances the performance of laterally loaded piles, referred to as fin-efficiency, by incorporating fins with optimal parameters as listed in Table 4.2.

4.7 SUMMARY

In this chapter, the performance of finned piles in resisting lateral loads was investigated through a combination of small-scale experiments and numerical studies in c-ϕ soil. Parametric studies were conducted to examine the behavior of finned piles under various parameters such as fin position, fin length, fin width, fin orientation, and loading eccentricity. The results obtained from both small-scale and large-scale analyses were compared to assess the scaling effect. Additionally, a material cost-benefit analysis was conducted to evaluate the construction economy associated with implementing finned piles in a project.

The major findings from the study are summarized below:

- Finned piles work more efficiently than regular piles against applied eccentric load (e=3.2D_p), i.e., when compared with lateral loading of e=0, the lateral resistance was reduced by 30% and 40% for finned and regular piles, respectively.

- Fin-length has a greater impact on lateral resistance than fin-width, even though both factors enhance lateral resistance. The optimum values of W_f and L_f are D_p and 12D_p, respectively, increasing lateral resistance by 56% without causing greater displacement.

- Fin-embedment in the pile cap influences L_u; for fin-orientation (θ) of 0° and 45°, respectively, a FP-FEPC resists 17.3% and 23.64% more load than a FP-WFE. Thus, the finned-pile group will be more efficient at resisting the lateral loads than the individual finned piles.

- To achieve the L_u of a finned pile with optimal fin parameters, the regular pile must have an equivalent pile diameter $(D_p)_{eq}$ that is 1.9 times the D_p of a finned pile with optimal fin parameters. i.e., 21.21% of the material more than a finned pile. Hence, the finned pile is a cost-effective alternative to the large-dimension regular pile.

- A finned pile with $(L_p)_{eq}$ of only 30% of the regular pile's L_p is sufficient to resist the load of L_u, reducing material usage by 46%.

CHAPTER 5

PILE-GROUP EFFICIENCY OF FINNED PILE GROUP

5.1 INTRODUCTION

Piles are commonly utilized together as a foundation, but as the number of piles in a group increases, the efficiency of the pile group (η_g) decreases. In regular pile groups, the η_g is typically below 90%. This study aims to enhance the lateral resistance of the pile group ($(L_u)_g$) by implementing innovative finned piles. To explore this matter further, small-scale model experiments were carried out on both regular and finned pile groups that were embedded in soil exhibiting c–ϕ characteristics. Additionally, numerical studies were conducted utilizing the Finite Element Approach. This chapter examines and presents the impacts of different factors, including the influence of fins on the pile group, pile spacings (s) and the number of piles (n), within the pile group, and the behavior of the group when subjected to eccentric loading

As the number of piles in a group increases, the η_g decreases. However, in order to withstand larger lateral loads, a higher group efficiency is necessary, which regular pile groups often fail to provide. Finned piles can resist greater lateral loads than conventional or regular piles Bariker et al. (2020); Nasr (2014); Peng (2005). Therefore, this study aims to investigate the impact of FP-groups on enhancing the L_u, specifically the η_g, of the pile group.

$(L_u)_g$ is lower than the combined capacity of individual piles and rises as the pile spacing increases (Prakash, 1962). The cumulative lateral resistance of the pile comprises the combined resistance at the pile cap's front, the pile cap's base, and the passive resistance of the soil in front of the pile (Agarwal and Prakash, 1967).

A method for determining the Group Reduction Factor (GRF) was introduced by Davisson (1970). Additionally, Franke (1988) observed that the lateral displacement (Δ) of the pile group was greater in cases where the pile spacing was less than $6D_p$. The decline in the efficiency of the pile group can be attributed to the shadowing effect caused by the trailing row of piles, with the majority of resistance being generated by the leading row of the pile group (Brown et al., 1990). Furthermore, with increased piles and variations in pile-group configurations result in a reduction of the $(L_u)_g$ (Gandhi and Selvam, 1997).

Ashour et al. (2004) proposed a model to ascertain the interaction between soil and piles in pile groups under lateral loading. The interaction between piles within the group intensifies as the lateral load is applied. For piles embedded in sand, the presence of group effects can be eliminated by maintaining a s_{min} of $6D_p$ for loose and medium sand, and a spacing greater than $8D_p$ is recommended. The behavior of the piles within the group closely resembles that of individual piles (Kim et al., 2011). With an increase in both the 's' and 'n' in the group, the $(L_u)_g$ experiences an increase. Moreover, compared to the RP-group, the FP-group exhibits greater resistance against larger lateral loads (Albusoda and Alsaddi, 2017).

This chapter investigates the performance of both RP-group and FP-groups under lateral loads through experimental and numerical studies. Parametric studies on pile-spacing (s), number of piles (n) in the group, and lateral load eccentricity (e) are attempted to optimize these pile parameters to resist maximum lateral load with minor lateral deformation that leads to a higher pile-group efficiency (η_g). The cost-benefit analysis of finned pile groups was performed compared to regular pile groups. A regression analysis to develop a standard correlation to determine the finned pile group's lateral resistance is also attempted in this chapter.

5.2 MESH SENSITIVITY ANALYSIS

Mesh sensitivity analysis was conducted on the 3D FE model of both RP and FP-group systems. For mesh sensitivity analysis, coarse, medium, fine, and refined element distributions were considered for the study, as shown in Figure 5.1. The symmetrical half model of both the regular and the finned pile groups produced 1431, 7394, 32872, and 92544 elements with the regular pile group model and 1591, 8402, 34472, and 94688 elements for the soil with the finned pile group model. The results have shown a marginal variation in lateral load. Hence, it is found that refined element distribution predicts the lateral load considerably under reasonable computational time, matching that of experimental data, as shown in Figure 5.2. Hence, the same refined meshing method is adopted for all parametric studies.

5.3 RESULTS AND DISCUSSION

The current study involved experimental and numerical analyses, which were carried out until the normalized lateral displacement (Δ/D_p) of 40%. The load at the normalized displacement (Δ/D_p) of 10% was considered the ultimate lateral load for both the regular and finned piled groups. The pile-group efficiency (η_g) is expressed by

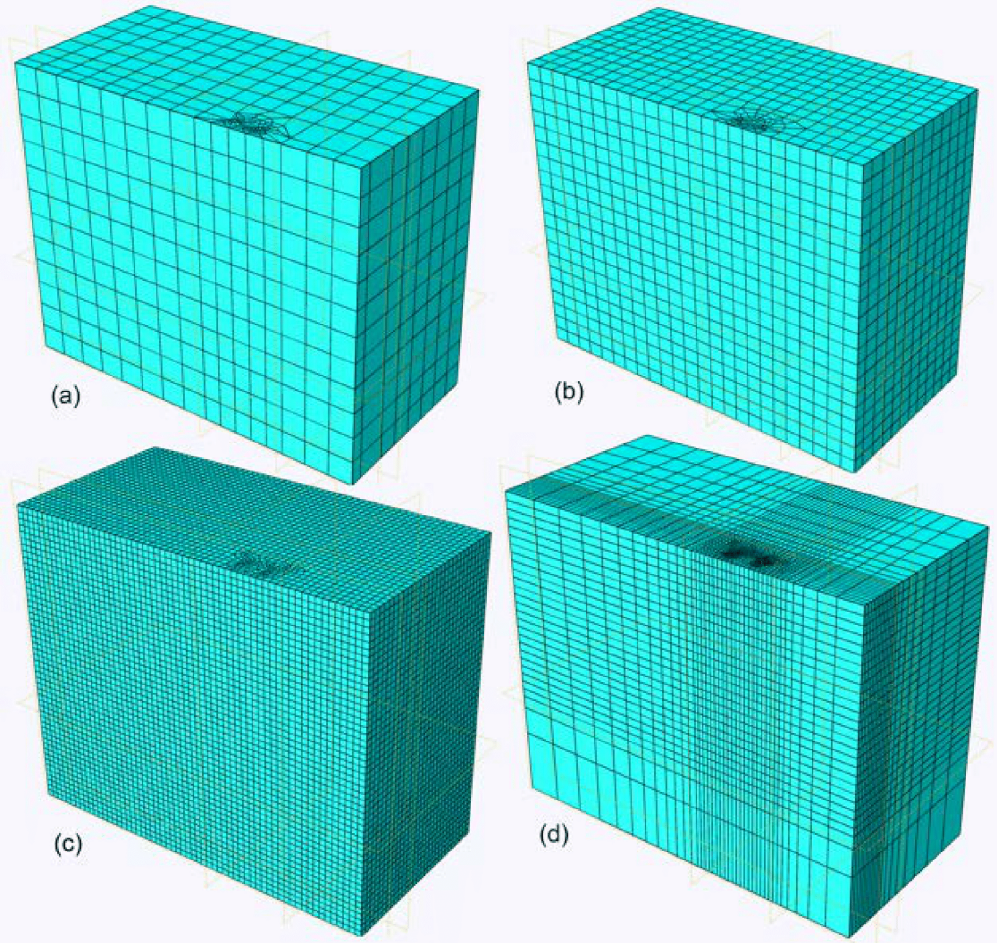

Figure 5.1 3D mesh generated for various element distributions (a) Coarse mesh; (b) Medium mesh; (c) Fine mesh; and (d) Refined mesh

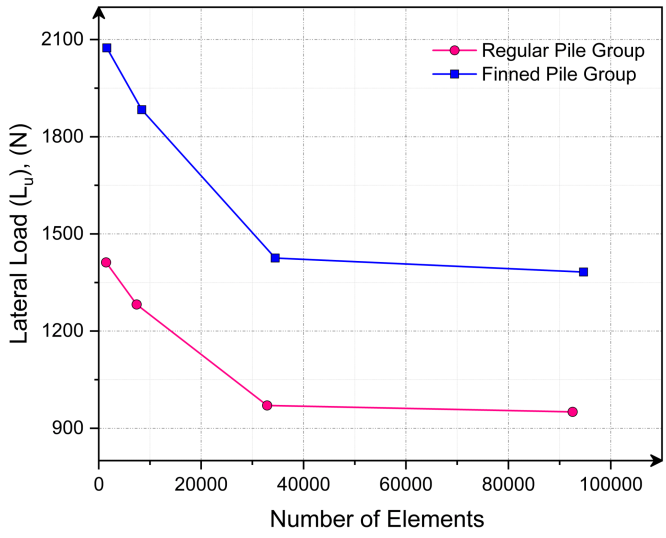

Figure 5.2 Mesh sensitivity analysis for regular and finned pile group model

a dimensionless factor, as shown in (5.1) and (5.2) for regular and finned pile groups, respectively.

$$(\eta_g)_{RP} = \left\{ \frac{[(L_u)_g]_{RP}}{n \times (L_u)_{RP}} \right\} \times 100 \tag{5.1}$$

$$(\eta_g)_{FP} = \left\{ \frac{[(L_u)_g]_{FP}}{n \times (L_u)_{RP}} \right\} \times 100 \tag{5.2}$$

Where $(\eta_g)_{RP}$ and $(\eta_g)_{RP}$ represent the pile-group efficiencies for regular and finned pile groups, respectively (%). $[(L_u)_g]_{RP}$ and $[(L_u)_g]_{FP}$ represent the ultimate lateral load for the RP-group and FP-groups, respectively. n is the number of piles in the group, $(L_u)_{RP}$ is the ultimate lateral load of the individual regular pile, i.e., the reference load for calculating the pile-group efficiency even for the finned-pile group so that it considers the effect of fins effectively.

These experimental and finite element analysis programs were conducted on the laterally loaded finned pile for refined meshing. To examine the resistance of the finned pile group against lateral loads, several parametric studies were conducted. Table 5.1 presents the results of these studies, which were performed on long RP and FP-groups.

Table 5.1 FE analytical and experimental program for RP and FP-groups

Series	Constant parameters	Variable Parameters
I	Individual regular and finned piles, L_p = 0.665 m,	e/D_p of 0 and 3.2
II	Regular and finned pile-group: n[a]= 4, and s[b]= $4D_p$.	e/D_p of 0 and 3.2
III	Regular and finned pile-groups: s = $4D_p$.	n = 4 and 5, e/D_p
IV	Regular and finned pile-groups: n = 4, and 5	s = $4D_p$ and $6D_p$, e/D_p

[a] n - No. of piles in group

[b] s - spacing between piles in group

5.4 PARAMETRIC STUDIES ON FINNED PILE GROUPS

Piles are commonly employed in groups as a general practice. When investigating FP-groups, it is essential to utilize the optimal fin parameters specific to the finned pile, as illustrated in Table 4.2. Its utilization is most economical by considering the most suitable fin parameters. Table 5.1 shows that Series I tests were initially performed over reference piles, i.e., individual regular and finned piles, for studying lateral load resistance. Series II tests were performed to examine the impact of fins in the pile group.

Series III tests were carried out to examine the impact of the number of piles (n) within the group, whereas Series IV tests were conducted to investigate the influence of the pile spacing (s) within the group.

The outcomes obtained from individual regular and finned piles (Figure 4.3), utilizing the optimal fin parameters (Table 4.2), were employed to examine the impact of pile groups under different parameters, as demonstrated in Series I of Table 5.1. The resistance developed by individual reference piles (i.e., regular and finned piles) was necessary for calculating the η_g.

5.4.1 Effect of Fins in the Pile Group

Both model experiments and numerical analyses were conducted on four pile groups (n=4) with a pile spacing (s) equivalent to $4D_p$. This study encompassed both the regular pile group (RP–P_4S_4) and the finned pile group (FP–P_4S_4), utilizing the optimal fin parameters illustrated in Figure 5.3 and Table 4.2. The pile group models are shown in Figure 5.4 and Series II of Table 5.1. For both eccentricity cases of e =

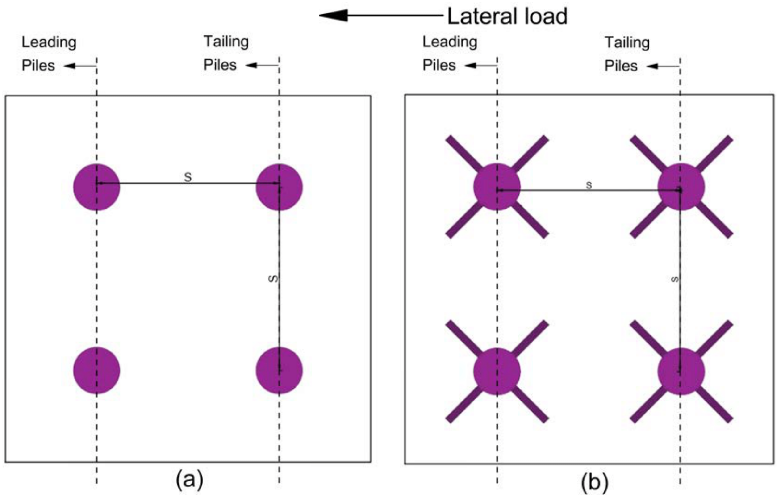

Figure 5.3 Schematic diagram of the piled group with four piles: (a) Regular pile group: $RP - P_4S_4$; and (b) Finned pile group: $FP - P_4S_4$

0 and e = $3.2D_p$, it was observed that the finned-pile group ($FP - P_4S_4$) exhibited higher lateral resistance ($[L_u]_g$) compared to the regular piled-group ($RP - P_4S_4$), as illustrated in Figure 5.5. The fins were affixed at the crucial location on the piles within the pile group, where the lateral load was exerted. This attachment of fins contributed to an increase in the flexural rigidity, thereby enhancing the lateral resistance of the pile group. As a result, the pile-group efficiency (η_g) was elevated , i.e., $(\eta_g)_{FP} > (\eta_g)_{RP}$, as shown in Figure 5.6.

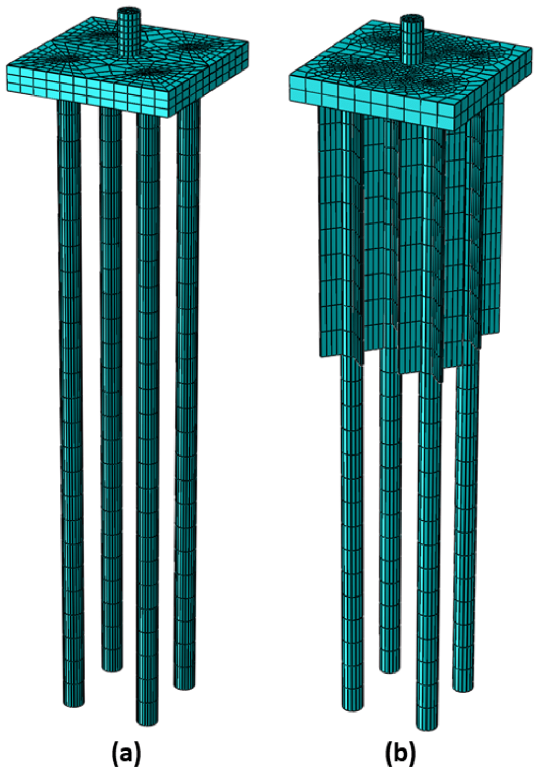

Figure 5.4 3D model of piled groups in ABAQUS: (a) Regular pile group: $RP - P_4S_4$; and (b) Finned pile group: $FP - P_4S_4$

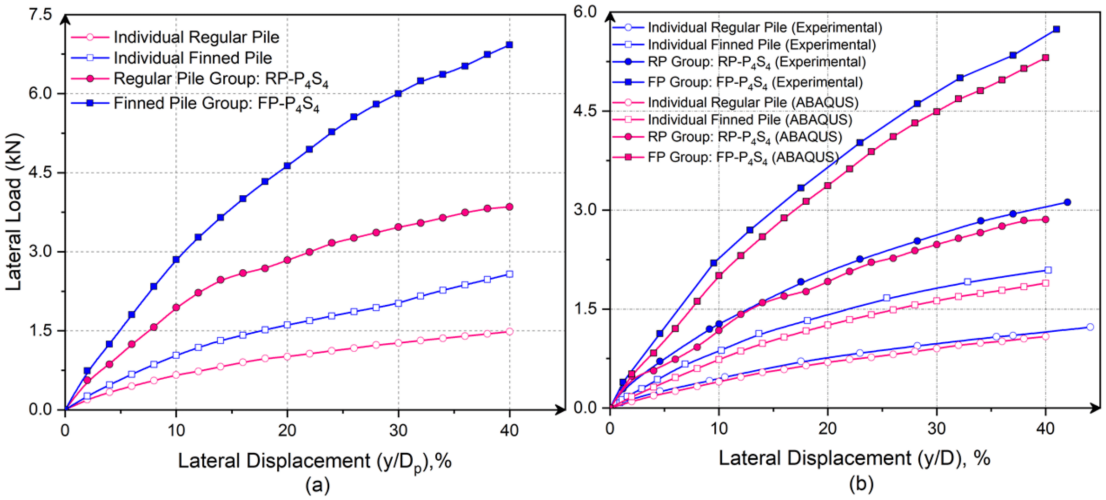

Figure 5.5 Variation of lateral resistance for individual piles and piled-groups for: (a) ABAQUS (e = 0); and, (b) Experimental and ABAQUS (e = $3.2D_p$)

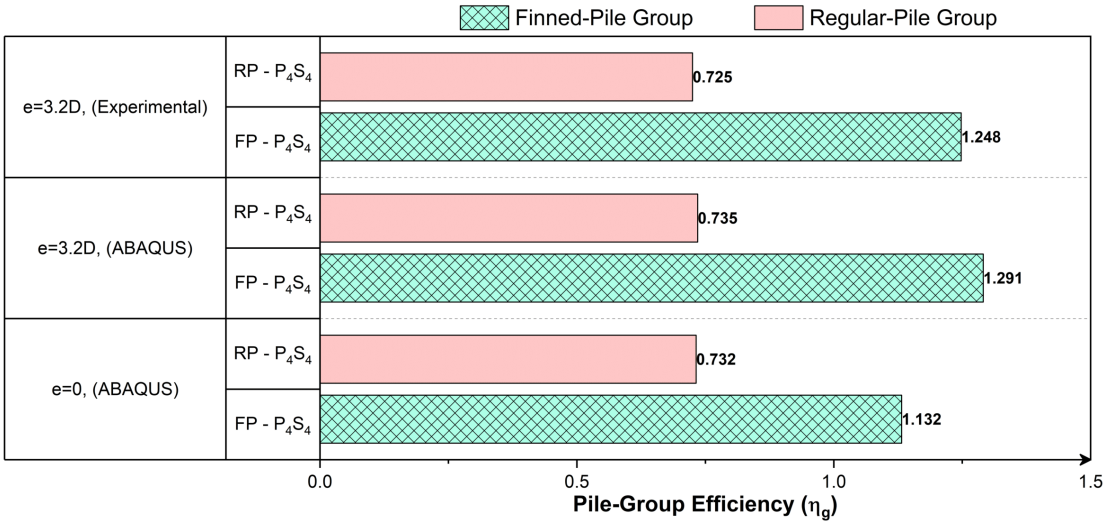

Figure 5.6 Variation of pile-group efficiencies for $RP-P_4S_4$ and $FP-P_4S_4$ piled groups for varying study types

It was observed that the finned pile groups developed higher lateral resistance to the applied lateral deformation than the regular pile groups, as shown in Figure 5.7. The finned pile groups increase the efficiency η_g by about 54.62% and 75.65% for eccentricities of e of 0 and $3D_p$, respectively. When a lateral load is applied with certain eccentricity, the FP-group demonstrates superior performance compared to the RP-groups.

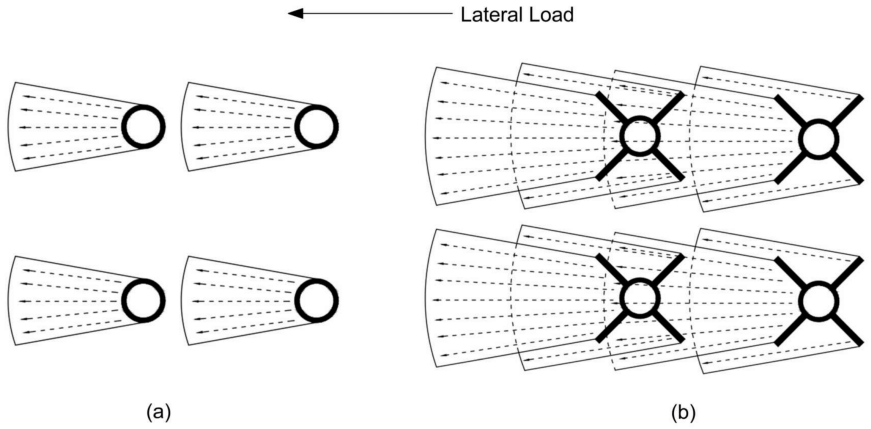

Figure 5.7 Resistance developed by piles in group against lateral load: (a) Regular pile group; and (b) Finned pile group

Figure 5.8 illustrates the changes in strain and stress within a pile when subjected to a lateral load. It is evident that the individual regular pile exhibits higher levels of strain and stress compared to the individual finned pile. The leading piles in the group experience marginally lower strain and stress than tailing piles. Since piles in the group

experience less strain and stress than individual RP and FP, the chance of pile bending and failure will be less for piles in the group. Hence, piles in a group work better than individual piles, complemented by resisting the higher lateral load for the FP-group.

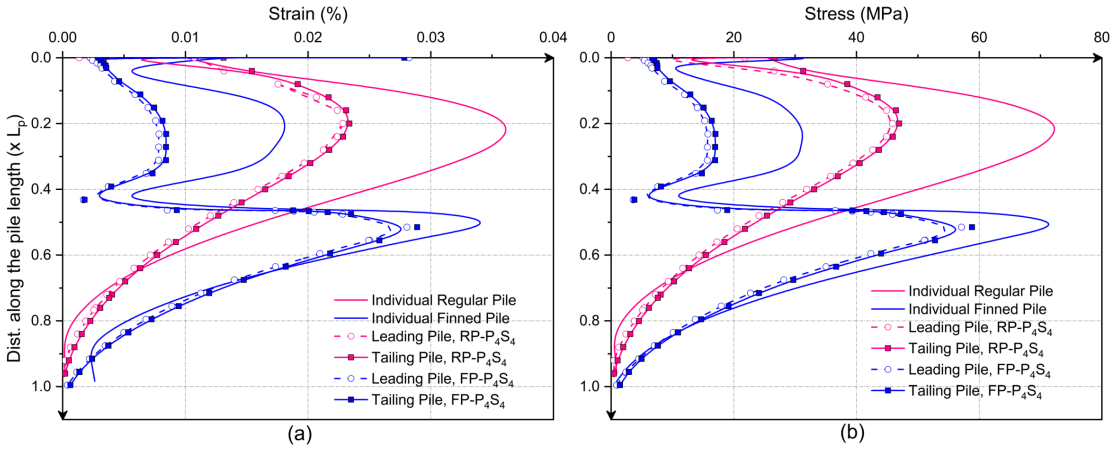

Figure 5.8 Variation of the strain and stress for regular and finned pile groups: (a) Strain; and (b) Stress

5.4.2 Impact of the pile numbers in the group

To examine the impact of the number of piles (n) within a group on the lateral resistance of both regular and finned pile groups, analyses were conducted on pile groups consisting of four and five piles. These pile groups had spacing (s) of $4D_p$ forming $RP-P_4S_4$, $RP-P_5S_4$, $FP-P_4S_4$, and $FP-P_5S_4$ as shown in Figure 5.9 and Figure 5.10, and Series III of Table 5.1. Optimal fin parameters were used for piles in the finned-pile groups.

The variation of lateral resistance for various groups, with varying pile numbers (n) for both regular and finned pile groups, is shown in Figure 5.11. With the addition of an extra pile (middle pile), the $[L_u]_g$ increases due to the enhanced resistance provided. The variation of η_g for the varying number of piles (n) in pile group is shown in Figure 5.12. Furthermore, it was observed that the pile group efficiency (η_g) of the $FP-P_4S_4$ group is 75.65% higher than that of the $RP-P_4S_4$ group, and for the $FP-P_5S_4$ group, it is 59% higher than that of the $RP-P_5S_4$ group. For the RP-group, η_g increases with the number of piles from four (P_4) to five (P_5) with pile spacing (s) of $4D_p$. However, η_g decreases for an increase in pile numbers (n) for the finned pile group because of the overlapping of stress bulbs for finned-piles. It is due to the lesser pile spacing (s) between piles in the P_5 group, as fins activate larger soil in front of it for developing larger resistance.

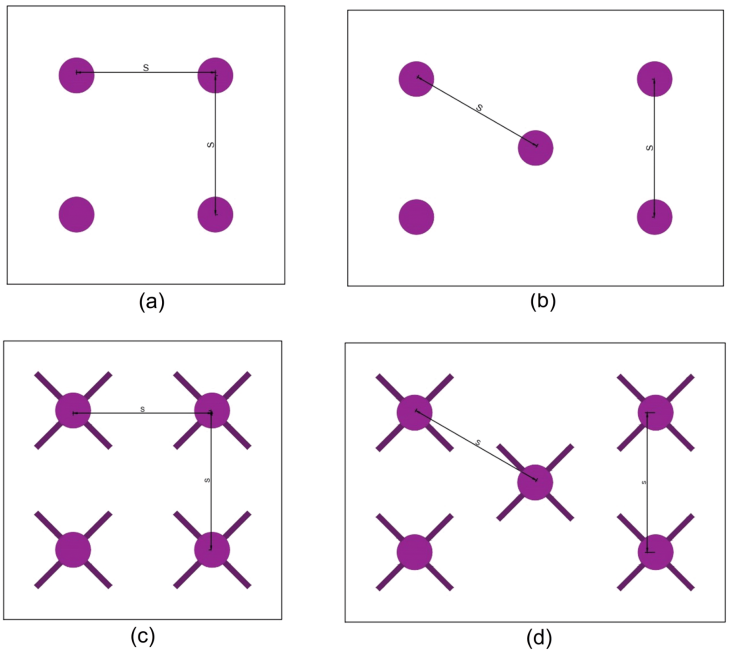

Figure 5.9 Schematic diagram of the piled groups with varying pile numbers (n) in the pile group: (a) $RP-P_4S_4$; (b) $RP-P_5S_4$; (c) $FP-P_4S_4$; and (d) $FP-P_5S_4$

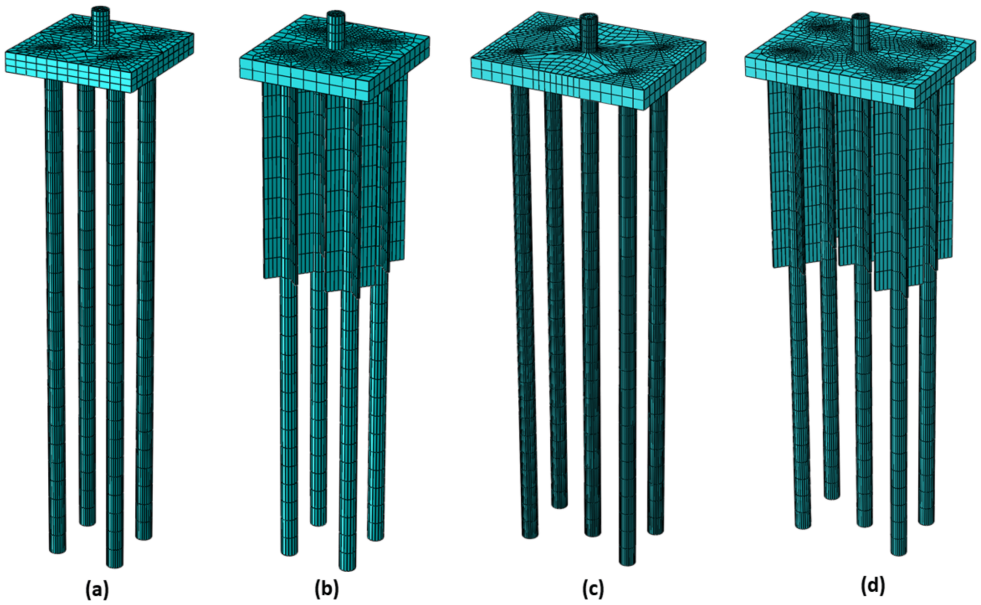

Figure 5.10 Pile-Groups used in studying the effect of the number of piles: (a) $RP-P_4S_4$; (b) $FP-P_4S_4$; (c) $RP-P_5S_4$; and (d) $FP-P_5S_4$

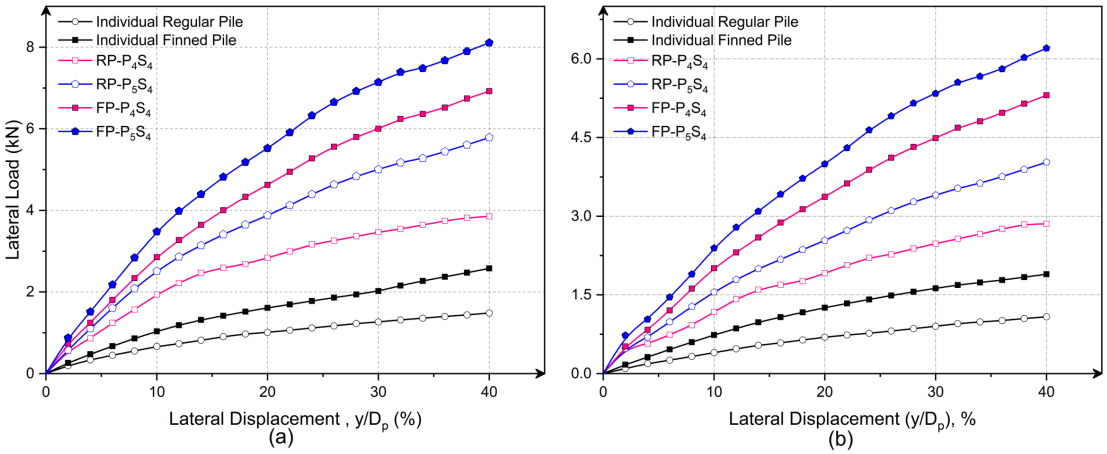

Figure 5.11 Variation of lateral resistance of piled groups with varying pile numbers in the group for (a) e = 0; and it's (b) e = 3.2D_p

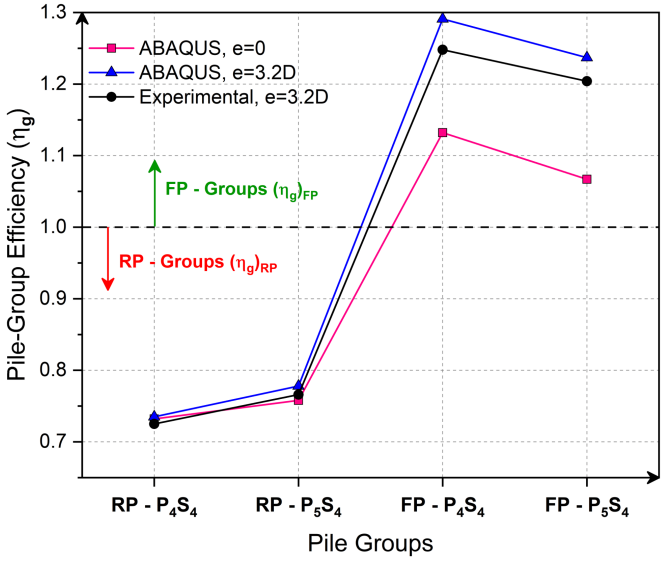

Figure 5.12 Variation of pile-group efficiencies (η_g) for the varying pile numbers (n) in the piled group

The variation of stress and strain developed in a pile for the applied lateral load is shown in Figure 5.13. In the P_5 group, no significant variations were observed in the stress and strain experienced by the different piles, including the leading, middle, and tailing piles. This suggests that the load applied to the pile group is effectively distributed among the additional pile in the P_5 group. Consequently, it was observed that the stress and strain levels in the P_5S_4 pile group were lower compared to those in the P_4S_4 pile group. Hence, it is safe against the serviceability or deflection of pile.

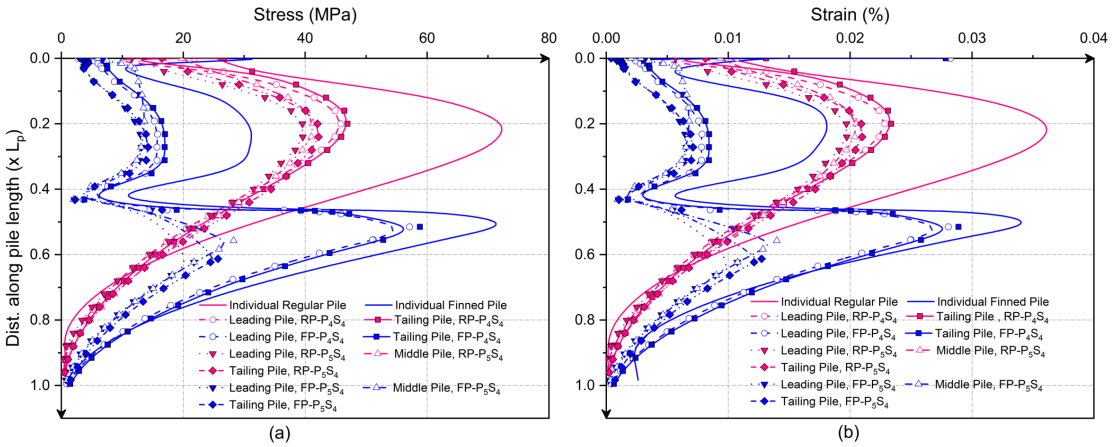

Figure 5.13 Variation of the strain and stress for regular and finned pile groups with four and five piles: (a) Stress; and (b) Strain

5.4.3 Impact of pile-spacing in group

The studies were conducted over P_4S_4, P_4S_6, P_5S_4, and P_5S_6 groups of regular and finned piles for eccentricity of 0 and $3.2D_p$ as shown in Figure 5.14 and Series IV of Table 5.1. These were performed to study the effect of pile spacing (s) over lateral resistance of regular and finned pile groups.

It is observed that $(L_u)_g$ with increased pile spacing (s) for both RP and FP-groups, as illustrated in Figure 5.15, and Figure 5.16. As the pile spacing increases, each individual pile within the group develops significant soil resistance independently. This phenomenon results in a higher overall lateral resistance for pile group.

Among $RP-P_4S_6$ and $RP-P_5S_4$ for regular pile groups under non-eccentric loading (e = 0) and eccentric loading (e = $3.2D_p$), the P_5S_4 group resists a lesser lateral load than that of P4S6 as illustrated in Figure 5.15. In RP-groups, the number of piles dominates the $(L_u)_g$ more than the pile spacing. The lesser pile-group flexural rigidity (E_pI_p) is due to the smaller cross-section area of the regular pile. The flexural rigidity (E_pI_p) of pile group is increased with increase in pile numbers (n) at the pile-head location.

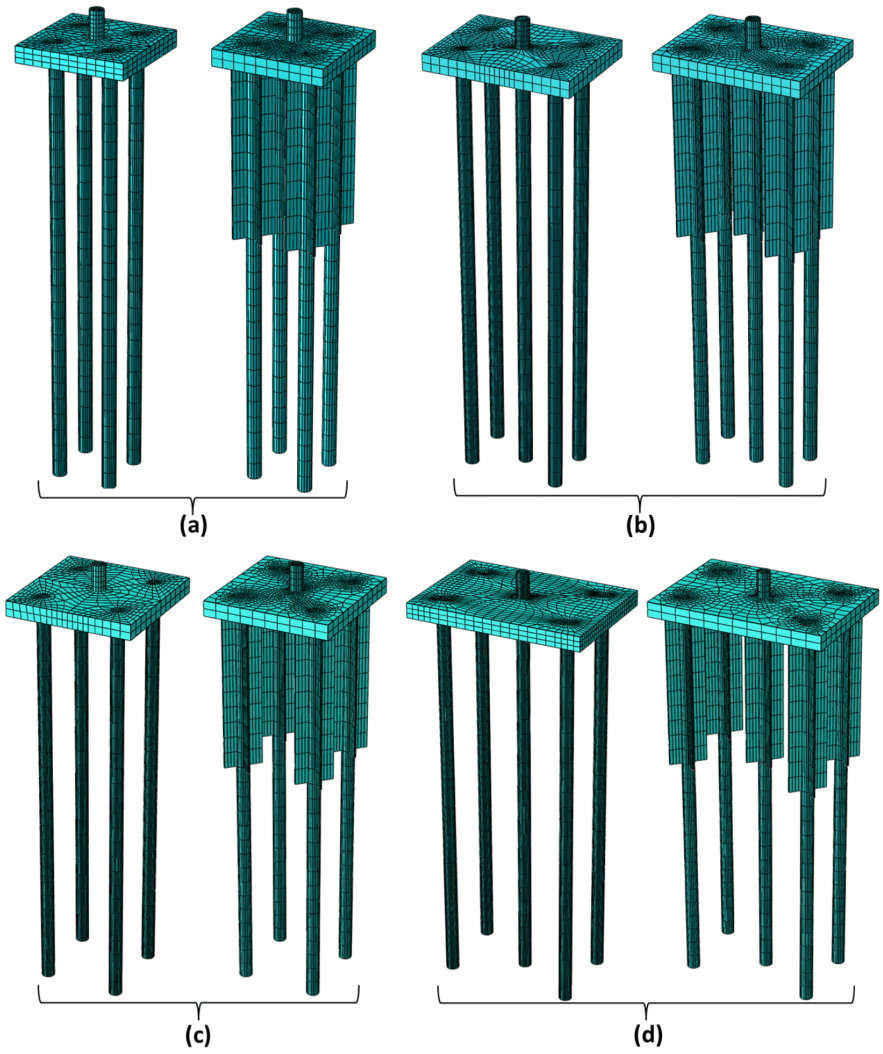

Figure 5.14 Regular pile and Finned pile groups used in studying the effect of pile spacing: (a) P_4S_4 groups; (b) P_5S_4 groups; (c) P_4S_6 groups; and (d) P_5S_6 groups

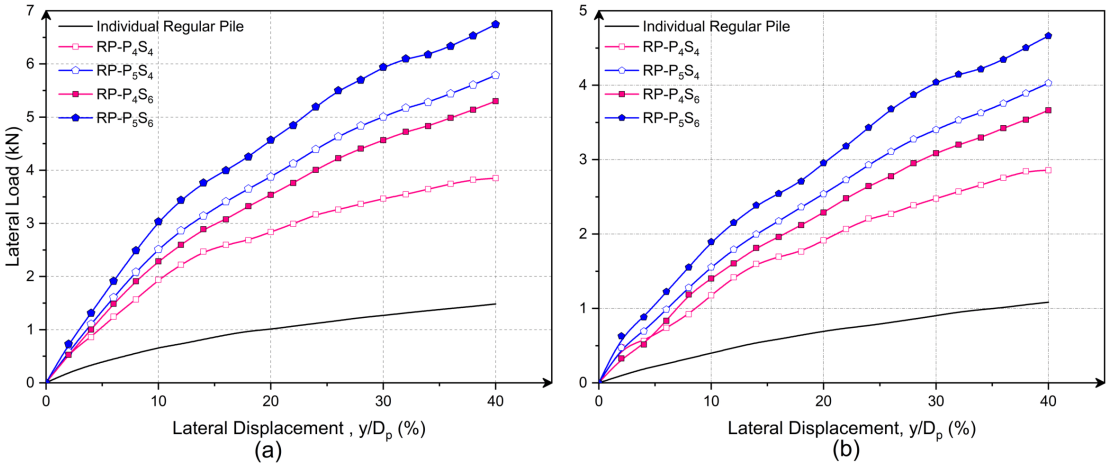

Figure 5.15 Lateral resistance developed by regular pile groups for varying pile spacings: (a) eccentricity, e = 0; and (b) e = $3.2D_p$

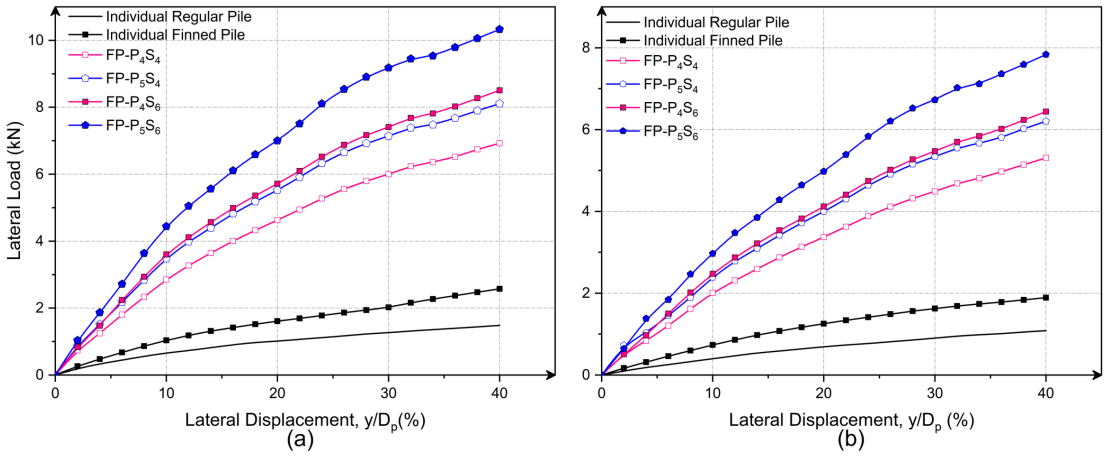

Figure 5.16 Lateral resistance developed by finned pile groups for varying pile spacings: (a) eccentricity, e = 0; and (b) e = $3.2D_p$

For finned pile groups, among $FP-P_4S_6$ and $FP-P_5S_4$, for non-eccentric loadings (e = 0) and eccentric loadings (e = $3.2D_p$), the P_4S_6 pile group resists marginally higher lateral load than P_5S_4 as shown in Figure 5.16. The finned piles increase the group's flexural rigidity (E_pI_p) by providing fins. Hence, the pile spacing (s) dominates the lateral resistance for finned piles rather than the number of piles (n). As fins increase lateral resistance, larger pile spacings (s) provide a large enough zone for soil to resist greater lateral resistance. Hence, P_4 groups with larger pile spacing (s) resist larger lateral loads than P_5 groups with smaller spacing for finned pile groups.

The variation of the pile-group efficiencies (η_g) for regular and finned pile groups is shown in Figure 5.17. For both regular and finned piled groups, η_g increases with pile spacing (s) increase.

Regular pile groups have an efficiency $(\eta_g)_{RP}$ lesser than unity (100%). However, the efficiency of finned pile groups $(\eta_g)_{FP}$ is greater than unity, i.e., they have higher lateral resistance than regular pile groups. For regular pile groups, the higher number of piles (n) resist higher lateral load, i.e., $RP-P_5S_4 > RP-P_4S_4$, $RP-P_5S_6 > RP-P_4S_6$. In contrast, for finned-pile groups, the spacing (s) between piles assumes a crucial role in enhancing the lateral resistance, surpassing the influence of the number of piles (n) within the group. This is because the presence of fins activates the soil between the piles to a greater extent, effectively countering the applied lateral load. Consequently, by providing larger pile spacing, the detrimental effects of stress bulb overlapping or pile grouping under lateral loading are reduced.

Along with strength criteria, stress and strain developed in a pile must also be satisfied in serviceability criteria. The variation of stress and strain in a pile for various pile groups of the regular and finned piles is illustrated in Figure 5.18 and Figure 5.19,

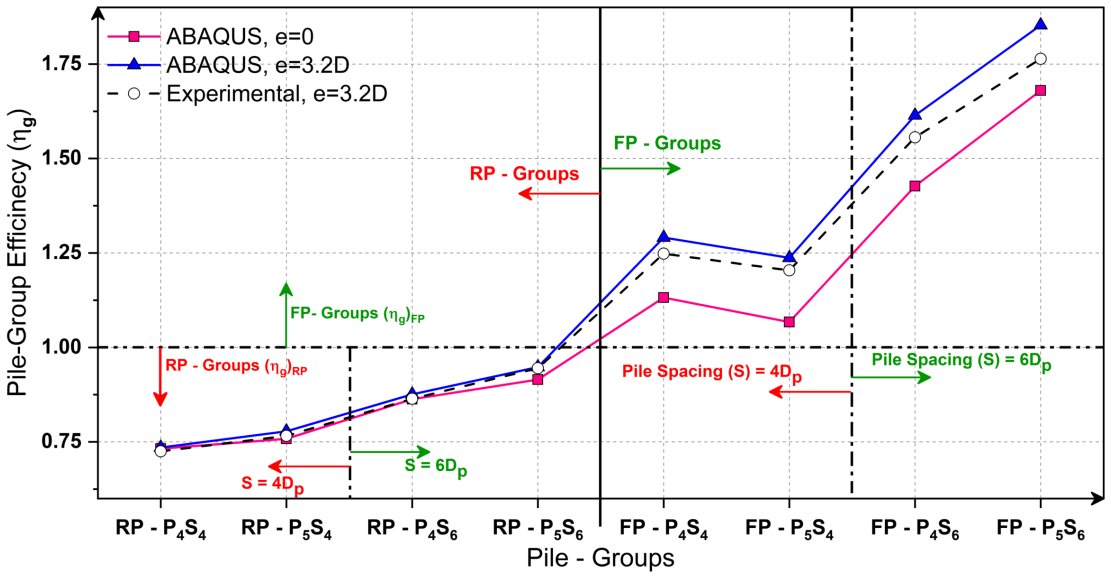

Figure 5.17 Variation of pile group efficiencies for varying pile spacing (s) in regular and finned pile groups

respectively. For RP-groups, the stress and strain developed in all piles are almost similar for all the pile groups since the pile alone has to carry all the applied lateral load, as shown in Figure 5.18. However, for FP-groups, as the fins have their influence in resisting applied lateral loads, stress and strain developed in a pile vary based on the pile position in group, as demonstrated in Figure 5.19.

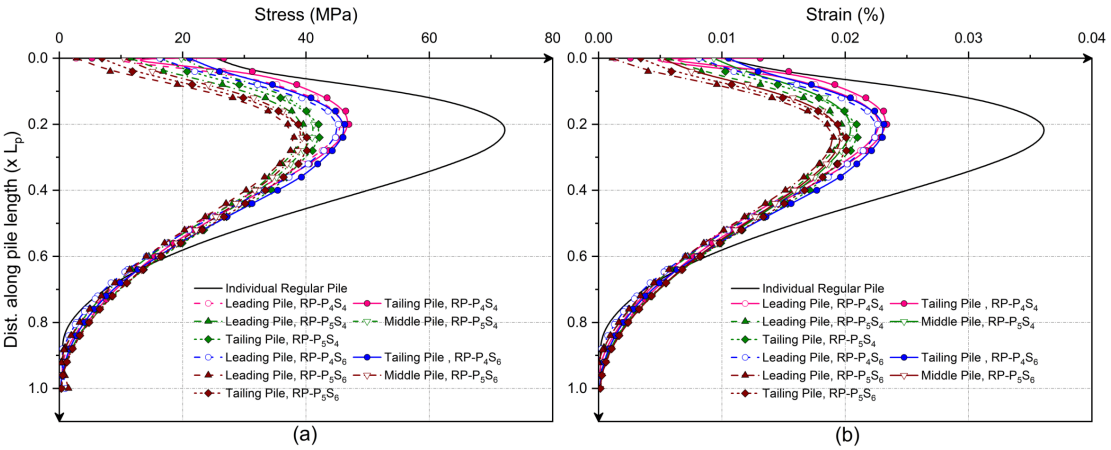

Figure 5.18 Variation of the strain and stress for regular pile groups of various pile spacings: (a) Stress; and (b) Strain

With an increase in pile spacing (s), the stress and strain developed in a pile decreased for the P_4 group, whereas stress and strain increased for the P_5 groups. The leading pile in $FP-P_4S_6$ has less stress and strain than the tailing pile in the group. The provision of fins resists marginally higher load at the fin position, i.e., till $L_f = 0.4L_p$.

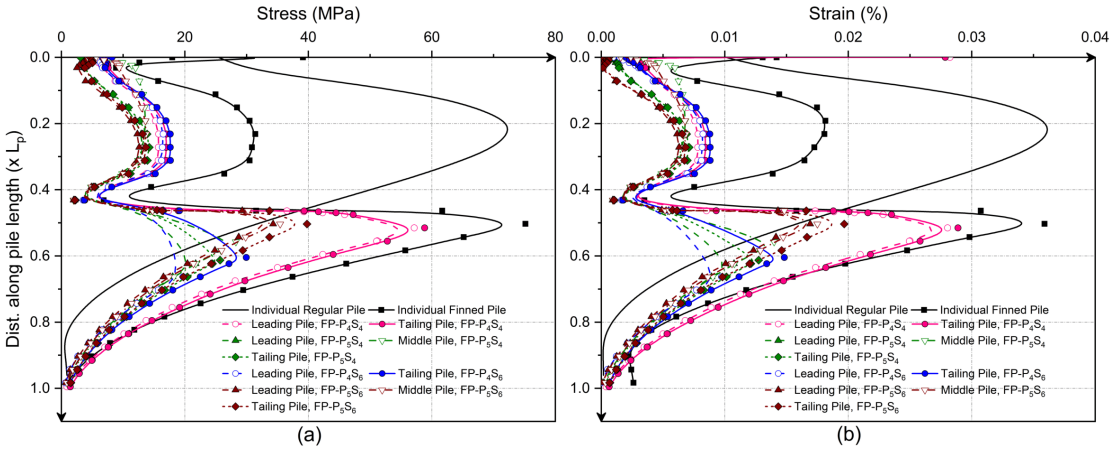

Figure 5.19 Variation of the strain and stress for finned pile groups of various pile spacings: (a) Stress; and (b) Strain

It diminishes below the fins, i.e., between $0.4L_p$ to $1.0L_p$, indicating that the individual pile effect dominates group action. $FP-P_5S_6$ develops larger stress and strain in a pile than $FP-P_5S_4$, i.e., for the FP-group, the block action dominates the individual pile effect, leading to larger stress and strain.

Hence, for P_4 finned pile-groups, irrespective of pile spacing (s), the individual pile action dominates over the pile-group or block effect, leading to a higher pile-group efficiency. However, in the P_5 finned pile groups, the pile-group effect dominates the individual pile effect, as shown in Figure 5.17.

5.5 MATERIAL-COST BENEFIT ANALYSIS

The innovative finned pile technique is advantageous in enhancing lateral resistance and reducing the construction cost of the foundation. By reducing the dimensions of the piles in a pile group, such as the length (L_p) and diameter (D_p), the construction cost of pile foundations can be minimized. The findings from both experimental and numerical studies indicate that the finned pile group exhibits superior resistance against lateral forces compared to the regular pile group. To investigate the cost-saving benefits of finned pile groups in construction, a series of small-scale studies were conducted, involving variations in pile diameter and length. The results were evaluated based on the Group Capacity Ratio (GCR), as depicted in equation (5.3).

$$Group\ Capacity\ Ratio = GCR = \frac{[(L_u)_g]_{RP}}{[(L_u)_g]_{FP}} \tag{5.3}$$

5.5.1 Equivalent Pile Diameter

Numerical analyses were conducted on RP-groups with different pile diameters (D_p), namely 21mm, 25mm, 28mm, and 30mm. The $(L_u)_g$ of the FP-groups, with a D_p of 21mm, served as the reference for comparison. The results of these analyses are presented in Table 5.2. The purpose of these studies was to examine the influence of pile diameter on the lateral resistance of pile groups. The equivalent pile diameter $(D_p)_{eq}$ refers to the diameter of regular piles within the group at which the developed resistance matches that of the reference FP-group. Since FP-groups have been used as a standard for determining the $(D_p)_{eq}$, the group capacity ratio (GCR) must be greater than or equal to unity (GCR $\geq$ 1.0), i.e., the regular pile group develops lateral resistance at least equal to the finned pile group.

Table 5.2 Summary of results from equivalent pile diameter study

Description	**Pile Diameter** (D_p)**, mm**	**GCR**	
		e = 0	**e = 3.2D_p**
$FP-P_4S_4$[a]-21mm	21	–	–
$RP-P_4S_4$-21mm	21	0.65	0.57
$RP-P_4S_4$-25mm	25	0.86	0.60
$RP-P_4S_4$-28mm	28	0.98	0.86
$RP-P_4S_4$-30mm	**30**	**1.07**	**1.03**
$FP-P_5S_4$[a]-21mm	21	–	–
$RP-P_5S_4$-21mm	21	0.71	0.63
$RP-P_5S_4$-25mm	25	0.91	0.83
$RP-P_5S_4$-28mm	**28**	**1.02**	**1.03**
$FP-P_4S_6$[a]-21mm	21	–	–
$RP-P_4S_6$-21mm	21	0.60	0.54
$RP-P_4S_6$-25mm	25	0.84	0.78
$RP-P_4S_6$-28mm	28	0.96	0.94
$RP-P_4S_6$-30mm	**30**	**1.06**	**1.03**
$FP-P_5S_6$[a]-21mm	21	–	–
$RP-P_5S_6$-21mm	21	0.55	0.51
$RP-P_5S_6$-25mm	25	0.72	0.71
$RP-P_5S_6$-28mm	28	0.83	0.84
$RP-P_5S_6$-30mm	30	0.94	0.96
$RP-P_5S_6$-32mm	**32**	**1.08**	**1.06**

[a] Finned Pile Group, (Reference group for evaluating GCR).

Table 5.2 indicates that in order to withstand the same lateral loads as the reference FP-group with a diameter of 21mm, the RP-groups required a larger pile diameter. The equivalent pile diameter $(D_p)_{eq}$ for $RP-P_4S_4$, $RP-P_5S_4$, $RP-P_4S_6$, and $RP-P_5S_6$ were 30, 28, 30, and 32 mm respectively. The material required for the above regular pile group with $(D_p)_{eq}$ for $RP-P_4S_4$, $RP-P_5S_4$, $RP-P_4S_6$, and $RP-P_5S_6$ is 47.5%, 25.3%, 70.2%, and 85.3% more than the corresponding finned pile groups respectively. Hence, finned pile groups are more economical than regular pile groups, especially for groups with greater pile spacing (s).

5.5.2 Equivalent Pile Length

To investigate the impact of pile length on reducing the construction cost of the foundation, a series of analyses were conducted on finned pile groups with different pile lengths. These analyses were compared to the regular pile, which had a length of 665mm and a diameter of 21mm. As the material cost can be reduced only by reducing the pile dimensions, in the present case, it is calculated in terms of the pile length (L_p). The analyses were carried out on finned piles by reducing the L_p until the resistance offered was equal to that of the corresponding RP-group, as shown in Table 5.3. The length of FP in the group resisting the L_u equal to that of the corresponding RP-group is termed equivalent pile-length $(L_p)_{eq}$. Since the lateral resistance provided by RP-groups was considered standard, the GCR must be less than and nearly equal to unity (i.e., GCR $\leq$ 1) to highlight the advantages, i.e., $[(L_u)_g]_{RP} \leq [(L_u)_g]_{FP}$.

The findings in Table 5.3 reveal that, in order to withstand the same lateral load as the reference RP-group with a length of 665mm, the corresponding FP-groups required a shorter pile length, specifically with an optimal fin length of $0.4L_p$. For $FP-P_4S_4$ and $FP-P_5S_4$, the equivalent pile lengths $(L_p)_{eq}$ were 233mm. Whereas for $FP-P_4S_6$ and $FP-P_5S_6$, $(L_p)_{eq}$ were determined to be 166 and 67mm for non-eccentric loading (e = 0), and 200 and 133mm for eccentric loading (e = $3.2D_p$) respectively. For $FP-P_4S_4$ and $FP-P_5S_4$, material usage was reduced by 24.1% and 29.7%. In contrast, for $FP-P_4S_6$ and $FP-P_5S_6$, material usage was reduced by 14.6% and 23.7%, for non-eccentric loading (e = 0) and 13.2% and 20%, for eccentric loading (e = $3.2D_p$) respectively. The analysis indicates that the material demand increases for pile groups with a greater number of piles under eccentric loads. Nevertheless, the overall material requirement for a FP-group is lower compared to the corresponding RP-group.

Table 5.3 Summary of results from equivalent pile length study

Description	Pile Length (L_p), mm	GCR	
		e = 0	e = 3.2D_p
$RP-P_4S_4$[a]-665mm	665	–	–
$FP-P_4S_4$-665mm	665	0.65	0.57
$FP-P_4S_4$-532mm	532	0.69	0.63
$FP-P_4S_4$-399mm	399	0.75	0.71
$FP-P_4S_4$-266mm	266	0.91	0.92
$FP-P_4S_4$-233mm	**233**	**0.96**	**0.99**
$RP-P_5S_4$[a]-665mm	665	–	–
$FP-P_5S_4$-665mm	665	0.71	0.63
$FP-P_5S_4$-532mm	532	0.75	0.68
$FP-P_5S_4$-399mm	399	0.82	0.76
$FP-P_5S_4$-266mm	266	0.94	0.95
$FP-P_5S_4$-233mm	**233**	**0.98**	**0.99**
$RP-P_4S_6$[a]-665mm	665	–	–
$FP-P_4S_6$-665mm	665	0.61	0.54
$FP-P_4S_6$-565mm	565	0.62	0.58
$FP-P_4S_6$-399mm	399	0.68	0.66
$FP-P_4S_6$-266mm	266	0.79	0.80
$FP-P_4S_6$-200mm	**200**	0.88	**0.97**
$FP-P_4S_6$-166mm	**166**	**0.97**	1.06
$RP-P_5S_6$[a]-665mm	665	–	–
$FP-P_5S_6$-665mm	665	0.55	0.51
$FP-P_5S_6$-532mm	532	0.57	0.54
$FP-P_5S_6$-399mm	399	0.62	0.60
$FP-P_5S_6$-266mm	266	0.67	0.70
$FP-P_5S_6$-133mm	**133**	0.76	**0.99**
$FP-P_5S_6$-67mm	**67**	**0.97**	2.20

[a] Regular Pile Group, (Reference group for evaluating GCR).

5.6 REGRESSION ANALYSIS

In order to establish a relationship between the $(L_u)_g$ of regular and finned pile groups, a regression model was developed using parameters such as the number of piles in a group (n), pile spacing (s), and eccentricity (e). This regression model was based on small-scale experiments conducted on regular and finned piles with varying parameters including pile diameter (D_p), length (L_p), fin length (L_f = 0.4L_p), fin width (W_f) of 21mm, and fin orientation (θ) of 45°. The piles were embedded in c-ϕ soil with properties described in Table 3.2.

Two distinct regression analyses were conducted on RP-groups and FP-groups, taking into account the factors influencing the $(L_u)_g$. The data shown in Table 5.4 and Table 5.5, obtained from the various parametric studies analyzed numerically, served as the input variables for the regression analyses. Two regression equations were proposed for regular and finned pile groups, respectively, using regression analyses as shown in (5.4) and (5.5).

$$[(L_u)_g]_{RP} = exp\Big\{(6.26\times10^{-2})D_p + 0.2877n + (5.328\times10^{-3})s - (5.815\times10^{-3})e + 4.594\Big\} \quad (5.4)$$

$$[(L_u)_g]_{FP} = exp\Big\{(9.40\times10^{-4})L_p + 0.3313n + (8.882\times10^{-3})s - (7.067\times10^{-3})e + 5.273\Big\} \quad (5.5)$$

Where $(L_u)_g$ in N, n is the pile numbers in pile-group (No.'s), s is the spacing in between piles (mm), and e is the factor defining the eccentricity of the load on the pile group, i.e., the distance of application of load (mm).

The validation of the developed correlation was done with the experimental results. The equations (5.4) and (5.5) mentioned above for calculating the $(L_u)_g$ predicts the load efficiently as that of the actual load obtained from the numerical analyses, as shown in Tables 5.4 and 5.5. The predicted load suits the actual load well and is accurate to 98.77% and 92.97% for regular and finned pile groups, respectively, as shown in Figure 5.20.

Table 5.4 Summary of results from regression analyses on regular-pile groups

Description	D_p (mm)	n	S (mm)	e (mm)	$(L_u)_{Actual}$ (N)	$(L_u)_{Predicted}$ (N)
$RP-P_4S_4$-D_p-21mm	21	4	84	0	1940.64	1821.16
$RP-P_5S_4$-D_p-21mm	21	5	84	0	2512.20	2428.22
$RP-P_4S_6$-D_p-21mm	21	4	126	0	2286.50	2277.93
$RP-P_5S_6$-D_p-21mm	21	5	126	0	3032.60	3037.25
$RP-P_4S_4$-D_p-21mm	21	4	84	67.2	1175.20	1232.12
$RP-P_5S_4$-D_p-21mm	21	5	84	67.2	1554.40	1642.83
$RP-P_4S_6$-D_p-21mm	21	4	126	67.2	1401.60	1541.15
$RP-P_5S_6$-D_p-21mm	21	5	126	67.2	1894.22	2054.88
$RP-P_4S_4$-D_p-25mm	25	4	84	0	2592.36	2339.64
$RP-P_5S_4$-D_p-25mm	25	5	84	0	3233.82	3119.53
$RP-P_4S_6$-D_p-25mm	25	4	126	0	3159.46	2926.45
$RP-P_5S_6$-D_p-25mm	25	5	126	0	3972.36	3901.95
$RP-P_4S_4$-D_p-25mm	25	4	84	67.2	1232.86	1582.90
$RP-P_5S_4$-D_p-25mm	25	5	84	67.2	2056.40	2110.54
$RP-P_4S_6$-D_p-25mm	25	4	126	67.2	2020.50	1979.92
$RP-P_5S_6$-D_p-25mm	25	5	126	67.2	2612.22	2639.90
$RP-P_4S_4$-D_p-28mm	28	4	84	0	2962.34	2823.25
$RP-P_5S_4$-D_p-28mm	28	5	84	0	3621.30	3764.35
$RP-P_4S_6$-D_p-28mm	28	4	126	0	3660.42	3531.36
$RP-P_5S_6$-D_p-28mm	28	5	126	0	4621.00	4708.50
$RP-P_4S_4$-D_p-28mm	28	4	84	67.2	1771.54	1910.09
$RP-P_5S_4$-D_p-28mm	28	5	84	67.2	2535.12	2546.80
$RP-P_4S_6$-D_p-28mm	28	4	126	67.2	2429.40	2389.17
$RP-P_5S_6$-D_p-28mm	28	5	126	67.2	3112.48	3185.58
$RP-P_4S_4$-D_p-30mm	30	4	84	0	3209.12	3200.00
$RP-P_4S_6$-D_p-30mm	30	4	126	0	3660.42	4002.61
$RP-P_5S_6$-D_p-30mm	30	5	126	0	5215.34	5336.83
$RP-P_4S_4$-D_p-30mm	30	4	84	67.2	2130.64	2164.99
$RP-P_4S_6$-D_p-30mm	30	4	126	67.2	2702.00	2708.00
$RP-P_5S_6$-D_p-30mm	30	5	126	67.2	3785.32	3610.68
$RP-P_5S_6$-D_p-32mm	32	5	126	0	6009.30	6049.01
$RP-P_5S_6$-D_p-32mm	32	5	126	67.2	4413.36	4092.51

Table 5.5 Summary of results from regression analyses on finned-pile groups

Description	L_p **(mm)**	**n**	**S (mm)**	**e (mm)**	$(L_u)_{Actual}$ **(N)**	$(L_u)_{Predicted}$ **(N)**
$FP-P_4S_4$-L_p-665mm	665	4	84	0	3000.66	2892.37
$FP-P_5S_4$-L_p-665mm	665	5	84	0	3537.20	4028.55
$FP-P_4S_6$-L_p-665mm	665	4	126	0	3783.60	4200.04
$FP-P_5S_6$-L_p-665mm	665	5	126	0	5554.96	5849.91
$FP-P_4S_4$-L_p-665mm	665	4	84	67.2	2065.36	1798.87
$FP-P_5S_4$-L_p-665mm	665	5	84	67.2	2473.60	2505.51
$FP-P_4S_6$-L_p-665mm	665	4	126	67.2	2580.40	2612.17
$FP-P_5S_6$-L_p-665mm	665	5	126	67.2	3700.52	3638.29
$FP-P_4S_4$-L_p-532mm	532	4	84	0	2823.60	2552.44
$FP-P_5S_4$-L_p-532mm	532	5	84	0	3346.04	3555.09
$FP-P_4S_6$-L_p-532mm	532	4	126	0	3664.40	3823.21
$FP-P_5S_6$-L_p-532mm	532	5	126	0	5387.56	5162.40
$FP-P_4S_4$-L_p-532mm	532	4	84	67.2	1877.98	1587.46
$FP-P_5S_4$-L_p-532mm	532	5	84	67.2	2289.76	2211.05
$FP-P_5S_6$-L_p-532mm	532	5	126	67.2	3523.92	3210.70
$FP-P_4S_4$-L_p-399mm	399	4	84	0	2574.20	2252.46
$FP-P_5S_4$-L_p-399mm	399	5	84	0	3081.80	3137.28
$FP-P_4S_6$-L_p-399mm	399	4	126	0	3357.08	3270.83
$FP-P_5S_6$-L_p-399mm	399	5	126	0	4950.10	4555.69
$FP-P_4S_4$-L_p-399mm	399	4	84	67.2	1658.28	1400.89
$FP-P_5S_4$-L_p-399mm	399	5	84	67.2	2042.12	1951.20
$FP-P_4S_6$-L_p-399mm	399	4	126	67.2	2128.00	2034.26
$FP-P_5S_6$-L_p-399mm	399	5	126	67.2	3156.54	2833.36
$FP-P_4S_4$-L_p-266mm	266	4	84	0	2142.84	1987.74
$FP-P_5S_4$-L_p-266mm	266	5	84	0	2662.30	2768.57
$FP-P_5S_6$-L_p-266mm	266	5	126	0	4527.50	4020.28
$FP-P_4S_4$-L_p-266mm	266	4	84	67.2	1279.15	1236.25
$FP-P_5S_4$-L_p-266mm	266	5	84	67.2	1639.28	1721.88
$FP-P_5S_6$-L_p-266mm	266	5	126	67.2	2694.10	2500.37
$FP-P_5S_4$-L_p-233mm	233	5	84	0	2568.22	2684.01
$FP-P_5S_4$-L_p-233mm	233	5	84	67.2	1572.80	1669.29
$FP-P_4S_6$-L_p-200mm	200	4	126	0	2612.10	2712.79
$FP-P_4S_6$-L_p-200mm	200	4	126	67.2	1452.24	1687.19
$FP-P_4S_6$-L_p-166mm	166	4	126	0	2465.48	2627.45
$FP-P_4S_6$-L_p-166mm	166	4	126	67.2	1313.20	1634.12

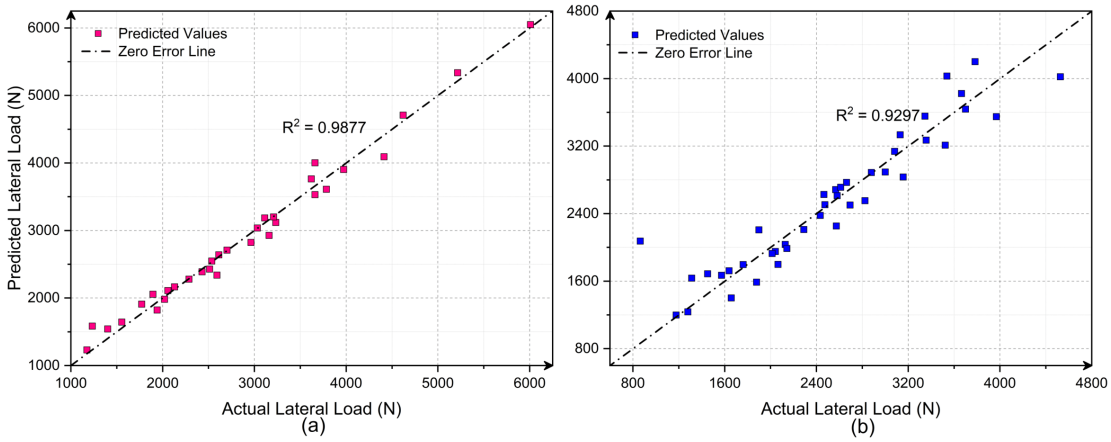

Figure 5.20 Comparison between actual and predicted lateral loads for pile-groups: (a) Regular pile-groups; and (b) Finned pile-groups

5.7 SUMMARY

The objective of this chapter was to assess the effectiveness of regular and finned pile groups in withstanding lateral loads. This was accomplished through a comprehensive investigation involving small-scale experiments and numerical simulations. Parametric studies were conducted to analyze the behavior of pile groups under different values of parameters such as the number of piles (n), pile spacing (s), and loading eccentricity. Additionally, a cost-benefit analysis was performed to compare the finned pile groups with the regular pile groups. Furthermore, the study aimed to establish a standardized correlation using regression analysis to predict the lateral resistance of both regular and finned pile groups.

he key findings of the study are summarized as follows.

- The FP-groups demonstrated a greater resistance to lateral deformation compared to the RP-group. Specifically, the pile-group efficiency (η_g) for the FP-group exhibited a 54.62% increase under non-eccentric (e=0) lateral loading conditions.
- The FP-group performs better than the regular ones when the lateral load is applied at eccentricity, i.e., the η_g for the FP-group increases by 75.65%, for eccentric (e=3.2D_p) lateral loading.
- In regular pile groups, the pile numbers in the group (n) dominates the L_u than the spacing (s). whereas in FP-groups, the spacing between piles (s) dominates the L_u than the pile numbers (n). Since fins enhance the lateral resistance, the larger pile spacing (s) provides a sufficient zone for soil to resist larger lateral resistance.
- In finned pile groups, for four piled groups (P_4), irrespective of pile spacing (s),

the individual pile action dominates over the pile-group effect, leading to higher pile-group efficiency. However, in the five piled groups (P_5), the pile-group effect dominates the individual pile effect.

- In pile group with pile spacing (s) of $4D_p$, on increasing the number of piles from four (P_4) to five (P_5), the pile group efficiency (η_g) increased for RP-group and decreased for FP-group respectively. The reduction in the efficiency (η_g) of the FP-group is attributed to the overlapping of stress bulbs caused by the smaller spacing (s) between piles in the case of the P5 group. Hence, pile spacing is crucial for FP-groups and must be higher than $4D_p$.

- The cost of regular pile groups increases by about 25% to 85% to perform similarly to the corresponding finned pile group. The finned pile groups can achieve the same level of lateral resistance as regular pile groups, with just about 75% of the material of the regular pile group.

CHAPTER 6

SEISMIC RESPONSE OF HIGH-RISE BUILDING RESTING ON FINNED PILE MAT

6.1 INTRODUCTION

Previous research in the field has typically treated the base of buildings as rigid when conducting seismic response studies. However, the amplification or de-amplification of vibrations depends on the characteristics of the structure and the properties of the soil on which it is built. When analyzing the seismic response of a rigid base multi-storied building, neglecting the amplification effects can lead to an underestimation of the actual vibrations experienced. Hence, it is beneficial to consider SSI while studying the seismic response of high-rise buildings (Fatahi et al., 2011; Kramer, 1996). The exchange of internal stresses within the system is largely influenced by the degradation of soil stiffness caused by seismic excitation, resulting in the dissipation of energy due to soil damping (Wolf and Obernhuber, 1985). Additionally, changes in the excitation across the system can also have an impact (Anand and Satish Kumar, 2018).

The performance of the structure is negatively affected by the dynamic loads resulting from both machine operation and earthquakes, leading to an amplification of damage parameters such as displacement and story drifts (Guin and Banerjee, 1998; Tabatabaiefar, 2012; Tabatabaiefar and Clifton, 2016). The response of multi-storied buildings equipped with shear walls holds greater significance, as their performance differs from buildings without shear walls (Zhang, 2022). Consequently, it is essential to implement appropriate measures that mitigate the adverse effects of earthquakes on high-rise structures.

Since lateral resistance will be of higher concern when dealing with the earthquake effects on the structure, that is responsible for creating damages of higher intensity. Hence, the sub-structure of the high-rise building must be innovative enough to resist these detrimental effects due to the high-intensity vibrations. From the recent research on finned piles, it was highlighted that they provide higher lateral resistance than conventional piles.

From the past research, finned pile foundation is one of the proven innovative

techniques (Bariker and Kolathayar, 2022a) in resisting the static lateral load. Hence, The primary objective of this study is to evaluate the seismic response of a 25-story building equipped with a shear-walls facility supported by a conventional piled-raft (RP-Mat). Additionally, an attempt is made to mitigate the seismic response of a similar building by employing the finned-pile mat system (FP-Mat). The investigation incorporates a numerical analysis approach utilizing the SSI model within the ABAQUS-CAE software.

6.2 MATERIALS AND METHODOLOGY

6.2.1 Structural Design

For the structural analysis of the high-rise building with 25-stories, the ETABS software (Etabs) was utilized, following the guidelines specified in IS 456 (2000) for concrete frame design. The plan details of the building are depicted in Figure 6.1. The dynamic analysis followed the guidelines outlined in IS 1893-1 (2016), incorporating time-history analysis using earthquake data from the El-Centro and Kobe earthquakes. The earthquake data was obtained from the PEER Earthquake database (PEER, 2022).

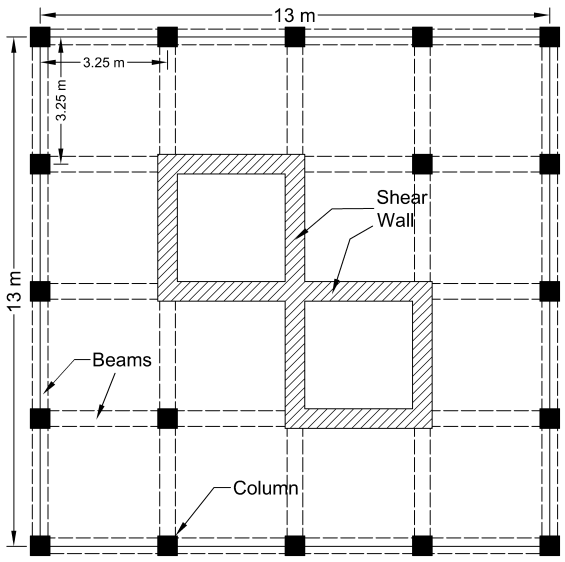

Figure 6.1 Detailed plan of the reference floor of the high-rise building used in study

The El-Centro earthquake had a magnitude (M_w) of 6.9, a time-period of 53.74 sec, and a peak acceleration of 0.349g. The Kobe earthquake had a M_w of 6.2, a time-period of 31.99 sec, and a peak acceleration of 0.276g. Figure 6.2 displays the relevant information.

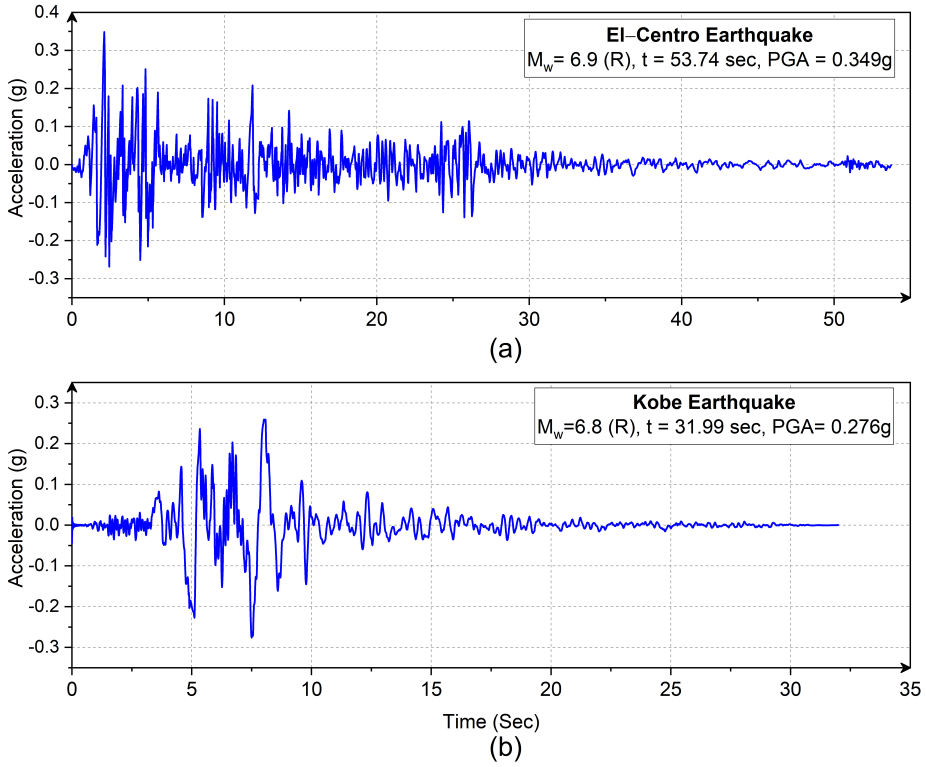

Figure 6.2 Earthquake data used for time-history analysis (a) El-Centro EQ; and (b) Kobe EQ (Source:PEER (2022))

All structural sections were of M35 grade concrete with f_{ck} of 35 MPa. The Young's modulus of concrete E_c=5000$(f_{ck})^{0.5}$ (29580 MPa) and unit weight of 25 kN/m^3, and steel rebar of Fe-500 grade steel, with f_y of 500 MPa, were used for the analysis and properties defined were as per (IS 456, 2000; CSI Computers and Structures INC, 2017). Damping of 5% within the structural members was considered for the dynamic analysis. Table 6.1 and Figure 6.3 list the structural elements' dimensions. The fixed base building's fundamental frequency and total mass were 0.547 Hz and 33.45 t. From the results of the dynamic structural design, the building period was found to be 1.827 sec and effective mass ratios was found to be 0.7195 and 0.9187 for the first three modes and at the end of all modes, respectively.

With the base reactions obtained from the structural analysis from the ETABS software, the foundation system was designed using the SAFE software. The details of the piled-raft foundation system were finalized, i.e., safe against one-way and punching shear criteria as per IS 456 (2000). The design details of the sub-structure, i.e., piled-raft foundation in which a 2m thick raft of 20m $\times$ 20m plan dimensions supported over 81 square piles with a cross-section of 0.25m^2 (9 $\times$ 9 piled configurations), and 30m length (L_p) with pile spacing's (s) of 2.25m as shown in Figure 6.3.

Table 6.1 Details of the designed sections used in the study

Section Type	**Column-1**	**Column-2**	**Column-3**	**Column-4**	**Column-5**	**Shear Wall**	**Slab**	**Beam**
Storey-level	1 to 5	6 to 10	11 to 15	16 to 20	21 to 25	1 to 25	1 to 25	1 to 25
Dimensions (m)	0.5 × 0.5	0.45 × 0.45	0.4 × 0.4	0.35 × 0.35	0.3 × 0.3	0.5m thick	0.25m thick	0.3 × 0.4
Cross section area (m^2)	0.25	0.2025	0.16	0.1225	0.09	0.5 (per m width)	0.25 (per m width)	0.12
Longitudinal Reinforcement (N#bar,mm)	12#24	12#24	12#24	12#20	12#20	#12@150	#16@250	3#12 (Top) 4#16 (Bot.)
Tie reinforcement (#bar@spac,mm)	#10@75	#10@125	#10@180	#10@200	#10@225	#10@200	–	#10@180

6.2.2 Material Properties

For this seismic soil interaction study, the soil was collected from one of the Mangalore Special Economic Zone (MSEZ) sites, and soil properties were tested as per SP 36 (Part1) (1987). The soil was classified as low compressible silt – sandy silt (ML-SM) as per ASTM D-2487-17e1 (2017). The high-rise building with 25 stories is modelled using M35 grade concrete in accordance with the specifications provided in IS 456 (2000). The building's sub-structure, known as the Piled-Mat, is designed to be embedded in silty soil. The properties of the soil and structural elements (M35 Concrete) used in the SSI analysis are consistent with those employed in the structural design. The specific details of these properties can be found in Table 6.2.. The dilation angle of 1° was used to avoid the divergence in the FEM analysis. The structural elements are defined as Visco-elastic materials, where a structural damping of 5% was employed in the analysis, which was incorporated using Rayleigh coefficients (α = 0.2015 and β = 0.012) determined based on the modal frequencies. The results were compared and validated against the findings of Zhang and Far (2022), specifically regarding the maximum lateral deformation of both fixed-base and flexible-base structures. Figure 6.4 illustrates the comparison between the present study and Zhang and Far (2022), demonstrating a strong agreement between the two models.

Table 6.2 Material properties used in the study

Characteristic Properties	**Soil**	**Structural Elements**
Material model	Mohr–Coulomb Model	Visco-elastic Model
Unit Weight, γ (kN/m^3)	15.5	25
Density, ρ (kg/m^3)	1580	2548
Young's Modulus, E (MPa)	28	29,580
Poisson's ratio, ν	0.33	0.2
Friction angle, ϕ (°)	22	–
Dilatancy angle, ψ (°)	1	–
Cohesion, c (kPa)	24	–
Void ratio, e	0.882	–

6.3 3D FEM MODELING

ABAQUS-CAE software was used to study the dynamic soil-structure interaction, in which the Rayleigh coefficients (α and β) were calculated considering the frequency-dependent damping from the different modes of the soil-foundation (Park

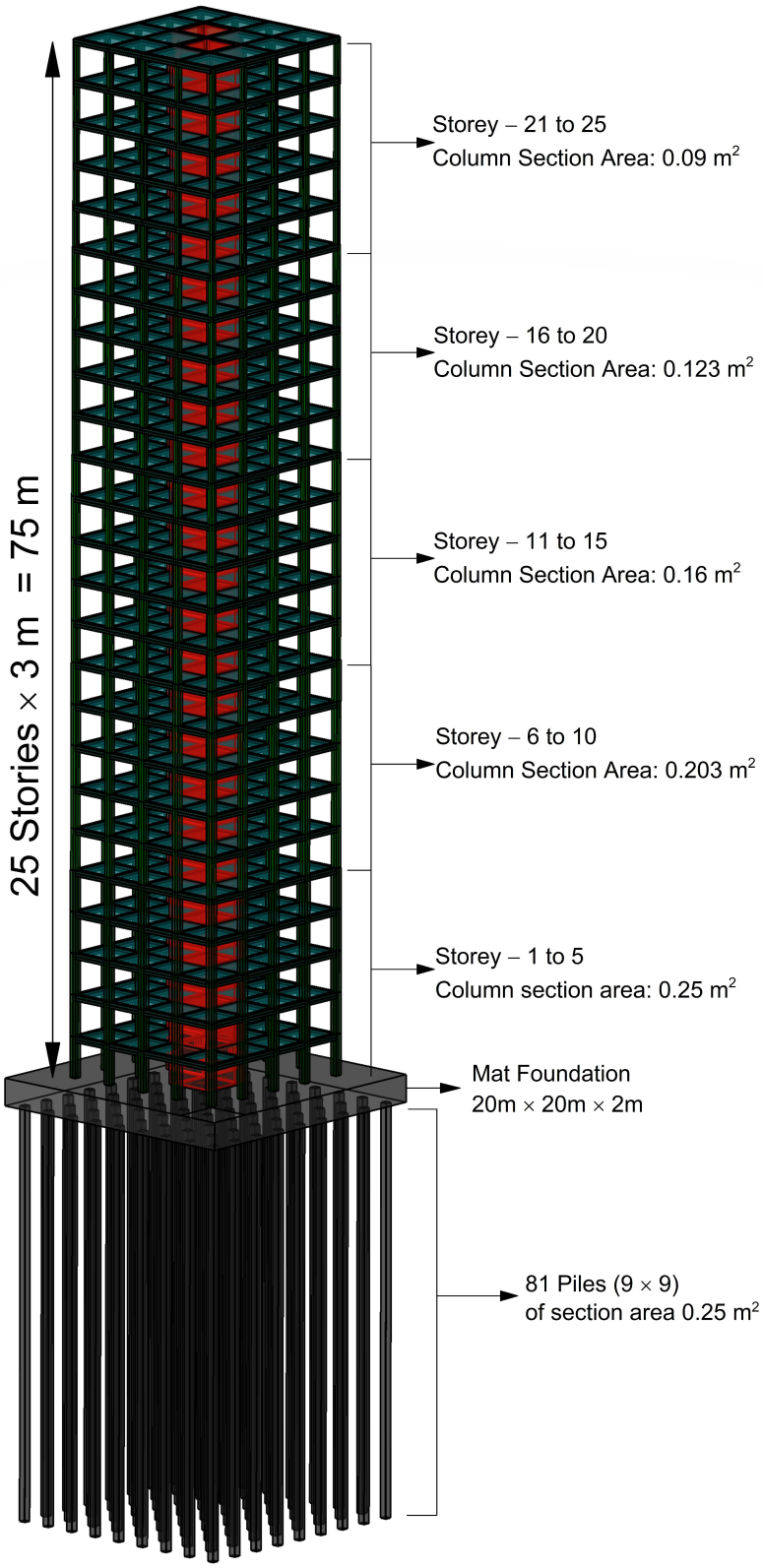

Figure 6.3 Detailes of designed sections of high-rise building used for analysis

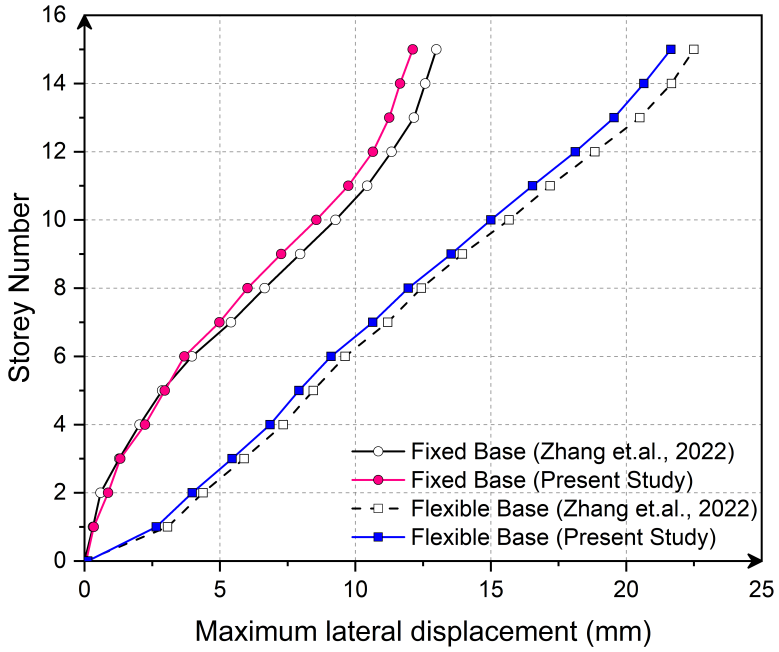

Figure 6.4 Variation of the lateral displacement with story height and validation of the present model with Zhang and Far (2022)

and Hashash, 2004). The α and β utilized in the study were 0.758 and 0.012, respectively. Each structural element detailed above in Table 6.1 was modelled as separate parts and assembled at their respective positions. It was later merged to form the super-structure part of the high-rise building, as shown in Figure 6.3. The Piled-Raft is modelled as a single part by defining the raft as 2m thick and extruding the piles of 30m length beneath it. Cut geometry command was used to cut the unwanted part of the soil, i.e., to excavate the soil portion occupied by pile-raft.

In order to account for soil-structure interaction, a surface-to-surface contact approach was employed to establish interactions between each pile, mat, and the surrounding soil. In cases involving softened soil between the soil and structure, the soil surface was designated as the slave surface, while the pile or mat served as the master surface for soil-pile and soil-mat interactions, respectively. Tangential contact (friction contact) was incorporated into the analysis through the definition of tangential contact, which was based on contact pressure data and aimed to simulate the Mohr-Coulomb failure criteria, as represented by equation (6.1). (Nasr, 2014; Van Nguyen et al., 2017; Yaghobi et al., 2019).

$$(Shear\ Strength)_{inter} = R_{inter}(Shear\ Strength)_{soil} \tag{6.1}$$

To account for practical geotechnical considerations, R_{inter} of 0.75 was implemented (Kim et al., 2011; Fatahi et al., 2014), this factor helps reduce the interface shear strength, which is influenced by factors such as the roughness of the pile and the construction method employed in the field (Belinchon et al., 2016).

To optimize computational efficiency, a mesh sensitivity analysis was conducted. Multiple element distributions were employed for meshing, ranging from very coarse to refined, resulting in element counts of 27,628, 68,248, 134,462, 268,612, 352,840, and 153,572, respectively. After evaluating both computational time and result accuracy, it was determined that the refined element distribution offered the most optimal balance for meshing, surpassing the other element distributions in terms of efficiency; hence, the refined element distribution was adopted for model meshing. Indeed, finer meshing was used near points where large amounts of stress were concentrated, and coarser meshing was used in places that were further away from these highly concentrated areas of stress. The soil and structural elements were defined as solid parts, and they were coupled with C3D8R elements to avoid reflecting earthquake vibrations into the model. The far-field soil was modelled using the infinite CIN3D8 elements that were used to absorb the vibrations from the unbound soil, as illustrated in Figure 6.5.

To prevent any translation of the soil base in all three directions during the initial step, appropriate boundary conditions were imposed ($U_X = U_Y = U_Z = 0$). Since earthquake loading was applied in the x-direction, translation in the x-direction (U_X) was allowed when performing the time–history analysis during the earthquake step. In addition, the sides of the soil model were constrained from undergoing translation in both the x and y directions ($U_X = U_Y = 0$) during both steps. The complete three-dimensional model used for the time–history analysis is shown in Figure 6.5.

6.4 NUMERICAL ANALYSIS PROGRAM

The provision of SSIs is a proven technique with which to predict the structure's actual response. Previous literature (Han, 2002; Galal and Naimi, 2008; Bilotta et al., 2015; Bagheri et al., 2018; Arboleda-Monsalve et al., 2020; Scarfone et al., 2020) has reached the consensus that the pile-raft technique serves as a viable alternative approach for investigating SSI and mitigating potential adverse effects on buildings. This is because remedial foundation techniques cannot nullify post-earthquake effects on buildings. However, they can be maximally reduced to reduce the detrimental effects of earthquakes on high-rise buildings.

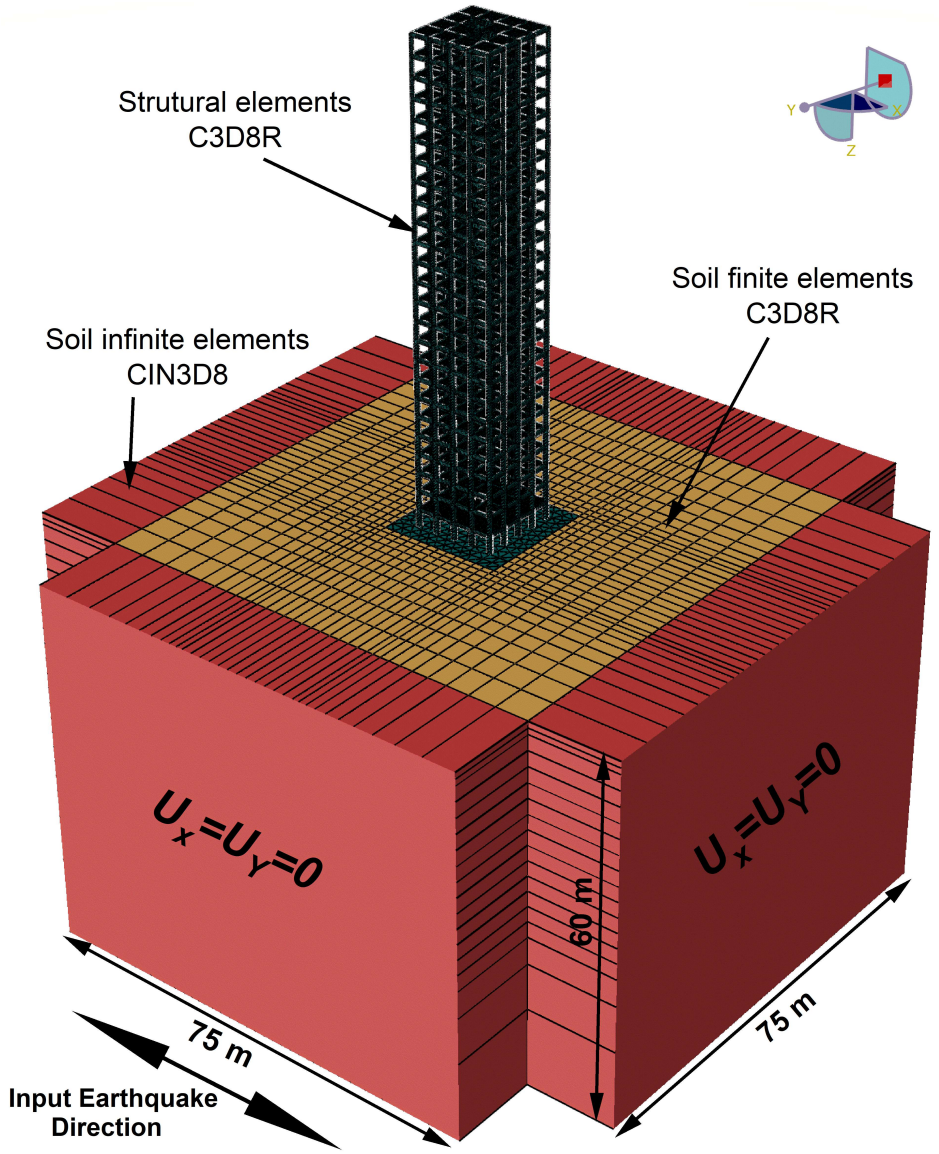

Figure 6.5 3D Finite element SSI meshed model in ABAQUS

The use of finned piles is an innovative technique that has an efficient lateral response over regular piles in a system. To establish the effectiveness of a finned pile-mat system, time-history analyses were conducted on a high-rise building. The response of the building supported by the finned pile-mat system was compared with that of a regular pile-raft system. The schematic view of the regular piled–raft and finned pile raft is shown in Figure 6.6. The size of each pile used in the study was calculated as B $\times$ B (0.5 m $\times$ 0.5 m), and their lengths were calculated as L_p (30 m). In addition, finned piles, with fin widths (W_f), assumed to have the same as pile width (B), i.e., 0.5 m, fin thicknesses t_f (0.15 m), and fin-lengths (L_f) as those in the regular pile.

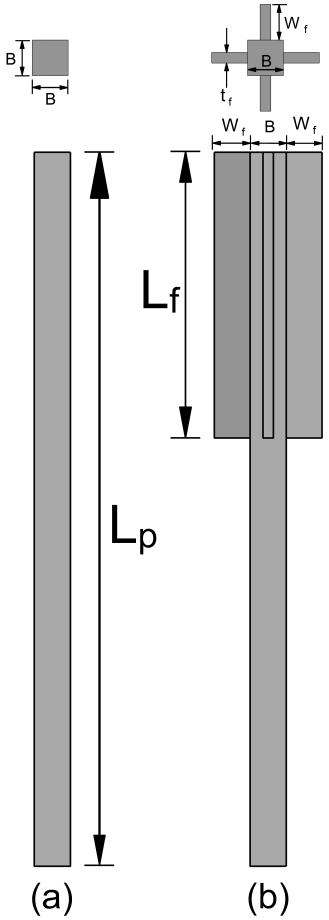

Figure 6.6 Schematic representation of the pile models: (a) regular pile and (b) finned pile

The SSI numerical analyses program performed using ABAQUS is shown in Table 6.3. The series I analyses were performed with an RP-Mat (regular pile-mat), and the response of the RP-Mat will serve as a reference for comparison. A set of Series II analyses was conducted utilizing an FP-Mat (finned pile-mat) system,

the analyses involved varying the fin lengths (L_f/L_p) at 0.2, 0.4, 0.6, and 0.8, respectively. The resulting responses from these analyses will provide crucial data to assess the effectiveness of the FP-Mat in mitigating the effects of earthquake loading conditions. The responses are recorded in terms of the seismic damage parameters: peak acceleration, peak displacement, inter-story drift, and drifting bounds. The story-drift (IS 1893-1, 2016) and inter-story drift (Zhang and Far, 2022) are calculated as shown in (6.2) and (6.3). The inter-story drift ratio plays an important role in deciding the detrimental effects of an earthquake on a building, as it defines the average rotation angle between the column and beams.

Table 6.3 Details of the designed sections used in the study

Series	Description	Constant parameters	Varying parameters
I	Regular Pile-Raft (RP-Raft)	Piles: L_p = 30 m, size = 0.5 m × 0.5 m, Mat: 2 m thick, size = 20 m × 20 m	–
II	Finned Pile-Raft (FP-Mat)		Fin-length (L_f/L_p) of 0.2, 0.4, 0.6, and 0.8

$$Storey\ Drift = \left\{ u_{(i+1)} - u_i \right\} \tag{6.2}$$

$$Inter\ Storey\ Drift = \left\{ \frac{Storey\ Drift}{Storey\ Height} \right\} \times 100 \tag{6.3}$$

Where, u is the displacement in each story, and i is the story number under consideration.

6.5 ANALYSIS OF REGULAR-PILE MAT

To study the response of the 25-story building that was supported using an RP-Mat, an analysis was performed using a 3D FEM model of an RP-Mat; the details for which are mentioned in series I of Table 6.3, and they are shown in Figure 6.6. The response of the model was aggregated in the form of time–history plots (i.e., acceleration variation and inter-story drift experienced by various floor levels of the building). Figure 6.7 and Figure 6.8 display the acceleration (time-history) plots for the El-Centro and Kobe earthquakes, respectively. It was observed that the building experienced higher acceleration levels at upper floor levels. The peak acceleration (a_p) varied from 0.012 g at the base to 0.25 g (equivalent to 71.6% of the applied earthquake) and from 0.0157 g at the base to 0.3238 g (equivalent to 117.3% on the top floor, 25^{th} floor) of the building.

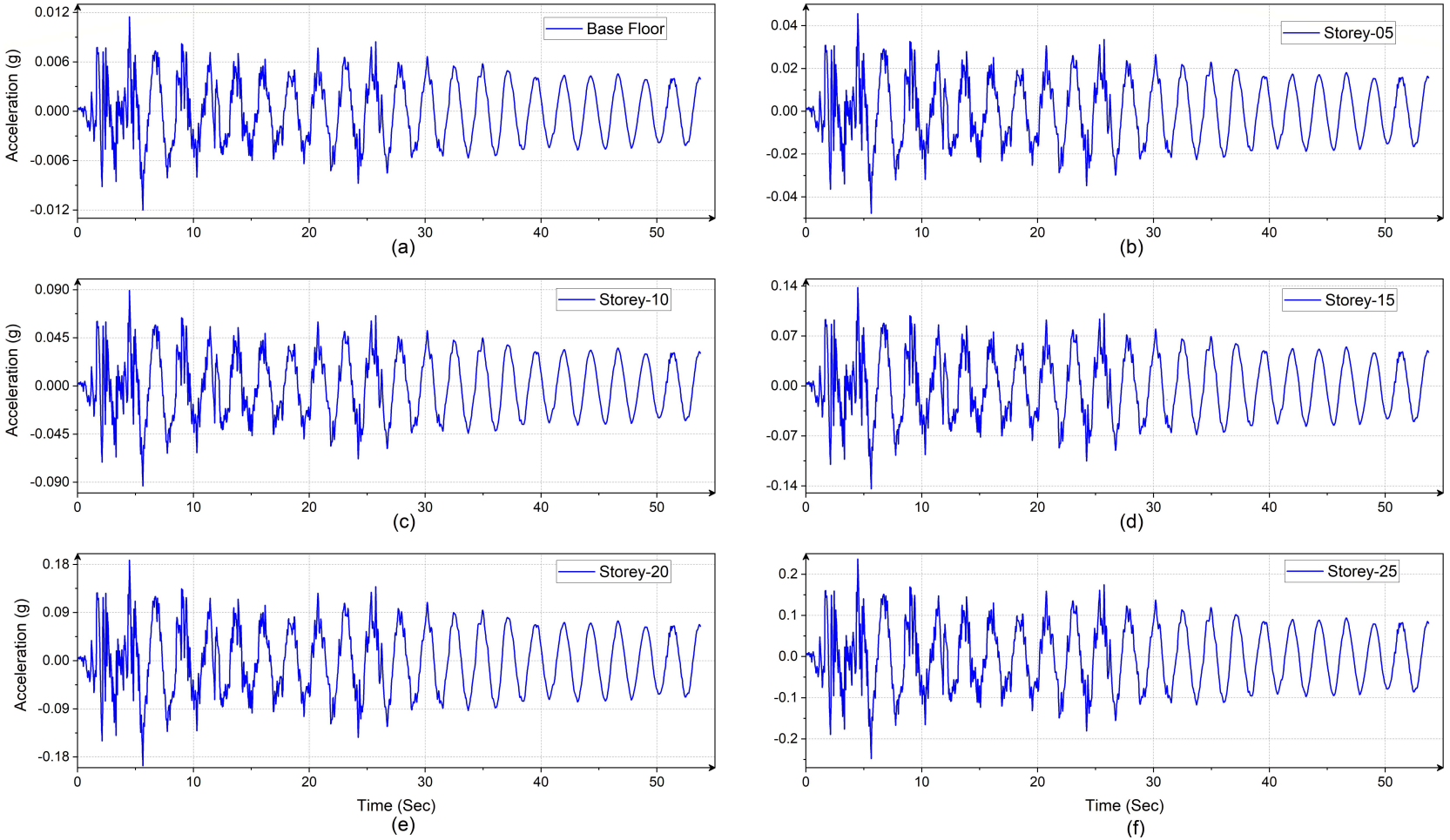

Figure 6.7 Acceleration (time–history) plots of the various story levels of the building under El-Centro Earthquake: (a) Base Floor; (b) Story-05; (c) Story-10; (d) Story-15; (e) Story-20; and (f) Story-25

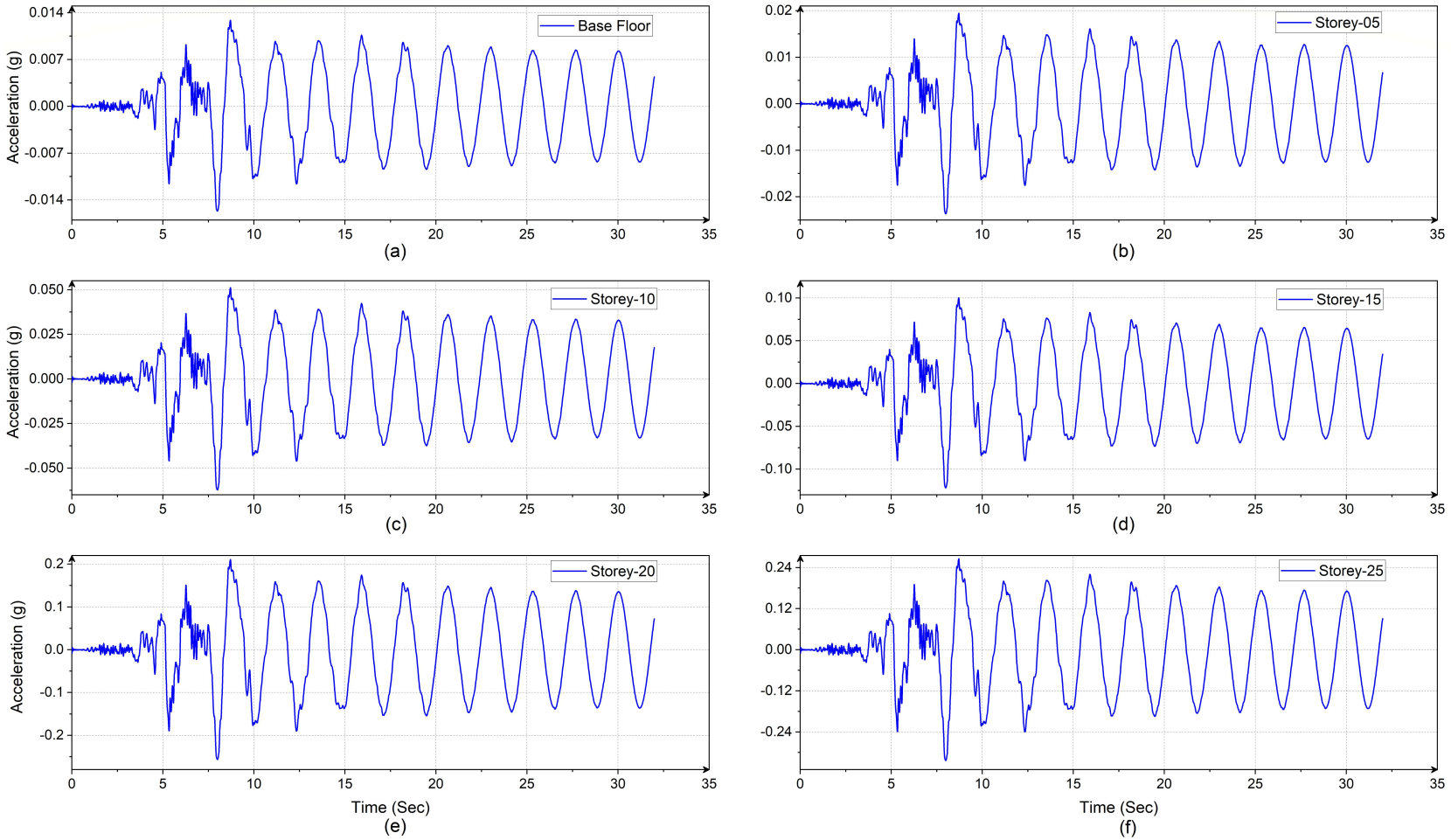

Figure 6.8 Acceleration (time–history) plots of the various story levels of the building under Kobe Earthquake: (a) Base Floor; (b) Story-05; (c) Story-10; (d) Story-15; (e) Story-20; and (f) Story-25

Figure 6.9 presents the variation of inter-story drifts. It was observed that the inter-story drifts increased progressively towards higher floors. This behavior can be attributed to the amplified vibrations experienced by the building, as depicted in Figure 6.7 and Figure 6.8.Furthermore, as the floor level increased, the building exhibited greater inter-story drifts of 6.82 s and 8.02 s. The maximum story drift measured approximately 0.0084 m and 0.0122 m, resulting in inter-story drifts of 0.28% and 0.41% for the El-Centro and Kobe earthquakes, respectively. As per IS 1893-1 (2016), the permissible story drift must be within 0.012 m, i.e., the building performs well under El-Centro earthquake but is not safe under Kobe earthquake (maximum story drift is 0.0122m $>$ permissible story drift); Therefore, in order to investigate the effectiveness of the FP-Mat in reducing the seismic response of the building, the available model was further analyzed to examine potential improvements.

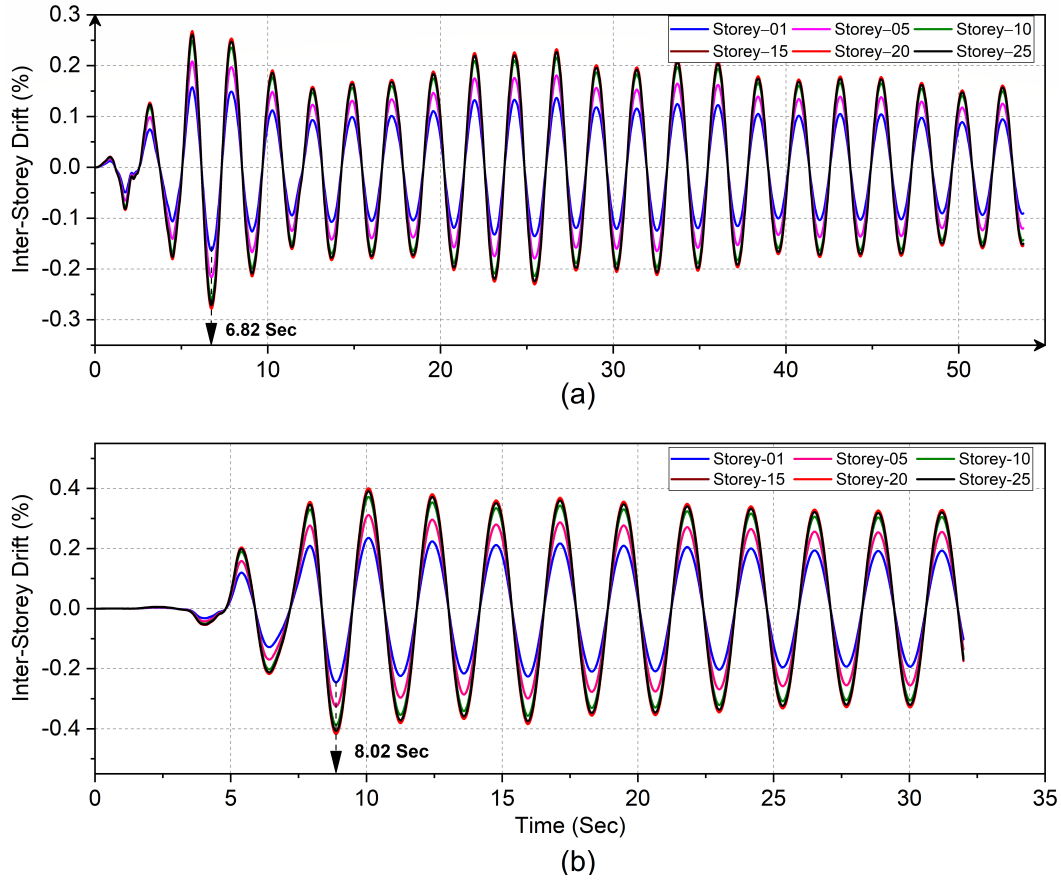

Figure 6.9 The time–history plot of the inter-story drift for various floors of the building resting on RP–Mats under (a) El-Centro EQ; and (b) Kobe EQ.

6.6 ANALYSIS OF FINNED-PILE MAT

In order to assess the impact of the finned pile-mat (FP-Mat) system on mitigating the seismic response of a high-rise structure, analyses were conducted on FP-Mats with different fin-lengths (L_f/L_p). The fin-lengths examined were 0.2, 0.4, 0.6, and 0.8, respectively. The 3D models of the FP-Mats utilized in this study are shown in Figure 6.10 below. The time–history analyses were performed on FP-Mats that were similar to RP-Mats, using the El-Centro and Kobe earthquake data (Figure 6.2).

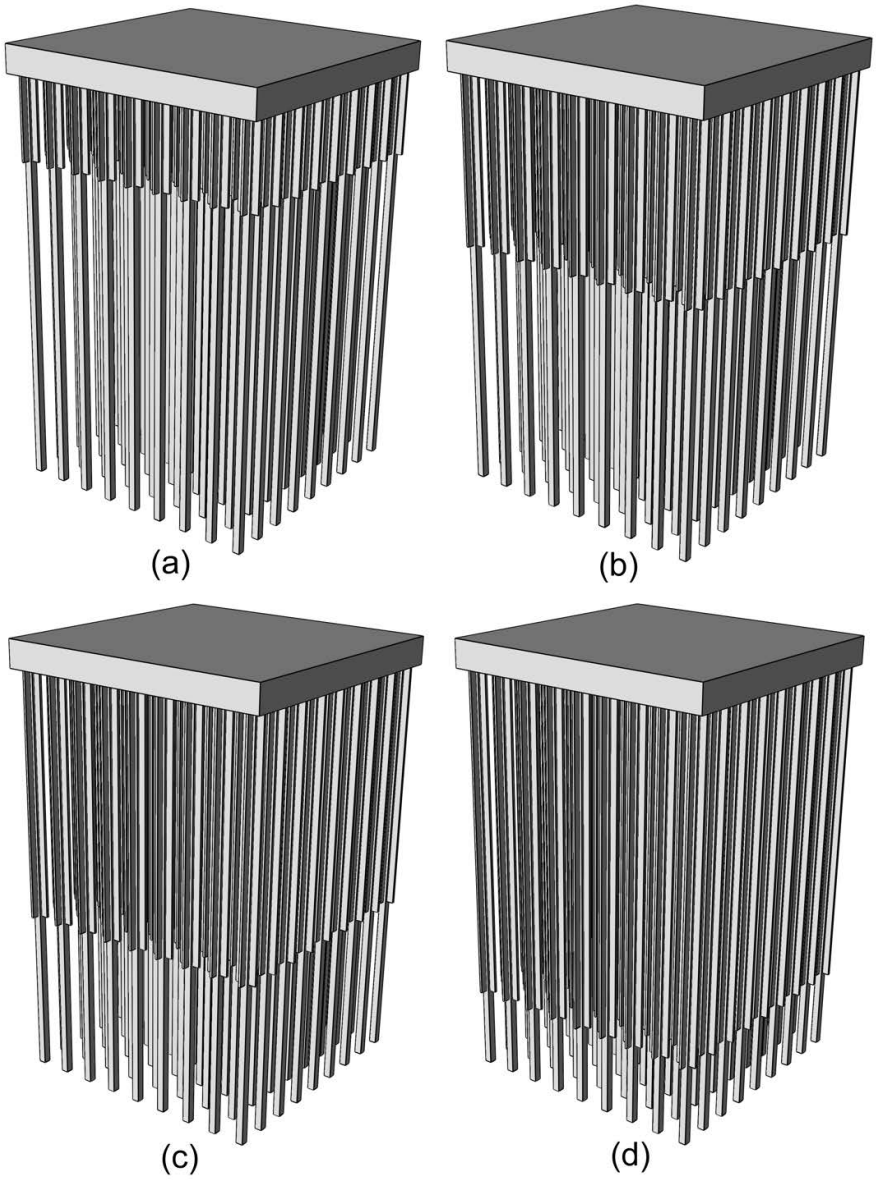

Figure 6.10 Three-dimensional finned pile-mats of varying fin-lengths (L_f/L_p) used in the SSI analyses: (a) $L_f = 0.2L_p$; (b) $L_f = 0.4L_p$; (c) $L_f = 0.6L_p$; and (d) $L_f = 0.8L_p$.

6.6.1 Time–History Plots

The time–history plots (acceleration and inter-story drift) for various floor levels of high-rise building, which were supported by the FP-Mats mentioned above, are illustrated in Figure 6.11 to Figure 6.14, respectively. Providing an FP-Mat under a high-rise building enhances the structure's performance under seismic loading. The peak acceleration and inter-story drift of the top floor were reduced by more than 90%, compared with the RP-Mat, thereby reducing the effects of detrimental vibrations on the building.

6.6.2 Impact of Fin-Length on the Seismic Response of the Structure

In order to investigate the influence of the fin-length (L_f) of finned piles in FP-Mats on a high-rise building, a visualization module in ABAQUS was utilized to create a path spanning from the base floor to the top story of the building. This path allowed for the extraction of key output parameters, such as peak acceleration, peak horizontal displacement, and inter-story drift, along the defined path. The analysis focused on the natural period of the piled-mat system, and the results are presented in Figure 6.13 and Figure 6.14.

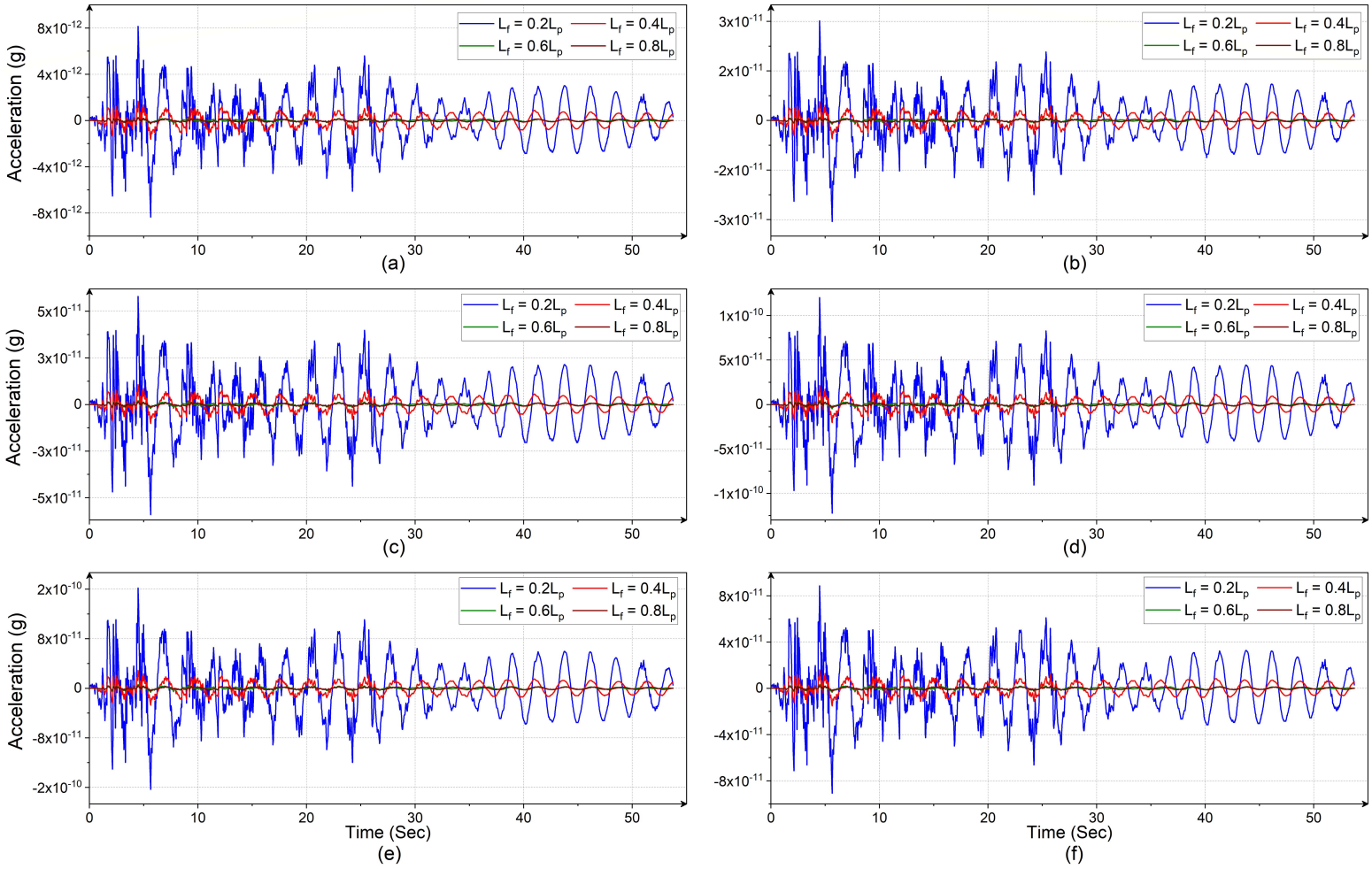

Figure 6.11 Time–history plots of the FP-Mats for the various floor-levels of the high-rise building under El-Centro earthquake: (a) Base Floor; (b) Floor-05; (c) Floor-10; (d) Floor-15; (e) Floor-20; and (f) Floor-25

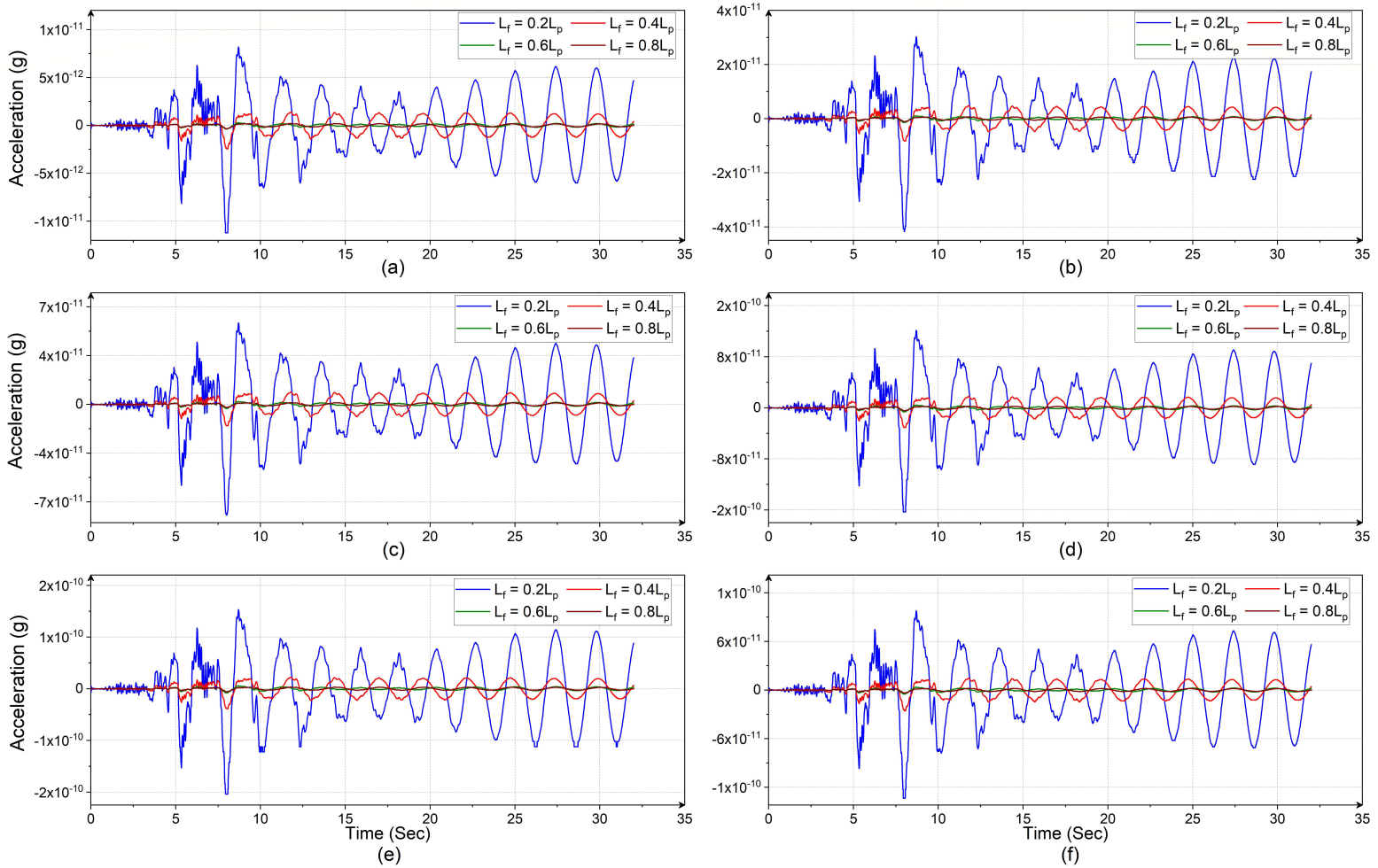

Figure 6.12 Time–history plots of the FP-Mats for the various floor-levels of the high-rise building under Kobe earthquake: (a) Base Floor; (b) Floor-05; (c) Floor-10; (d) Floor-15; (e) Floor-20; and (f) Floor-25

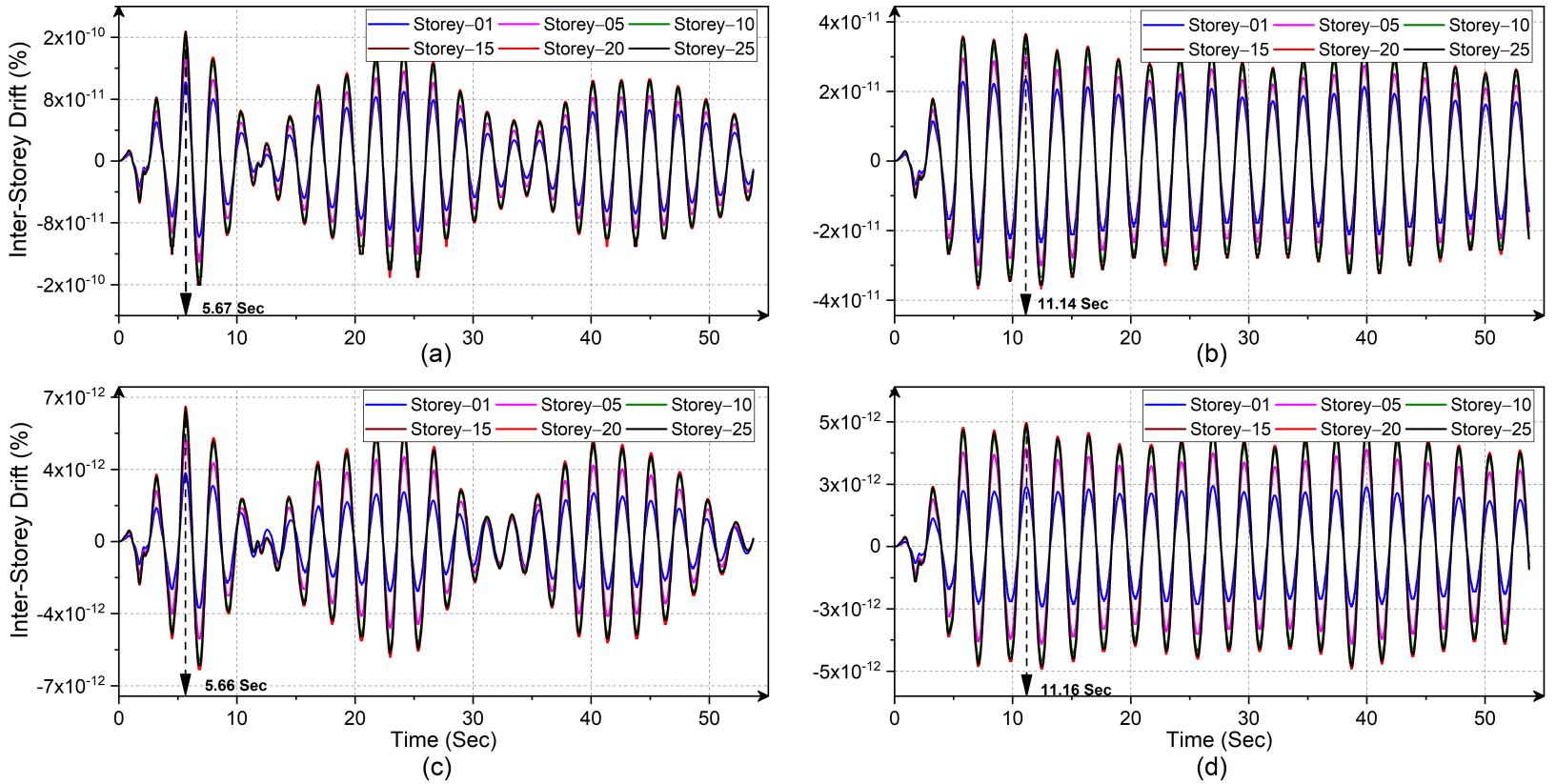

Figure 6.13 Time–history plots for the inter-story drifts of various floor levels for the structure resting on FP-Mats of different fin-lengths under El-Centro earthquake: (a) $L_f = 0.2L_p$; (b) $L_f = 0.4L_p$; (c) $L_f = 0.6L_p$; and (d) $L_f = 0.8L_p$

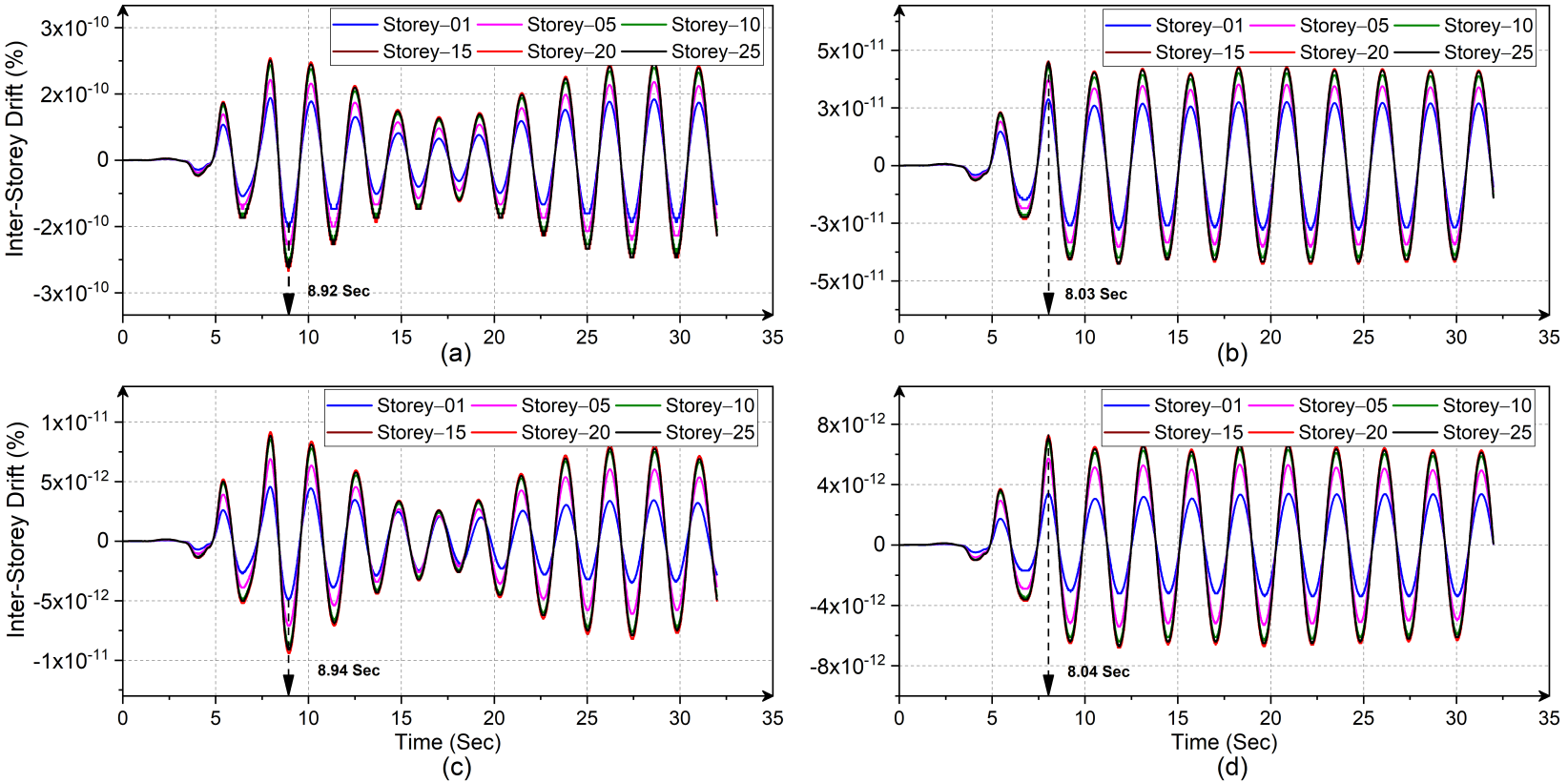

Figure 6.14 Time–history plots for the inter-story drifts of various floor levels for the structure resting on FP-Mats of different fin-lengths under Kobe earthquake: (a) $L_f = 0.2L_p$; (b) $L_f = 0.4L_p$; (c) $L_f = 0.6L_p$; and (d) $L_f = 0.8L_p$

6.6.2.1 Variation in Peak Acceleration

The variation in peak acceleration for all floor levels was plotted for all considered FP-Mats of various fin-lengths, as shown in Figure 6.15. Observations revealed that the building exhibited increased stiffness for all piled mats beyond the 10th story. This observation is further supported by the similarity in the time-history plot of inter-story drift for floor levels above Story-10, as depicted in Figure 6.11 and Figure 6.12. Figure 6.15 shows that the peak acceleration experienced by the top floors ranges between 15 to 20 times that of the base floor. Additionally, the presence of the FP-Mat resulted in a reduced reduction in peak acceleration compared to the RP-Mat.

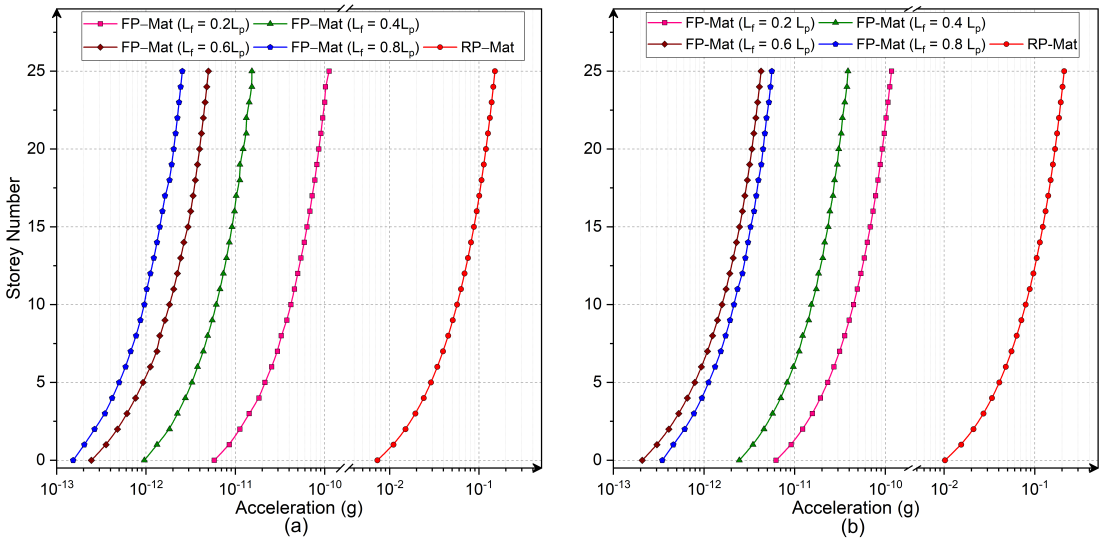

Figure 6.15 Variation in peak accelerations along the height of building resting on FP-Mats of varying fin-lengths for (a) El-Centro; and (b) Kobe EQ

6.6.2.2 Variation in Peak Horizontal Displacement

The variation in the peak horizontal displacement (u) of the high-rise building for all floor levels, using various piled mats, is presented in Figure 6.16. An observation was made that the horizontal displacement on the top story was around 20.7 times larger than that of the base floor when employing the RP-Mat. With the utilization of the FP-Mat, the horizontal displacement on the top floor was found to be 16 to 18 times greater than that of the base floor for the El-Centro earthquake, and 16 to 19 times greater for the Kobe earthquake. Notably, the horizontal displacement values for the FP-Mats with fin-lengths (L_f) of $0.6L_p$ and $0.8L_p$ were observed to be identical. This suggests that the structure becomes less vulnerable to vibrations, further reinforcing its stability. Considering the seismic performance and economical construction, $0.6L_p$ may be considered the optimum fin-length for improving the seismic response.

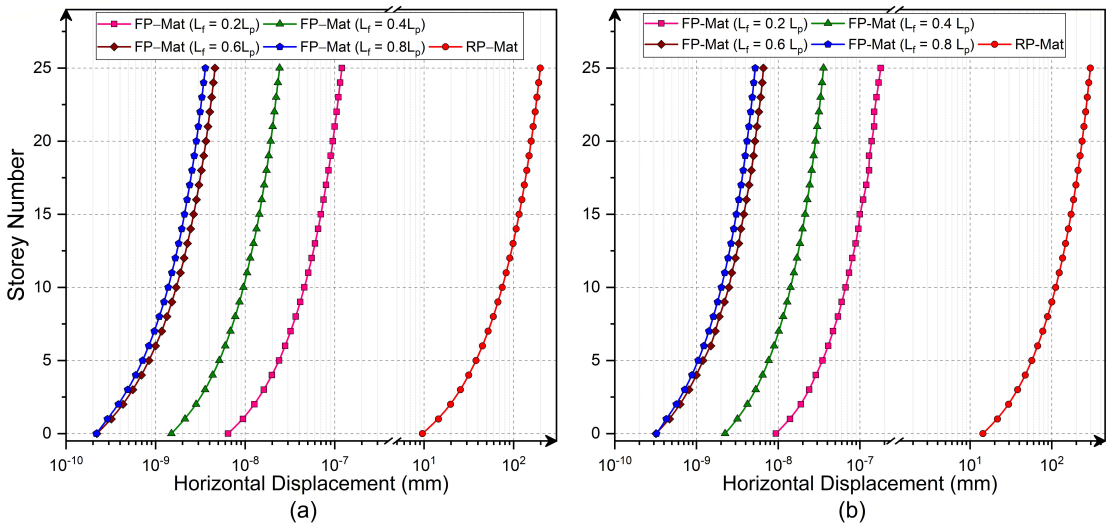

Figure 6.16 Variation in the peak horizontal displacements for various FP-Mats with varying fin-lengths for (a) El-Centro EQ; and (b) Kobe EQ

6.6.2.3 Variation in Inter-Story Drift

The variation of the inter-story drift for high-rise buildings resting on various FP-Mats and RP-Mats is shown in Figure 6.17 and Figure 6.18. It was observed that buildings resting on RP-Mats show softened inter-story drift variations, and FP-Mats show stiffer responses than RP-Mats. In terms of FP-Mats, an increase in the fin-length (L_f) increases the stiffening behaviour of the building. Stiffer behaviour means the same horizontal displacement for two consecutive floors (i.e., inter-story drift). To ensure that the building exhibited stiff behaviour, the story numbers 16, 13, 11, and 9 corresponded with fin-lengths (L_f/L_p) of 0.2, 0.4, 0.6, and 0.8, respectively. The lower the inter-story drift, the less damage is caused to the building due to seismic activities.

As the buildings supported by FP-Mats experience fewer vibrations, displacements, and inert-story drifts, FP-Mats are more advantageous for high-rise buildings than RP-Mats. Furthermore, the utilization of varying fin lengths in a piled-mat system led to a reduction in the difference between the maximum and minimum inter-story drifts. The drifting bounds of the FP-Mat system were diminished by increasing the fin lengths. Specifically, the difference between the maximum and minimum inter-story drifts was found to be 0.115% for the RP-Mat. However, for FP-Mats with fin lengths (L_f/L_p) of 0.2, 0.4, 0.6, and 0.8, the differences were 6.57×10^{-11}%, 1.23×10^{-11}%, 3.0×10^{-12}%, and 2.6×10^{-12}%, respectively. This signifies that as the fin length increased, the average rotation between the beam and column within the same story was significantly reduced, resulting in a more sustainable design.

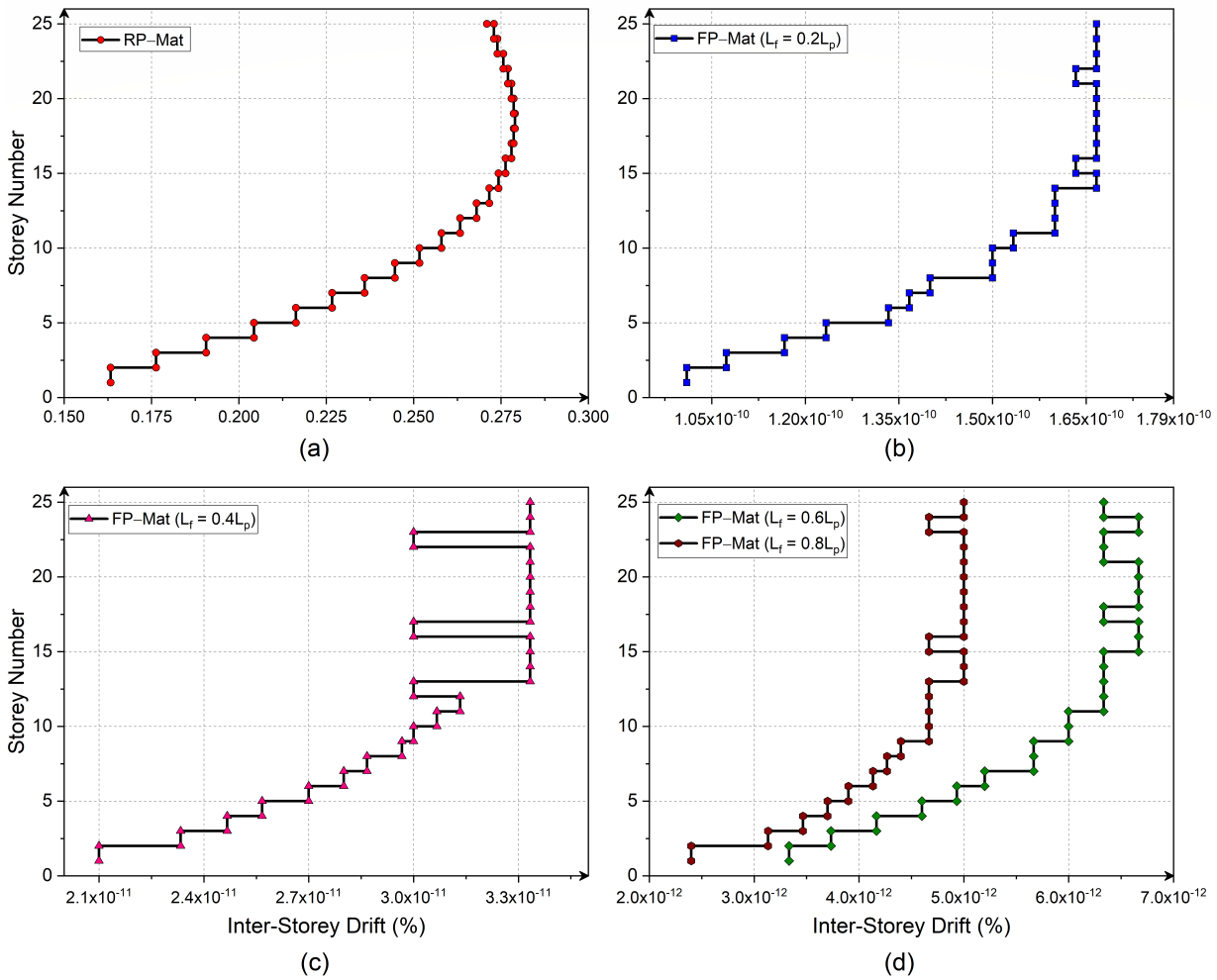

Figure 6.17 Variation in the inter-story drifts for buildings resting on various piled-mats under El-Centro earthquake: (a) RP-Mat; (b) FP-Mat: $L_f = 0.2L_p$; (c) FP-Mat: $L_f = 0.4L_p$; and (d) FP-Mats: $L_f = 0.6L_p$, and $0.8L_p$.

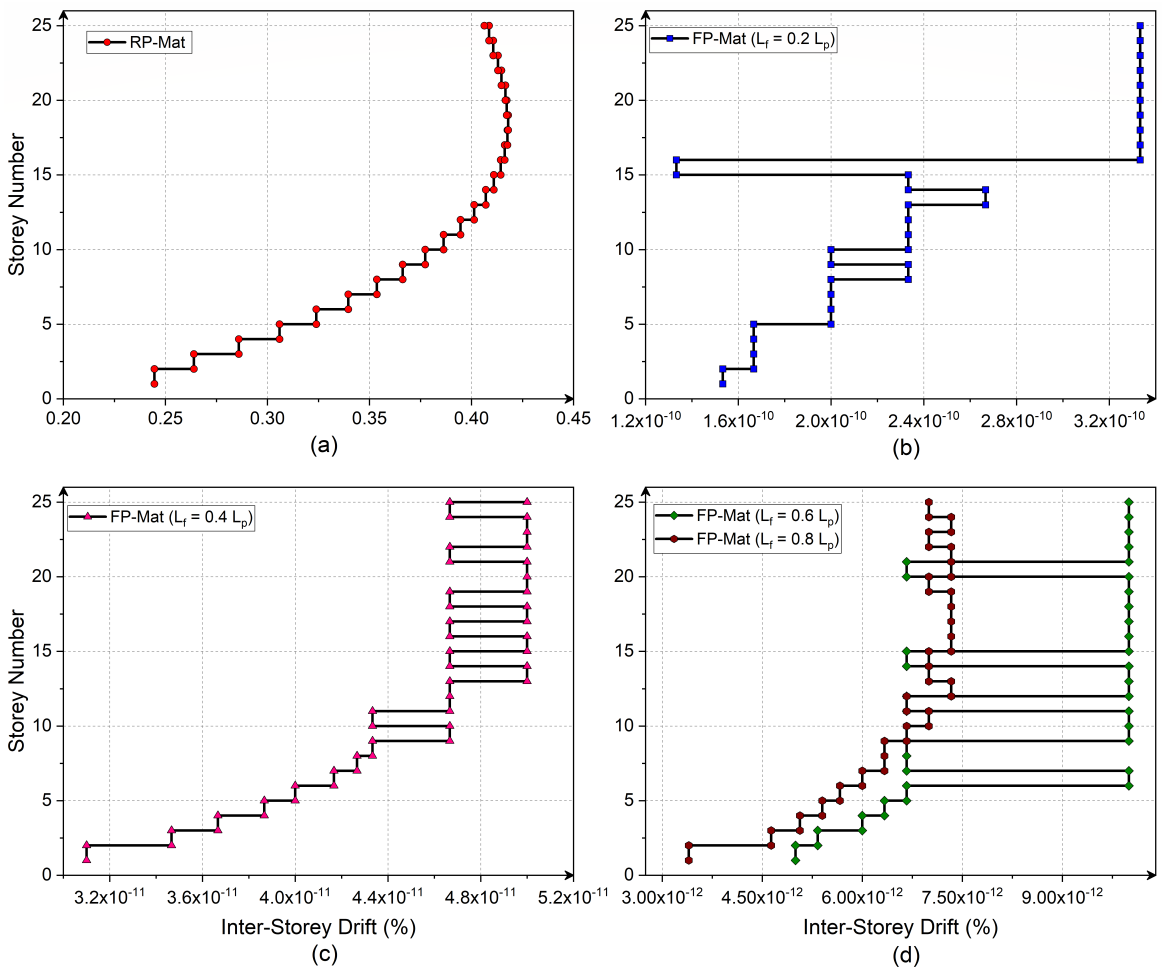

Figure 6.18 Variation in the inter-story drifts for buildings resting on various piled-mats under Kobe earthquake: (a) RP-Mat; (b) FP-Mat: $L_f = 0.2L_p$; (c) FP-Mat: $L_f = 0.4L_p$; and (d) FP-Mats: $L_f = 0.6L_p$, and $0.8L_p$.

6.7 SUMMARY

In this chapter, a novel approach was undertaken to evaluate the seismic response of RP-Mats by incorporating numerical analysis of SSI. Additionally, the effectiveness of FP-Mats with varying fin lengths in mitigating the adverse effects of earthquakes on high-rise buildings was investigated. The following conclusions were drawn based on a series of numerical SSI simulations conducted on a 25-story high-rise building, utilizing far-field time history data from the El-Centro and Kobe earthquakes.

- The maximum peak acceleration and horizontal displacement of the high-rise building supported by piled mats stay the same as we move toward the top story. Instead, it shows stiffer behaviour in a particular story (Story-10 in the present study), and variation after that remains almost linear.

- Provision of fins in the piled mats drastically reduces detrimental vibrations due to earthquakes. Finned piles, with a fin-length (L_f) of just $0.2L_p$, can reduce the seismic response of multi-storied buildings by more than 98%.

- The fin-length (L_f) has a high level of influence over the effect of the seismic response (i.e., regarding FP-Mats, as the fin-lengths increase, the variation between inter-story drift readings remain constant (i.e., stiffer behaviour) in subsequent stories). It is responsible for reducing story displacements due to seismic loading.

- FP-Mats with fin-lengths (L_f) of $0.6L_p$ and $0.8L_p$ showed nearly identical horizontal displacement variation; hence, considering the seismic performance and economical construction, $0.6L_p$ may be considered the optimum fin-length for reducing the seismic response.

- Compared with the RP-Mat, the using FP-Mats during the construction of high-rise buildings can reduce horizontal displacement by 1.7×10^9, 8.2×10^9, 4.3×10^{10}, and 5.5×10^{10} for FP-Mats with fin-lengths (L_f/L_p) of 0.2, 0.4, 0.6, and 0.8, respectively.

- The drifting bounds of the FP-Mat system were reduced by increasing the fin lengths, thereby reducing the average rotation between the beam and column within the same story.

CHAPTER 7

SEISMIC RESPONSE OF WIND TURBINE RESTING ON FINNED PILE MAT

7.1 INTRODUCTION

The global cumulative capacity of wind power has been experiencing a significant growth rate, approximately doubling every three years, as stated in the annual report by Global Wind Energy Council (2014). This trend is expected to continue, and the expansion rate may even accelerate. While the structural design and evaluation of wind turbines against environmental factors have been the primary focus of research in this field, there is now a growing need to carefully assess their seismic performance. The need is emphasised by the recent construction of many wind turbines in earthquake-prone regions across the world (Katsanos et al., 2016).

In 2021, the wind turbines contributed about 6.6% of the world's electricity, which rose from 3.5% in 2015 after signing the Paris Agreement and is aimed to increase the contribution to 20% by 2030 (Zieliński et al., 2022). Hence governments support using renewable energy resources. As a benefit of wind turbines being more over areas with higher wind speeds, larger height wind turbines are being constructed to provide more power. Even though the turbines resting on piled mats are safe enough to resist the wind load, they proved critical during the earthquake. Since sensitive instruments such as electronic controllers, anemometers, hydraulics systems, nacelle, and blades are installed on wind turbines, the impacts of earthquakes may cause these components to collide and become inoperable. Hence, there is a need to reduce the earthquake effects on wind turbines by using innovative foundation techniques.

Due to its tall and slender nature, the wind turbine is susceptible to lateral stresses and deformations caused by horizontal loading. This loading can arise from wind profiles or seismic excitations, as highlighted by Katsanos et al. (2016). The concentrated lumped mass at the top of the turbine further contributes to its vulnerability to these forces.

Lateral resistance of the soil is of prime concern while dealing with the wind turbine, as wind or earthquakes indirectly induce lateral deformation, leading to severe

damages. Hence, the foundation must withstand these detrimental effects due to earthquakes. Finned-pile mat is equally eligible to reduce the vibrations induced in the high-rise building subjected to earthquake loading (Bariker and Kolathayar, 2022b). No studies are available on the analysis of finned pile foundations for special structures like wind turbines.

The objective of this chapter is to conduct a numerical analysis to assess the response of a wind turbine placed on both a regular pile mat (RP-Mat) and a finned pile mat (FP-Mat) under different earthquake excitations. The analysis will employ a finite element approach that takes into account the interaction between the soil, piles, and structure. It is important to note that the wind turbine will be assumed to be in a parked condition throughout the analyses.

7.2 METHODOLOGY

7.2.1 Structural Design

The wind turbine chosen for this study is modeled after the Siemens Gamesa SG 8.0-167 DD, which has a rotor diameter of 167m and a tower height of 130m. The tower of the wind turbine is represented schematically in Figure 7.1(a), and it features a consistent tapering design. For the foundation study, the tower and foundation part of the wind turbine was modelled of M35 concrete, with f_{ck} of 35MPa and has Young's modulus (E) of 29580 MPa as per IS 456 (2000). The tower is modelled as a chimney structure, with constant tapering throughout its length. As increased damping in the system can reduce excessive vibrations (Bisoi and Haldar, 2014; Valamanesh and Myers, 2014), this study's structural damping of 3% was considered. By conducting a modal analysis on the fixed base tower with a concentrated tip mass using STAAD Pro software, the fundamental frequency was determined to be 0.475Hz. Subsequently, a dynamic analysis of the fixed base structure yielded a period of 2.104s. Considering all modes, the participation factor was found to be 0.925.

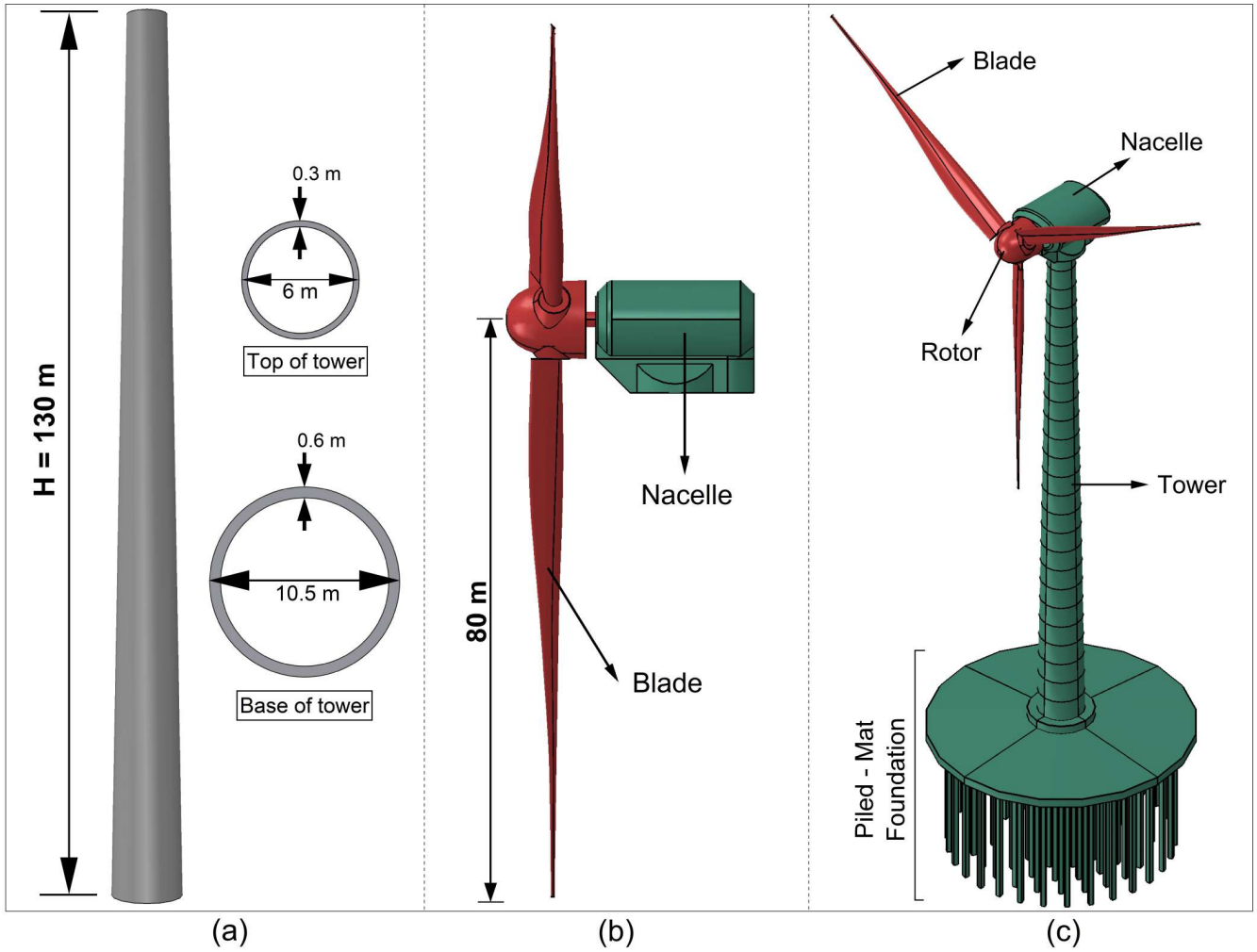

Figure 7.1 Details of (a) Tower; (b) Rotor and Nacelle Assembly (RNA); and (c) Complete 3D model of the wind turbine.

From the support reactions obtained from STAAD Pro analyses performed on the tower structure, the sub-structure part of the tower or wind turbine was designed using SAFE software. The details of the piled-raft foundation, including the capacity to endure one-way and punching shear, were finalised in accordance with IS 456 (2000).

Figure 7.2 depicts the specifications of the substructure, which is a piled-mat foundation supported by 91 square piles with a cross-section of 1 m^2. These piles were 30 m long (L_p), with pile spacing of 5 m (5 times the pile width; s = 5B), to avoid stress bulb overlapping. The sub-structure part (piled-mat) of the wind turbine was embedded in the silty soil. The properties of the soil and concrete utilized in the SSI study are presented in Table 6.2.

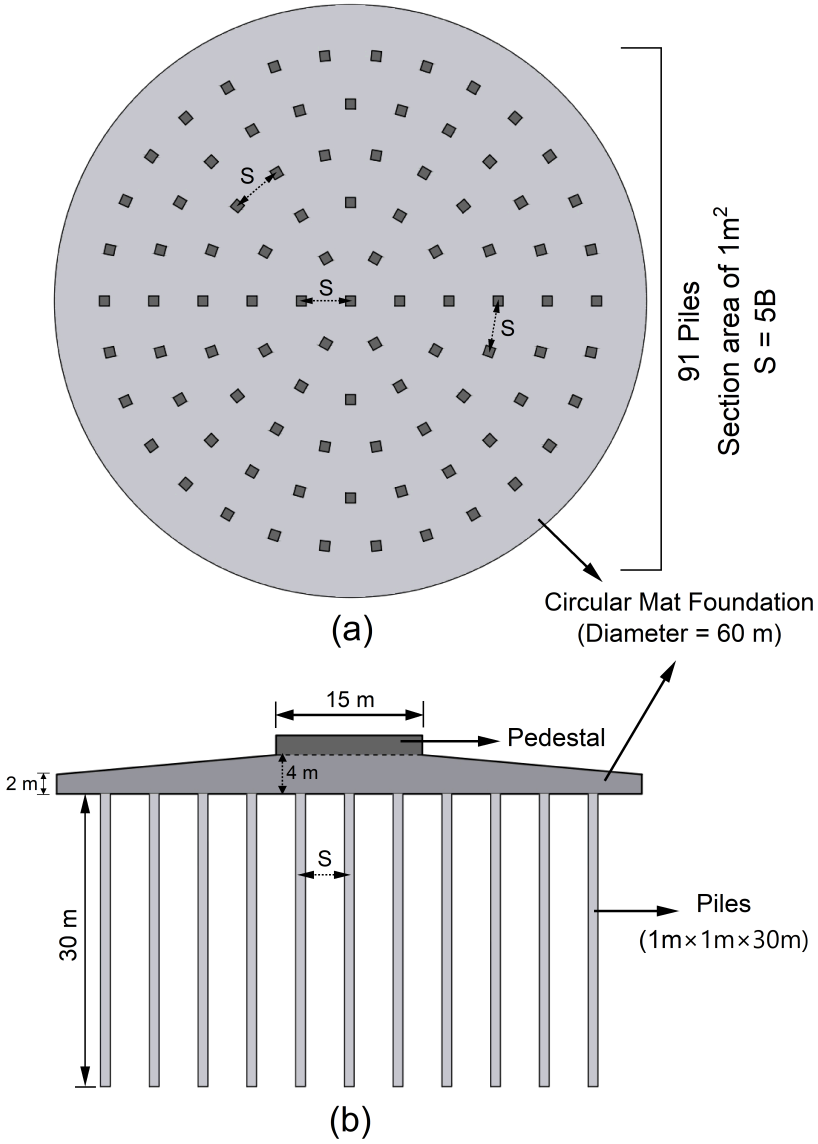

Figure 7.2 Schematic diagram of the Piled-Mat used in the study:
(a) Plan view, and (b) Sectional View

For the FEM study, a dilation angle of 1° was employed to prevent divergence errors. The tower and sub-structure were modelled as visco-elastic materials with M35-grade concrete properties. To incorporate a structural damping value of 3% in the analysis, Rayleigh coefficients, namely α and β, were employed. These coefficients, with values of 0.182 and 0.015 respectively, were determined based on the modal frequencies.

7.2.2 3D Finite Element Modeling

Each part of the turbine, i.e., blades, rotor, nacelle, tower with foundation, and soil, were modelled as separate parts and assembled to form a wind turbine. Since this study focuses on understanding the advantages of finned pile mat (FP-Mat), the blades and rotor-nacelle assembly (RNA) are not included in the analysis; instead, they are considered as the lumped mass (Ishihara and Sarwar, 2008). The tower and foundation part of the turbine structure was modelled as a single part, assigned as concrete material, and embedded in the soil.

The investigation involved examining the interactions between each pile, mat, and soil using a surface-to-surface contact approach. In this approach, the surfaces of stronger materials (such as piles and mats) were designated as master surfaces, while the surface of the softer material (soil) was designated as slave surface. Tangential contact, representing frictional behavior, was employed to model the interaction between the soil, mat, and piles. This contact was formulated to simulate the Mohr-Coulomb failure criteria, utilizing contact-pressure dependent data as described in (6.1) (Nasr, 2014; Van Nguyen et al., 2017; Yaghobi et al., 2019).

In addition to the accuracy of the analyses, the computation time is also a crucial factor to consider. To optimize the computational efficiency, mesh sensitivity analyses were conducted using different mesh sizes varying between very coarse and refined meshing. All meshing strategies generated elements of uniform size throughout the model, irrespective of the zones of higher stress variation, that either led to consuming higher computational time (for the finer meshing) or failed to provide accurate results (for the coarser meshing). Whereas refined meshing is a special strategy with smaller elements near the zone of higher stress variation and larger elements at the zone of lower variation in stress and the gradual variation in element sizes between these two zones. Refined meshing was adopted in all analyses of the present study as it produced relatively accurate results while taking less time. To prevent the reflection of applied earthquake loads back into the model and effectively absorb the vibrations, all elements

were assigned as C3D8R elements, while side boundary elements were specifically assigned as CIN3D8 elements. This choice of element types ensured the appropriate handling of boundary conditions and facilitated the absorption of the applied vibrations. Figure 7.3 depicts the comprehensive and detailed model utilized for the SSI analysis.

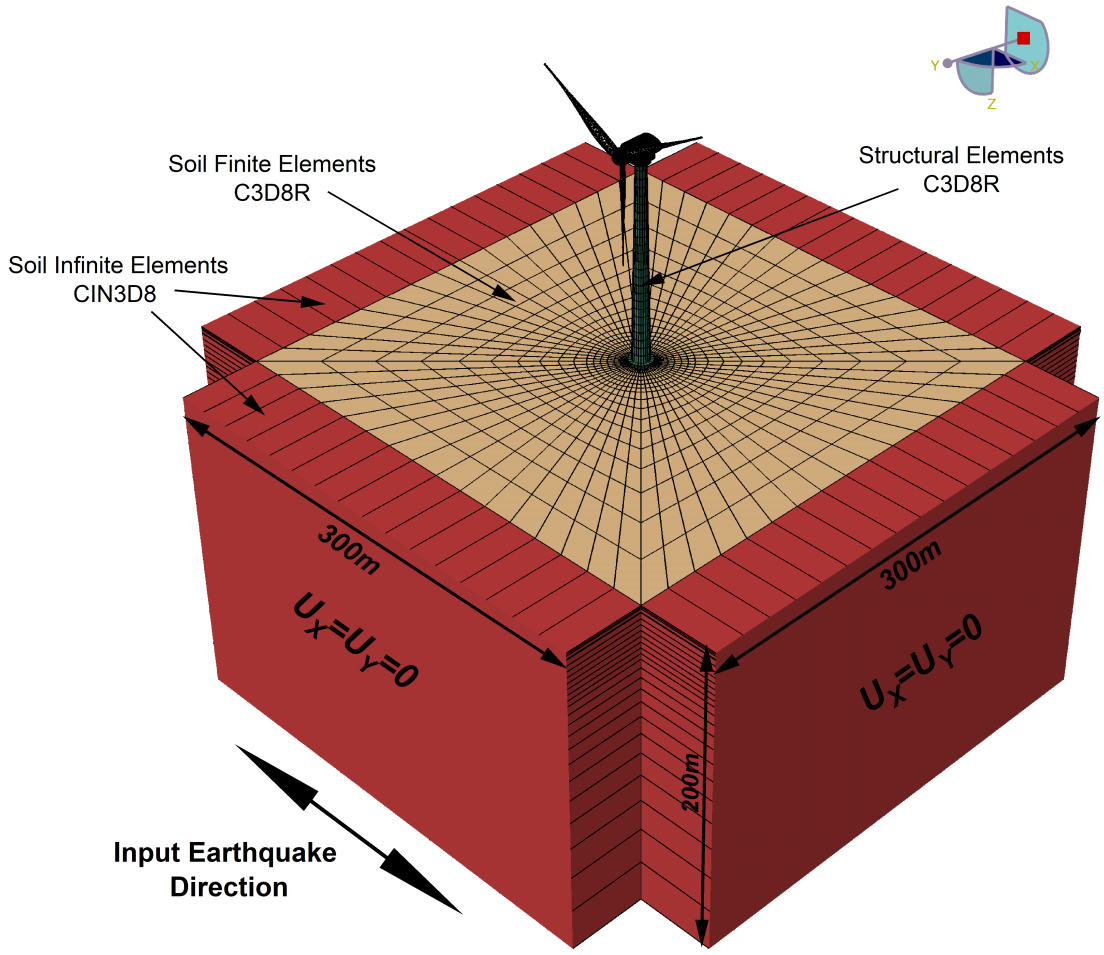

Figure 7.3 Three-dimensional finite element meshed model used in the present study

7.3 NUMERICAL ANALYSIS PROGRAM

Time-history analyses were performed on a wind turbine supported by a finned pile-mat (FP-Mat) system, and the response of the FP-Mat system was compared to that of the conventional pile-raft (RP-Mat) system. Figure 7.4 shows a schematic representation of the regular and finned pile used in piled mat system. The size of each pile adopted in this study was (B $\times$ B) of 1m $\times$ 1m, measuring a sectional area of 1m^2 and a length L_p of 30m. For finned piles, additional fins of fin-width (W_f) equal to the width of the pile (B), i.e., 1m as per (Bariker and Kolathayar, 2022b), fin-thickness (t_f) of 0.3m with various fin-lengths (L_f).

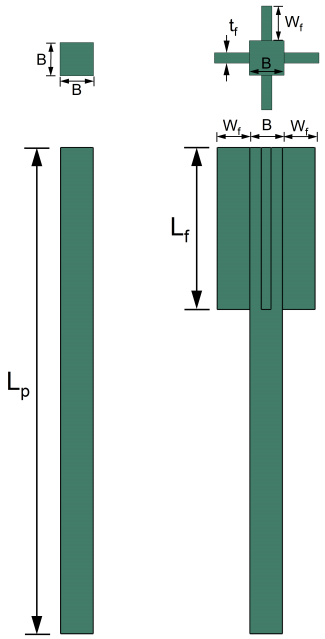

Figure 7.4 Schematic representation of regular pile and finned pile used in the study

As, Wind-turbine stay in an elastic regime even under seismic events, time-history analyses were conducted over wind turbines resting on RP-Mat and FP-Mat in the ABAQUS software to understand the response. Even though the tower with constant tapering was considered for the analyses, the tower is partitioned into segments of 5m in length each to gather its seismic response efficiently along its length. The results obtained for the wind turbine resting on RP-Mat serve as a reference for comparison with that of FP-Mat systems. The results of these analyses will offer data for determining the efficiency of the FP-Mat under earthquake loading conditions. Peak acceleration, peak displacement, and inter-segmental drift along the tower length are recorded as seismic damage characteristics. Segmental drift as per IS 1893-1 (2016) and inter-segmental drift (Bariker and Kolathayar, 2022b) play an important role in deciding any foundation system's efficacy and are calculated as from (7.1) and (7.2).

$$Segmental\ Drift = \left\{ u_{(i+1)} - u_i \right\} \tag{7.1}$$

$$Inter\ Segmental\ Drift = \left\{ \frac{Segmental\ Drift}{Segment\ Height} \right\} \times 100 \tag{7.2}$$

Where, u is the displacement in each segment and i is the segment number under consideration.

The time-history analyses were performed for various earthquakes such that the analyses consider earthquakes of higher duration, i.e., El-Centro (M_w=6.9) of t=53.74s, Kobe earthquake (M_w=6.9) of t=31.99s, data collected from the PEER (2022) earthquake database, and Koynanagar earthquake (M_w=6.3) of t=10s, data collected from Smith (2009); the details of the earthquakes are as presented in Figure 7.5 and Table 7.1.

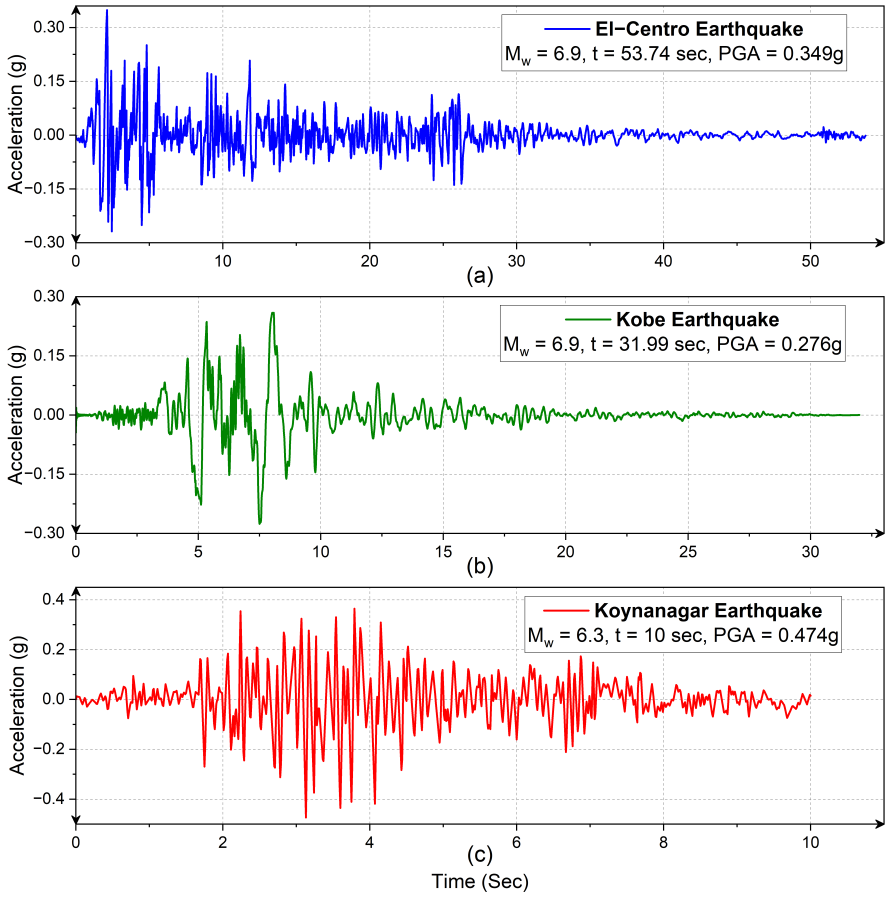

Figure 7.5 Earthquake data used for time-history analysis (Source: PEER (2022); Smith (2009))

Table 7.1 Characteristics of earthquakes used in the study

Earthquake	Country	Year	PGA (g)	M_w (R)	Duration (s)
El-Centro	United States	1940	0.349	6.9	53.74
Kobe	Japan	1995	0.276	6.9	31.99
Koynanagar	India	1967	0.474	6.3	10

7.4 ANALYSIS OF REGULAR PILE MAT

Time-history analyses were performed using the 3D FE model with RP-Mat to study its response. The response is noted as time-history plots, i.e., acceleration variation, displacement variation at the base, mid-height and tip of the tower. Figure 7.6 and Figure 7.7 presents the acceleration and displacement time-history plots. It was observed that irrespective of the earthquakes, the tower top experienced more acceleration and displacement than the other two levels, i.e., mid-height and base levels of the tower. Hence, the tower top is more critical for the study than the other two levels. From Figure 7.6, wind turbines experienced maximum acceleration at 2.12s, 7.5s, and 3.13s and maximum displacement at 27.4s, 4.88s, and 9.73s, respectively, for El-Centro, Kobe and Koynanagar earthquakes; these data serve as a reference for comparing the results with that of finned pile mat (FP-Mat).

The permissible segmental drift of any structure under the action of an earthquake, as per IS 1893-1 (2016), is 0.004h (0.4% of segmental height). In the present study, the tower of wind-turbine has 26 segments of 5m height (h). Hence, the permissible segmental drift for the tower was found to be 20mm, but when subjected to the El-Centro earthquake, the wind turbine experienced a segmental drift of 26.83mm, as shown in Figure 7.8. Thus, the structure is safe against Kobe and Koynanagar earthquakes but unsafe when subjected to the El-Centro earthquake. Hence, suitable measures must be taken to reduce this segmental drift well below permissible. Although the wind turbine tower supported by the RP-Mat system was found to be safe against the Kobe and Koynanagar earthquakes, the study was conducted using the FP-Mat system to evaluate the enhancement in seismic response of the wind turbine under different earthquake conditions.

7.5 ANALYSIS OF FINNED PILE MAT

In order to investigate the impact of the finned pile mat on enhancing the seismic response of the wind turbine, a series of time-history analyses were performed on a 3D finite element model. The model consisted of the wind turbine resting on an FP-Mat with a fin-length (L_f) of 0.5m. The FP-Mat used in the analyses is illustrated in Figure 7.9(b). Time-history analyses were conducted on all models utilizing FP-Mat, which were comparable to RP-Mat, for three different earthquake scenarios: El-Centro, Kobe, and Koynanagar earthquakes, as depicted in Figure 7.5. The time-history plots for wind turbines resting on finned pile mat (FP-Mat), i.e., acceleration and displacement plots, were plotted.

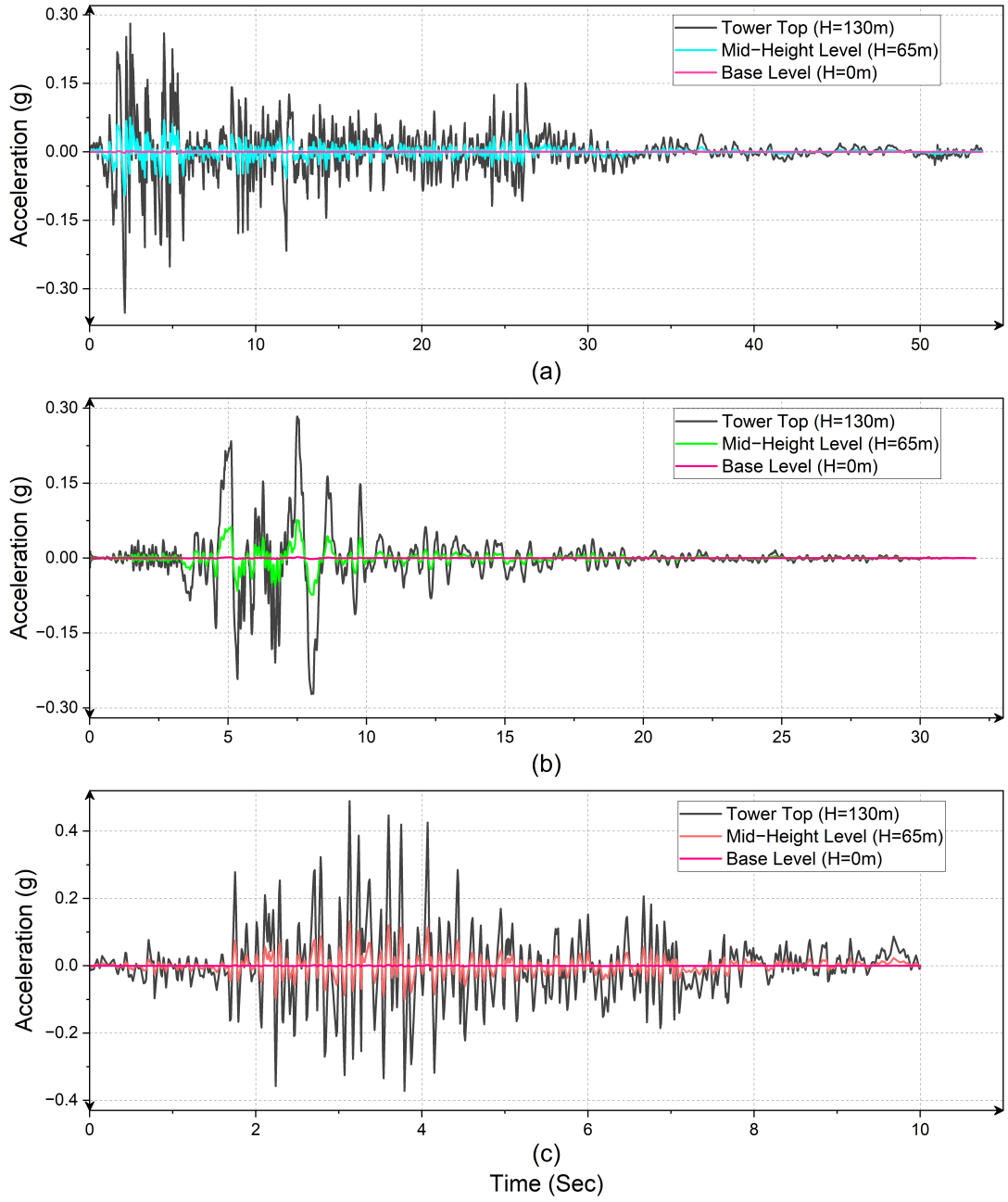

Figure 7.6 Acceleration time-history plots at various levels of wind turbine for: (a) El-Centro EQ, (b) Kobe EQ, and (c) Koynanagar EQ

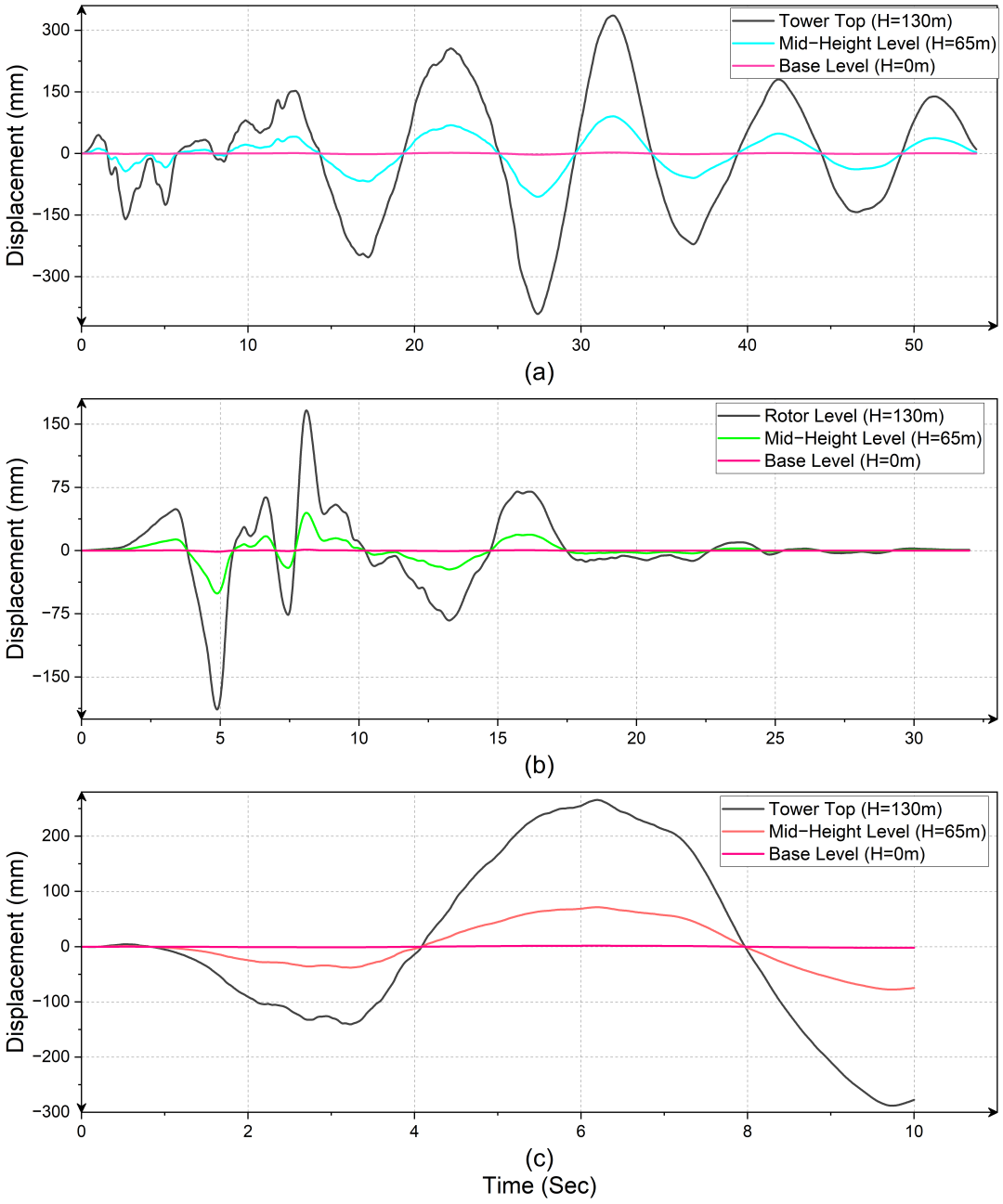

Figure 7.7 Displacement time-history plots at various levels of wind turbine for: (a) El-Centro EQ, (b) Kobe EQ, and (c) Koynanagar EQ

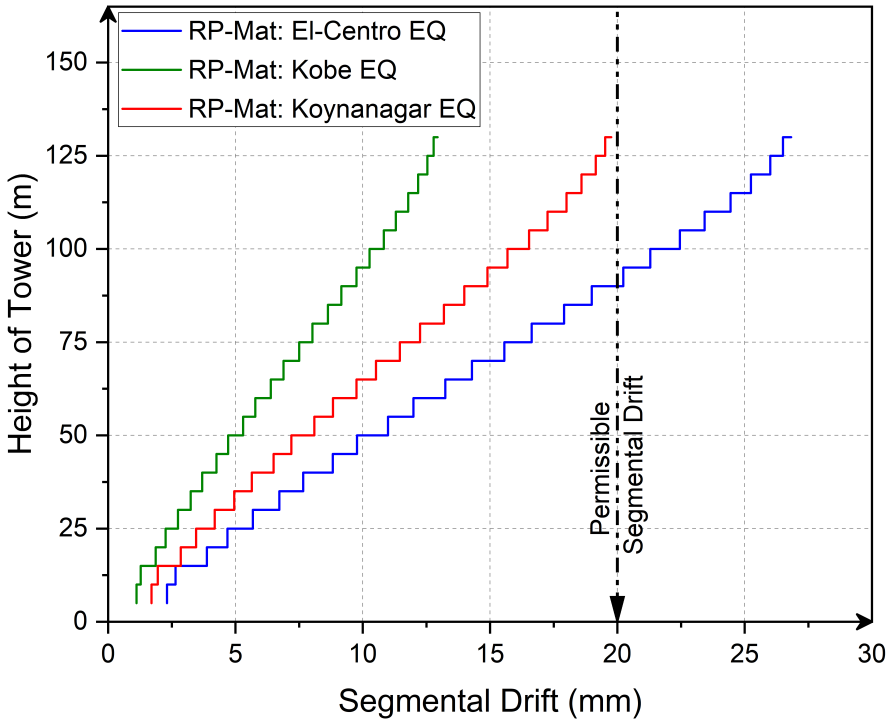

Figure 7.8 Variation of segmental drift along tower height for different earthquakes

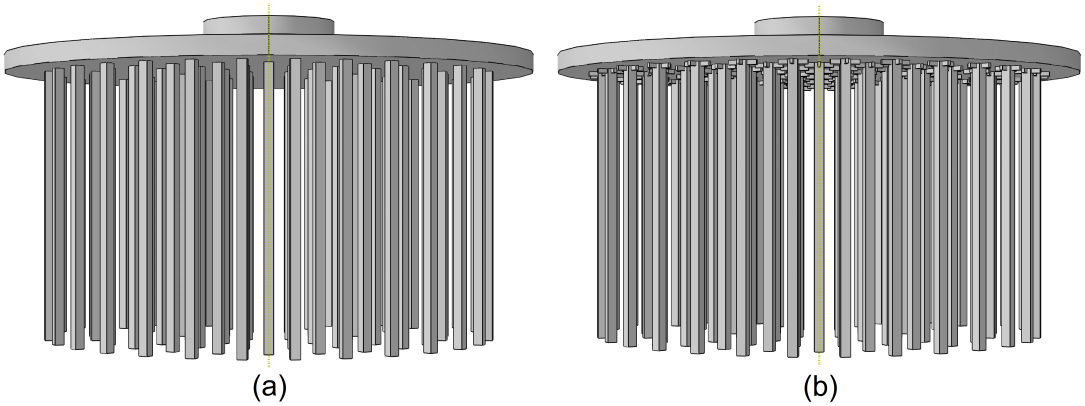

Figure 7.9 Three-dimensional piled mat used in the study (a) RP-Mat; and (b) FP-Mat

7.5.1 Time-history Plots

7.5.1.1 Acceleration Plots

The time-history plots for wind turbines resting on finned pile mat (FP-Mat), i.e., acceleration plots for all the three-earthquake data, at every time step-lengths of 0.02s, 0.01s and 0.01s for El-Centro, Kobe and Koynanagar earthquakes respectively are shown in Figure 7.10. It was noted that the acceleration plots for wind turbines resting on FP-Mats decreased regardless of the type of earthquake motion. Like the wind turbine resting on RP-Mats, FP-Mat has the tower top in the critical position because the acceleration was highest compared to the other two levels, namely the mid-height and base levels, as shown in Figure 7.10.

7.5.1.2 Displacement plots

To examine the impact of the finned pile mat in mitigating the tower displacement caused by earthquake excitation, a set of time-history analyses were conducted for different earthquake events, as illustrated in Figure 7.5. The displacement plots at various levels of the wind turbine are shown in Figure 7.11. Peak displacement for the model with FP-Mat was observed to be reduced than that of RP-Mat. The displacement was maximum at the tower top than the other two levels, similar to RP-Mat.

7.5.2 Effect of Fins on Wind-tubine Response

In addition to investigating the turbine's response at critical levels, it is essential to comprehend the variations of peak acceleration (A_{peak}), peak displacement (U_{peak}), segmental drift, and inter-segmental drift throughout the height of the wind turbine. Therefore, a series of SSI analyses were conducted to assess the seismic response along the turbine's height under various earthquake excitations. The results were presented in the form of a height-wise variation of peak values.

7.5.2.1 Variation of peak acceleration and peak displacement

The variation of the peak acceleration (A_{peak}) and peak displacements (U_{peak}) along the height of the wind turbine at every segment for both RP and FP-Mats under different earthquake excitations are illustrated in Figure 7.12 and Figure 7.13, respectively.

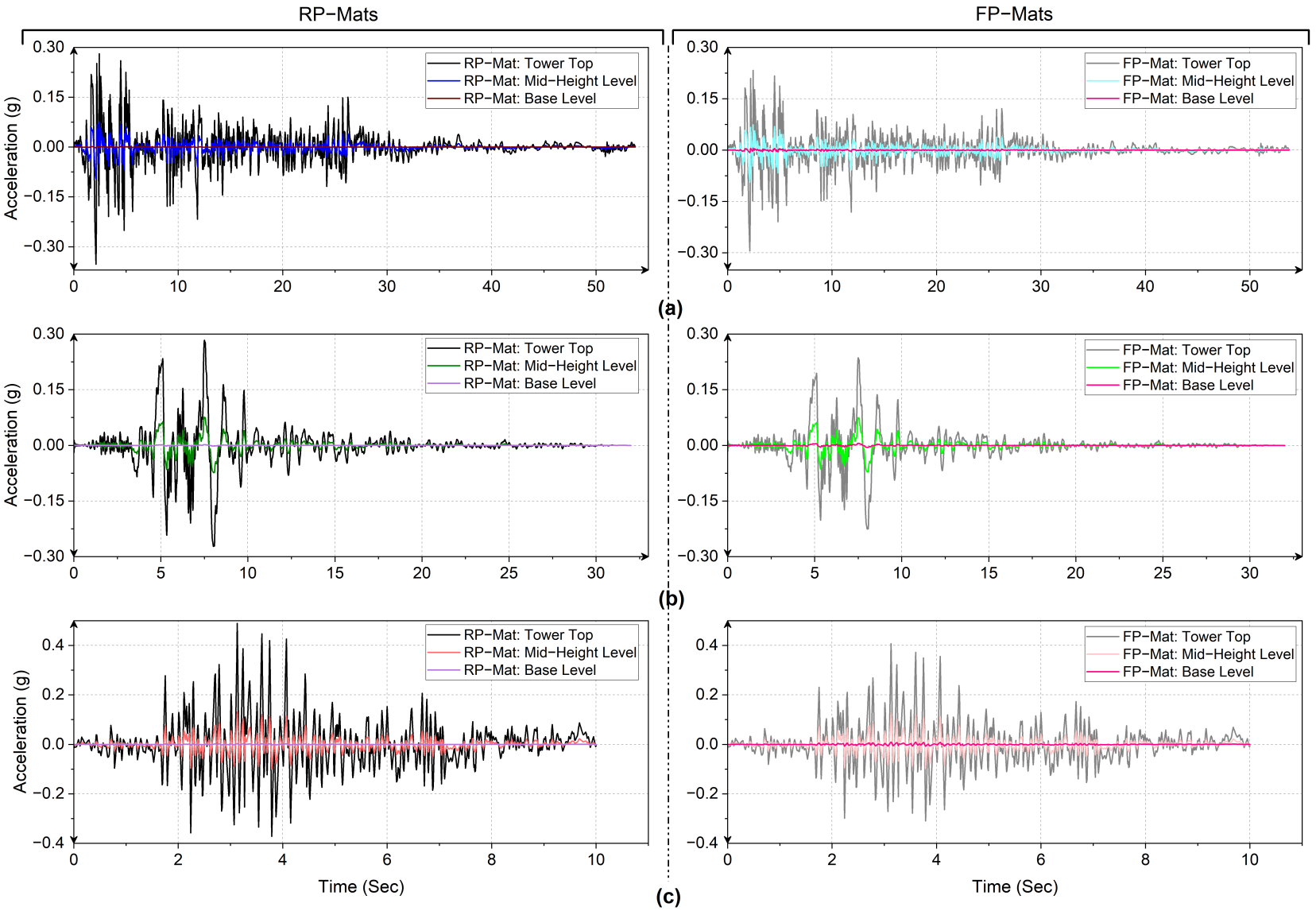

Figure 7.10 Time-history plots for wind turbine resting on FP-Mat at various levels for: (a) El-Centro EQ; (b) Kobe EQ; and (c) Koynanagar EQ

Upon comparing the peak values at the top of the tower with those at the base level, it was observed that the wind turbine supported on RP-Mat experienced A_{peak} and U_{peak} values that were about 148 times higher than those at the base level. However, in the case of FP-Mat, the A_{peak} and U_{peak} values at the top were about only 41 times higher than those at the base level. This indicates that the provision of FP-Mat with a fin length (L_f) of 0.5m reduced the peak acceleration and displacements at the top of the tower by 27.7% compared to RP-Mat.

In order to assess the reduction in acceleration achieved by incorporating FP-Mat compared to RP-Mat, the peak acceleration at the top of the tower was analyzed for all three earthquakes, as depicted in Figure 7.14. It was observed that the inclusion of 0.5m length fins resulted in a reduction of approximately 17% in peak acceleration, indicating a decrease in vibration levels.

The peak displacement experienced by the wind turbine at the tower top for both RP-Mat and FP-Mat cases is shown in Figure 7.15. Compared to the model with RP-Mat, the wind turbine resting on FP-Mat experienced 17.25%, 18.2%, and 32.54% lesser displacement for El-Centro, Kobe, and Koynanagar earthquakes, respectively.

7.5.2.2 Segmental drift and Inter-segmental drift

Figure 7.16 illustrates the variation of segmental drifts along the height of the wind turbine, while Figure 7.17 presents the variation of inter-segmental drifts. These figures provide insights into how the drift values change at different levels of the turbine structure. It was observed that the Wind-turbine resting on RP-Mat experienced softer behaviour than the FP-Mat, leading to greater displacement for the RP-Mat case. As per IS 1893-1 (2016), the permissible segmental drift is 0.004h (i.e., 20mm). Still, from Figure 7.16, it was observed that the wind turbine resting on RP-Mat experienced a higher value than the permissible segmental drift. However, the provision of FP-Mat with L_f of 0.5m has reduced the segmental drift within the system to a lesser extent than specified.

Figure 7.17 shows that the provision of FP-Mat has reduced the inter-segmental drift more than the case of RP-Mat. Lesser inter-Segmental drift sets lesser damage in the system due to seismic activity; hence it is called the damage deciding factor. Hence, the wind turbine supported on FP-Mat suffers less damage than that supported on RP-Mat. To quantify the reduction in inter-segmental drift under various earthquakes, the results of FP-Mat were compared with that of RP-Mat and are shown in Figure 7.18. It was observed that the provision of FP-Mat reduced the inter-segmental drift by

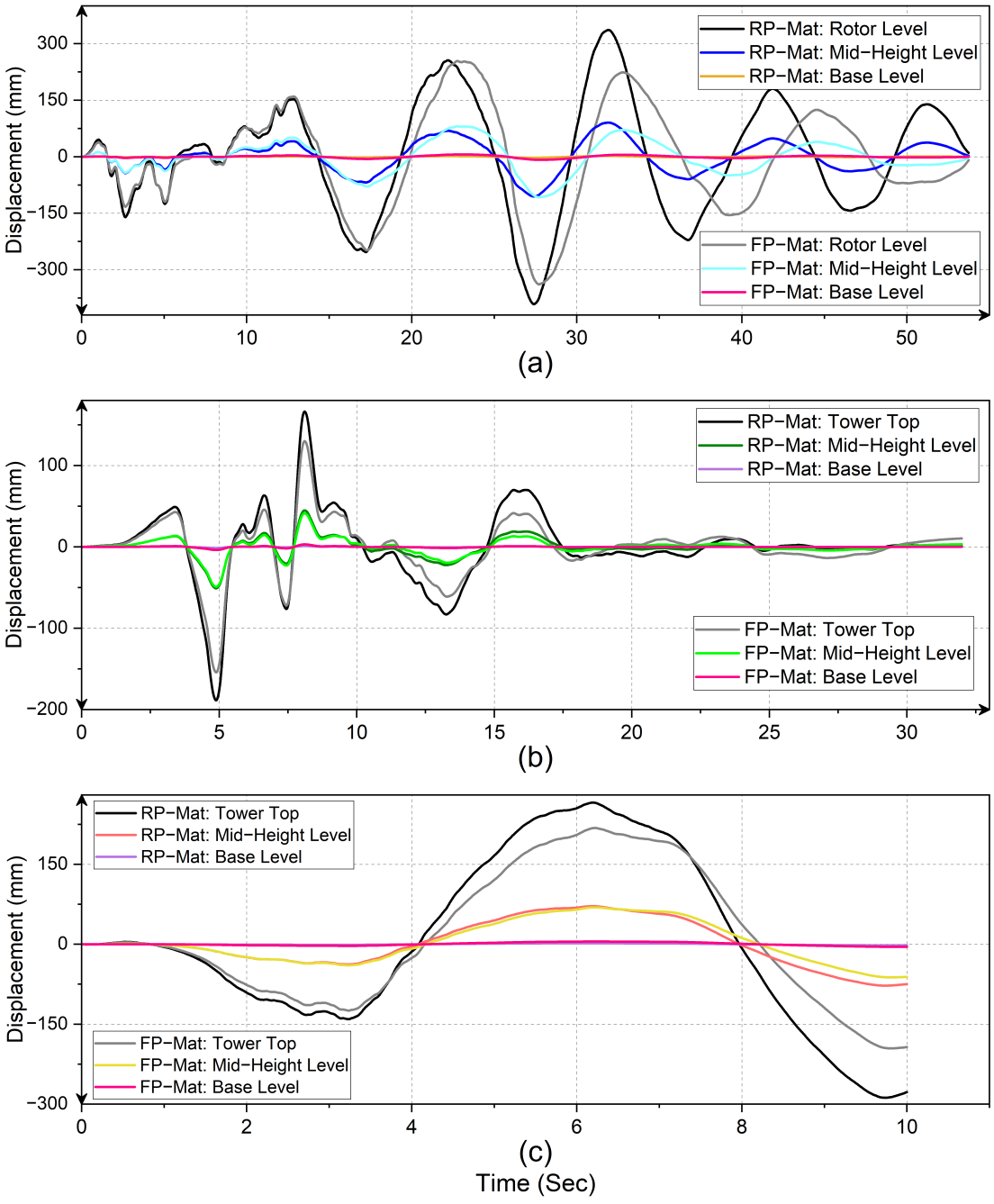

Figure 7.11 Displacement plots for wind turbine resting on RP and FP-Mat at various levels for: (a) El-Centro EQ; (b) Kobe EQ; and (c) Koynanagar EQ

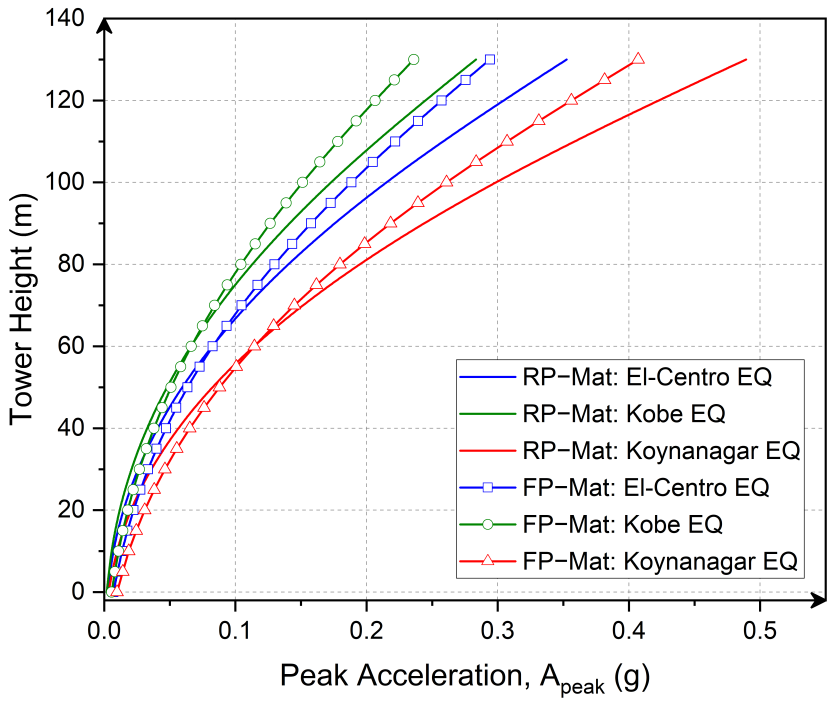

Figure 7.12 Variation of the peak acceleration along the height of wind turbine for different earthquake excitations

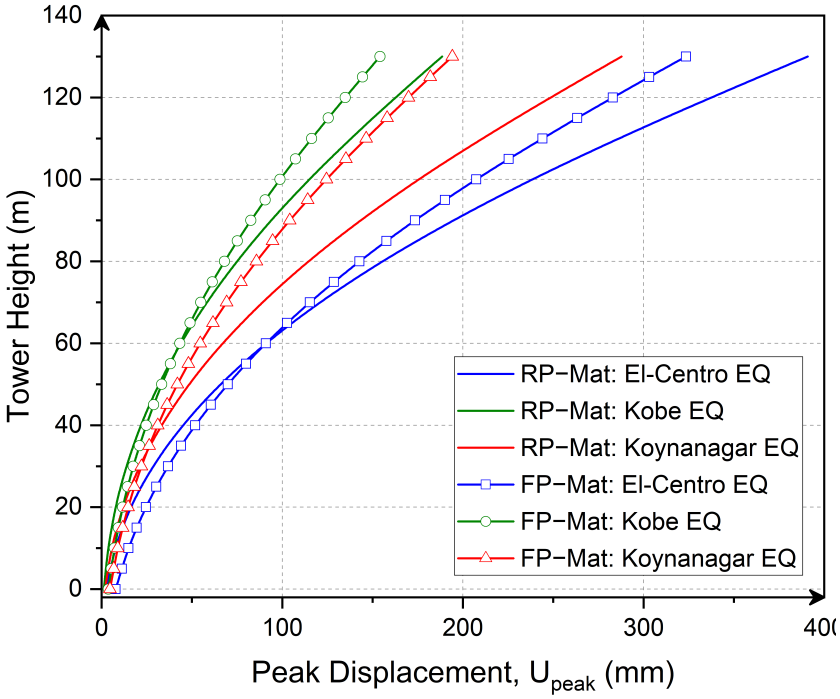

Figure 7.13 Variation of the peak displacement along the height of wind turbine for different earthquake excitations

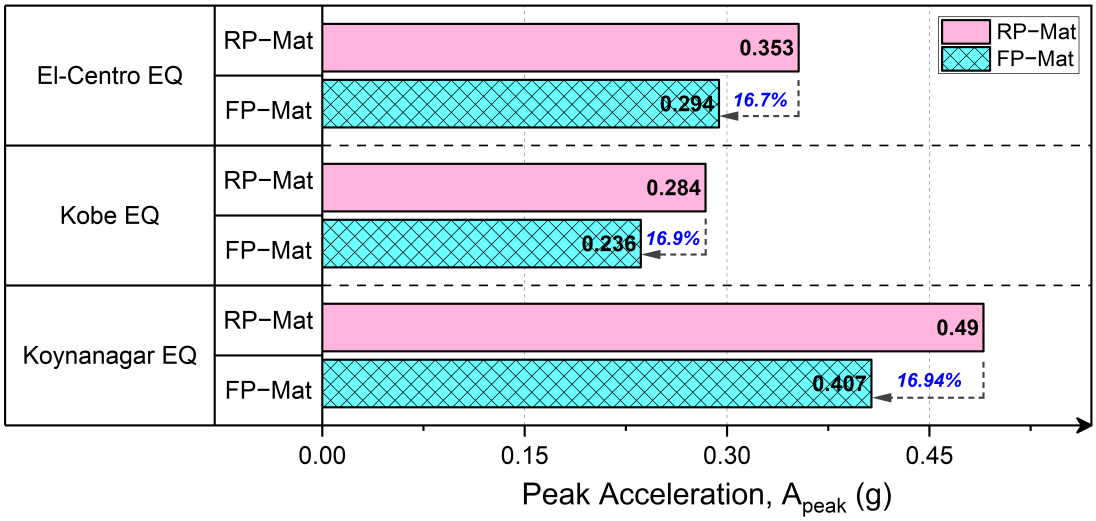

Figure 7.14 Reduction of peak acceleration for the model with FP-Mat at tower top

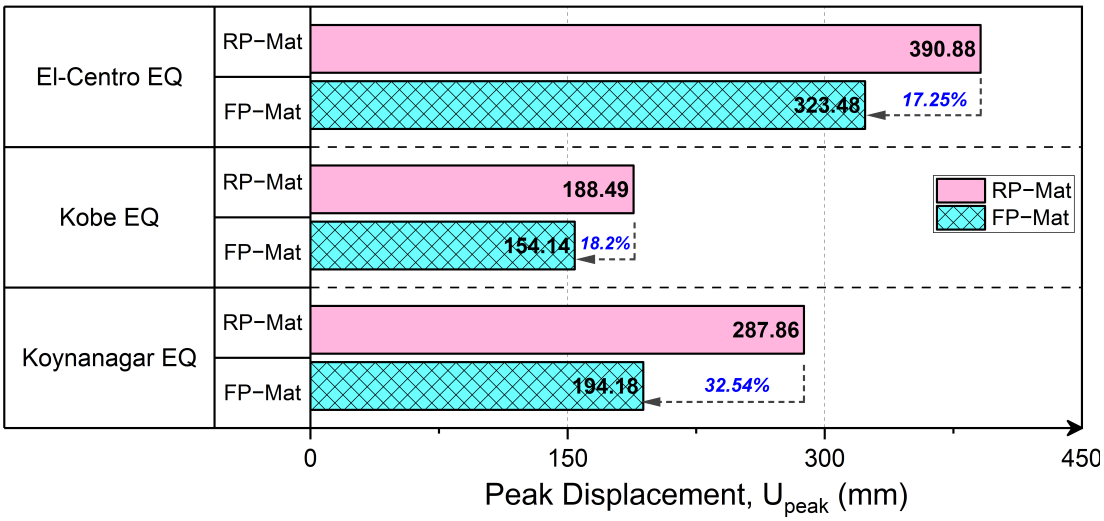

Figure 7.15 Reduction of peak displacement for the model with FP-Mat at tower top

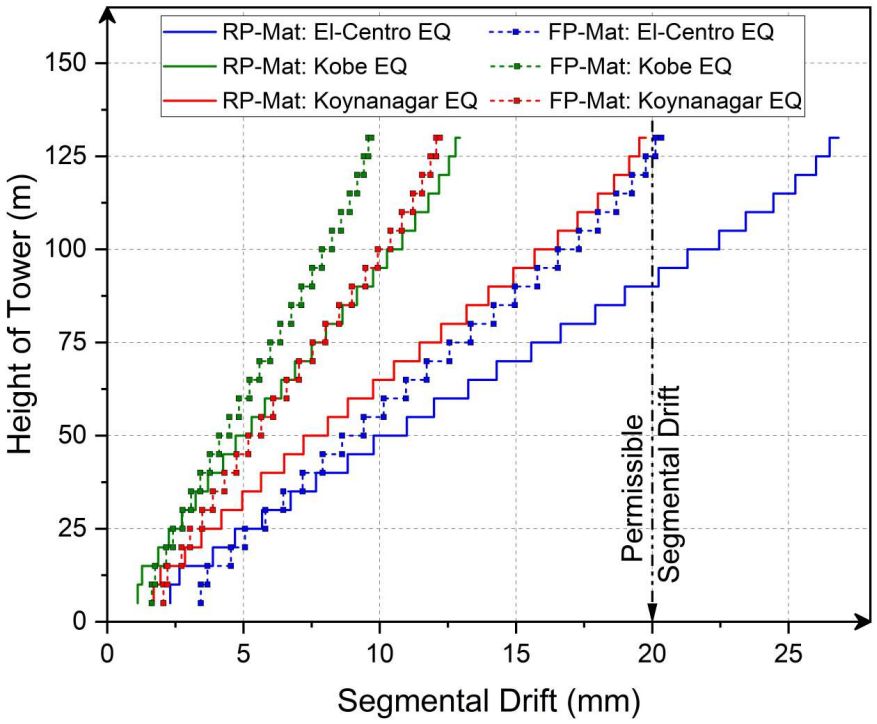

Figure 7.16 Variation of segmental drift along the height of wind turbines resting on RP-Mat and FP-Mat

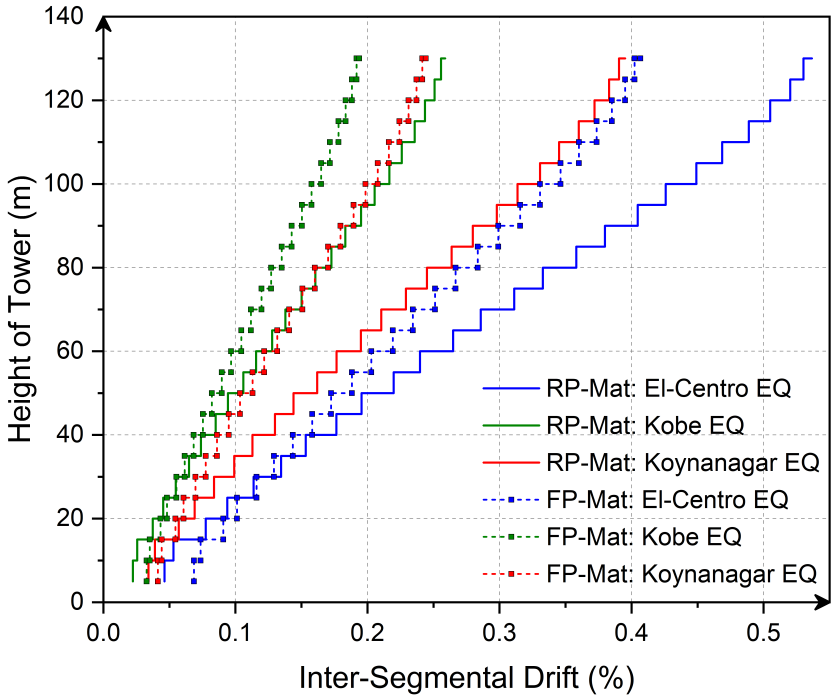

Figure 7.17 Variation of inter-segmental drift along the height of wind turbine resting on RP-Mat and FP-Mat

24%, 25.5% and 38% compared to RP-Mat under El-Centro, Kobe, and Koynanagar earthquakes, respectively. From the trend of results obtained, it can be concluded that the reduction in the inter-segmental drift for wind turbine resting on FP-Mats, was higher for lower-duration earthquakes (Koynanagar EQ) than that for high-duration earthquakes (El-Centro EQ).

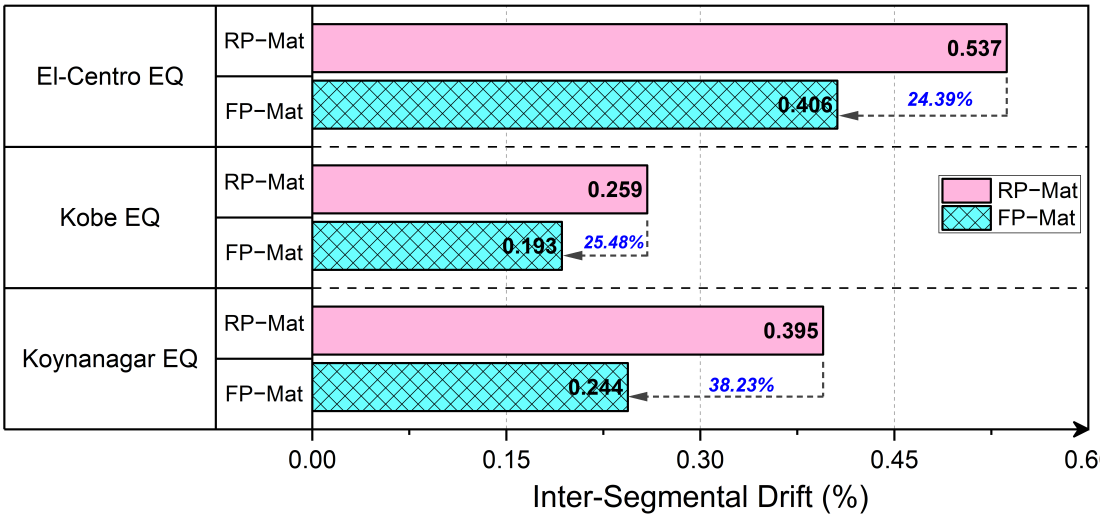

Figure 7.18 Variation of the inter-segmental drift for the wind turbine resting on FP-Mat under various earthquakes

The tilt of the tower during seismic events significantly impacts the operational status of the wind turbine, as excessive tilt can lead to collisions between the tower and the rotating blades. To study this effect of tilting, the difference between inter-segmental drifts at the tower top and base levels, termed as 'drifting bound', was employed as shown in equation (7.3). The higher the drifting bound, the higher the risk of collision and the comparison between RP-Mats and FP-Mats was done to study the risk of tilting.

$$Drifting\ bound = \left\{ (Inter\ segmental\ drift)_{Top} - (Inter\ segmental\ drift)_{Base} \right\} \quad (7.3)$$

In the case of a wind turbine resting on RP-Mat, the drifting bound was found to be 0.491%, 0.237%, and 0.361%, respectively, for the El-Centro, Kobe, and Koynanagar earthquakes. While the drifting bounds for the turbine resting on FP-Mats were found to be 0.338%, 0.161%, and 0.203%. FP-Mats reduce the drifting bound by 31.16%, 31.19%, and 43.8% more than RP-Mats. Hence, from the comparison between drifting bounds, it was found that installing the wind turbines on FP-Mats can reduce the tilting of the tower, thereby reducing the chances of collision between the tower and blades, leading to a sustainable design strategy.

Even though the model of FP-Mat with L_f of 0.5m experienced lesser segmental drift than the permissible as specified by IS 1893-1 (2016), several SSI analyses were made for various wind-turbine models with FP-Mats of increased fin-lengths. Still, they didn't show much improvement in results. It indicates that a fin length of 0.5m is optimum, giving the best results.

7.6 SUMMARY

In this study, a novel approach was taken to quantitatively assess the seismic response of conventional piled mats (RP-Mats) by incorporating SSI. Additionally, the effectiveness of finned-pile mats (FP-Mats) in mitigating the impact of earthquakes on wind turbines was investigated. The following conclusions were drawn based on a series of SSI simulations conducted on the wind turbine using different seismic data.

- The provision of fins in the piled mats (FP-Mat) reduces the vibrations caused due to earthquakes. Finned piles, with a fin length (L_f) of just 0.5m, can reduce the peak acceleration and displacements at the tower top by 27.7% compared to RP-Mat.
- The wind turbine resting on FP-Mat experienced 17.25%, 18.20%, and 32.54% lesser displacement than RP-Mat for El-Centro, Kobe, and Koynanagar earthquakes, respectively.
- The provision of FP-Mat with an L_f of 0.5m has reduced the segmental drift within the system to a lesser extent than the specified permissible segmental drift.
- The provision of FP-Mat reduced the inter-segmental drift by 24%, 25.5% and 38% compared to RP-Mat under El-Centro, Kobe, and Koynanagar earthquakes, respectively. Also, the reduction in the inter-segmental drift for wind turbines resting on FP-Mats was higher for lower-duration earthquakes (Koynanagar EQ) than for high-duration earthquakes (El-Centro EQ).
- The wind turbines resting on FP-Mats reduced the tower tilting by 31.16%, 31.19%, and 43.8% than RP-Mat under El-Centro, Kobe, and Koynanagar earthquakes, respectively. Thereby reducing the chances of collision between the tower and the blades.

From the above findings, it can be concluded that the finned pile mat is one of the best alternatives to regular pile mats to support wind turbines. Finned pile mat performs better under earthquake excitation. This can be an economic alternative to wind turbines in seismically active regions.

CHAPTER 8

CONCLUSIONS AND FUTURE SCOPE

8.1 CONCLUSIONS

This thesis presented an innovative finned pile foundation system as an alternative to regular pile foundations in resisting larger lateral loads and improving pile group efficiency in $c-\phi$ soil. This work also evaluated the lateral load resistance of finned piles for onshore foundation applications and compared its performance under seismic excitation with regular pile mats for high-rise buildings and wind turbines. In addition to physical model experiments, the numerical studies were performed in a FEM framework. Suggested fin parameters were determined to optimize the lateral resistance of finned pile foundations, aiming to enhance construction efficiency and cost-effectiveness. The major conclusions are summarized below:

8.1.1 Optimization of Fin-Parameters

- From the fin-parametric studies performed over the individual finned pile, the optimum fin position, fin width, and fin length were found to be top-position (pile-head position), $1.0D_p$, and $12D_p$ or $0.4L_p$ respectively, based on pile diameter (D_P), and pile length (L_p). While both fin width (W_f) and fin length (L_f) contribute to improving the L_u of the finned pile, it was observed that the fin length has a more significant influence on enhancing the L_u compared to the fin width.

- The improvement in the L_u of the finned pile was found to be 126%; this shows that the finned piles work more efficiently in $c-\phi$ soil, with the optimum fin length of $L_f = 0.4L_p$ or $12D_p$.

- To resist the lateral load same as that of the finned pile with optimum fin parameters, a conventional or regular pile with $(D_p)_{eq}$ of $1.9\times D_p$ of the finned pile was required, i.e., requires around 21% more material than the finned pile. Also, a finned pile with an $(L_p)_{eq}$ of just 30% of the regular pile's L_p is sufficient to resist the load of L_u, reducing material usage by around 46%. Hence, the finned

pile is a cost-effective alternative to the large-dimension regular pile.

8.1.2 Pile Group Efficiency of Finned Pile Groups

- In finned pile groups, with four piles (P_4), irrespective of pile spacing (s), the individual pile action dominates over the pile-group effect, leading to higher pile-group efficiency. But in the five piled groups (P_5), the pile-group effect dominates the individual pile effect.
- In a pile group with pile spacing (s) of $4D_p$, on increasing the number of piles from four (P_4) to five (P_5), the pile group efficiency (η_g) increased and decreased for regular and finned pile group respectively. The decrease in the $(\eta_g)_{FP}$ is due to the overlapping of stress bulbs for finned piles in the group due to the lesser pile spacing (s) between piles for the P_5 group. Hence, pile spacing is crucial in the case of FP groups and must be higher than $4D_p$.
- The cost of regular pile groups increases by about 25% to 85% to have performance similar to the corresponding finned pile group. The finned pile groups can achieve the same level of lateral resistance as regular pile groups, with just about 75% of the material of the regular pile group.

8.1.3 Response of High-Rise Building on FP-Mat

- The provision of fins in the piled mats drastically reduces detrimental vibrations due to earthquakes. Finned piles, with a fin-length (L_f) of just $0.2L_p$, can reduce the seismic response of high-rise buildings by more than 90%.
- The fin-length (L_f) has a high level of influence over the effect of the seismic response, i.e., the variation between inter-story drift readings remains constant (i.e., stiffer behaviour) in subsequent stories. It is responsible for reducing story displacements due to seismic loading.
- FP-Mats with fin-lengths (L_f) of $0.6L_p$ and $0.8L_p$ showed nearly identical horizontal displacement variation; hence, considering the seismic performance and economical construction, $0.6L_p$ may be considered the optimum fin-length for reducing the seismic response.
- The drifting bounds of the FP-Mat system were reduced by increasing the fin lengths, Thereby reducing the average rotation between the beam and column within the same story.

8.1.4 Seismic Response of Wind Turbine Resting on FP-Mat

- The provision of fins in the piled mats (FP-Mat) reduces the vibrations caused due to earthquakes. Finned piles, with a fin length (L_f) of just 0.5m, can reduce the peak acceleration and displacements at the tower top by 27.7% compared to RP-Mat.
- The provision of FP-Mat with an L_f of 0.5m has reduced the segmental drift within the system to a lesser extent than the specified permissible segmental drift.
- The provision of FP-Mat reduced the inter-segmental drift by 24%, 25.5% and 38% compared to RP-Mat under El-Centro, Kobe, and Koynanagar earthquakes, respectively. Also, the reduction in the inter-segmental drift for wind turbines resting on FP-Mats was higher for lower-duration earthquakes (Koynanagar EQ) than for high-duration earthquakes (El-Centro EQ).
- The wind turbines resting on FP-Mats can reduce the tower tilting by 31.16%, 31.19%, and 43.8% than RP-Mat under El-Centro, Kobe, and Koynanagar earthquakes, respectively. i.e., reducing the collision between the tower and blades.

8.2 FUTURE SCOPE

The potential scope for future research in the area of finned pile foundations are listed below:

- To study the behaviour of finned pile foundations under inclined loads.
- To develop design charts for the use of finned pile foundation system in the wider range of c-ϕ soils.
- To study the behaviour of finned piles as anti-slide piles for landslide mitigation.

REFERENCES

Agarwal, S. and Prakash, S. (1967). Determination of Laterl Load Carrying Capacity of Pile Groups in Fileds. *J. Inst. Eng. India*, pages 427–450.

Albusoda, B. S., Al-Saadi, A. F., and Jasim, A. F. (2018). An experimental study and numerical modeling of laterally loaded regular and finned pile foundations in sandy soils. *Comput. Geotech.*, 102(May):102–110.

Albusoda, B. S. and Alsaddi, A. F. (2017). Experimental Study on Performance of Laterally Loaded Plumb and Finned Piles in Layered Sand. *Appl. Res. J.*, 3(1):32–39.

Ambi, R., Ambi, R., and Unnikrishnan, N. (2019). Effect of fin shape on the behaviour of piles under combined loading conditions. In Sheela Evangeline, M.R. Rajkumar, S. G. P., editor, *Recent Adv. Mater. Mech. Manag.*, pages 44–48. CRC Press, London.

Ambi, R., Jayasree, P. K., and Unnikrishnan, N. (2020). Study of fin shape on the behaviour of finned piles under combined loading conditions. *IOP Conf. Ser. Earth Environ. Sci.*, 491(1):012051.

Anand, V. and Satish Kumar, S. R. (2018). Seismic Soil-structure Interaction: A State-of-the-Art Review. *Structures*, 16(October):317–326.

Arboleda-Monsalve, L. G., Mercado, J. A., Terzic, V., and Mackie, K. R. (2020). Soil–Structure Interaction Effects on Seismic Performance and Earthquake-Induced Losses in Tall Buildings. *J. Geotech. Geoenvironmental Eng. - ASCE*, 146(5):1–14.

Ashour, M., Pilling, P., Norris, G., and Asce, M. (2004). Lateral Behavior of Pile Groups in Layered Soils. *J. Geotech. Geoenvironmental Eng. - ASCE*, 130(6):580–592.

ASTM D-2487-17e1 (2017). *Standard Practice for Classification of Soils for Engineering Purposes (Unified Soil Classification System), ASTM standard D2487*. ASTM, West Conshohocken, Pa.

Babu, K. and Viswanadham, B. (2018). Numerical Investigations on Lateral Load Response of Fin Piles. In Shehata H., R. Y., editor, *Sustain. Civ. Infrastructures*, chapter 27, pages 317–329. Springer, Cham., numerical edition.

Babu, K. and Viswanadham, B. (2019). Numerical studies on lateral load response of fin piles. *Geomech. Geoengin.*, 14(2):85–98.

Bagheri, M., Jamkhaneh, M. E., and Samali, B. (2018). Effect of Seismic Soil–Pile–Structure Interaction on Mid- and High-Rise Steel Buildings Resting on a Group of Pile Foundations. *Int. J. Geomech.*, 18(9):1–27.

Bariker, P. and Kolathayar, S. (2021). A Study on Trenching Techniques for Vibration Isolation: An Overview. In *Lect. Notes Civ. Eng.*, volume 116 LNCE, pages 283–293. Springer, Singapore.

Bariker, P. and Kolathayar, S. (2022a). Appraisal of Innovative Finned-Pile Foundations to Resist Lateral Loads. In *C. N. V. Satyanarayana Reddy al. (eds.), Gr. Charact. Found. Lect. Notes Civ. Eng.*, pages 697–707. Springer, Singapore., vol. 167, edition.

Bariker, P. and Kolathayar, S. (2022b). Dynamic Soil Structure Interaction of a High-Rise Building Resting over a Finned Pile Mat. *Infrastructures*, 7(10):142.

Bariker, P., Rajesh, K. S., and Raju, K. V. (2020). A study on lateral resistance of finned piles in sands. In *S. Haldar al. (eds.), Adv. Offshore Geotech. Lect. Notes Civ. Eng.*, volume 92, pages 319–336. Springer, Singapore.

Belinchon, P., Sørensen, K. K., and Christensen, R. (2016). Finite element investigation of the interaction between a pile and a soft soil focussing on negative skin friction. *Proc. 17th Nord. Geotech. Meet.*, pages 513–522.

Bhushan, K., Haley, S. C., and Fong, P. T. (1979). Lateral Load Tests on Drilled Piers in Stiff Clays. *J. Geotech. Eng. Div. ASCE*, 105(No. GT 8):969–985.

Bienen, B., Dührkop, J., Grabe, J., Randolph, M. F., and White, D. J. (2012). Response of Piles with Wings to Monotonic and Cyclic Lateral Loading in Sand. *J. Geotech. Geoenvironmental Eng.*, 138(3):364–375.

Bilotta, E., Sanctis, L., Di Laora, R., D'Onofrio, A., and Silvestri, F. (2015). Importance of seismic site response and soil–structure interaction in dynamic behaviour of a tall building. *Géotechnique*, 65(5):391–400.

Bisoi, S. and Haldar, S. (2014). Dynamic analysis of offshore wind turbine in clay considering soil-monopile-tower interaction. *Soil Dyn. Earthq. Eng.*, 63:19–35.

Boulanger, R. W., Curras, C. J., Kutter, B. L., Wilson, D. W., and Abghari, A. (1999). Seismic Soil-Pile-Structure Interaction Experiments and Analyses. *J.*

Geotech. Geoenvironmental Eng., 125(9):750–759.

Bowles, J. (1974). *Analytical and Computer Methods in Foundation Engineering*. McGraw Hill, NewYork.

Bransby, P. and Smith, I. (1975). Side friction in model retaining wall experiments. *J. Geotech. Eng. ASCE*, 101(GT7):615–632.

Broms, B. (1964a). Lateral Resistance of Piles in Cohesionless Soils. *J. Soil Mech. Found. Eng. ASCE*, 90(3):123–156.

Broms, B. (1964b). Lateral Resistance of Piles in Cohesive Soils. *J. Soil Mech. Found. Eng. ASCE*, 90(2):27–63.

Brown, D. A., Morrison, C., and Reese, L. C. (1990). Lateral load behavior of pile group in sand. *J. Geotech. Eng.*, 116(8):1282–1283.

Christos, A. and Michael, G. (1993). Interaction of Axial and Lateral Pile Responses. *J. Geotech. Eng. ASCE*, 119(4):793–798.

CSI Computers and Structures INC (2017). *CSI Analysis Reference Manual*. CSI, 18 edition.

Davisson, M. T. (1970). Lateral Load Capacity of Piles. *Highw Res Rec*, 333(33):104–112.

Deendayal, R., Muthukkumaran, K., and Sitharam, T. (2016). Response of laterally loaded pile in soft clay on sloping ground. *Int. J. Geotech. Eng.*, 10(1):10–22.

Fatahi, B., Basack, S., Ryan, P., Zhou, W.-H., and Khabbaz, H. (2014). Performance of laterally loaded piles considering soil and interface parameters. *Geomech. Eng.*, 7(5):495–524.

Fatahi, B., Tabatabaiefar, H. R., and Samali, B. (2011). Performance Based Assessment of Dynamic Soil-Structure Interaction Effects on Seismic Response of Building Frames. In *GeoRisk 2011*, pages 344–351, Reston, VA. American Society of Civil Engineers.

Franke, E. (1988). Group action between vertical piles under horizontal loads. *Deep Found. bored auger piles*.

Franke, E. and Muth, G. (1985). Scale effect in 1g model tests on horizontally loaded piles. In *Proc. 11th Int. Conf. Soil Mech. Found. Vol. 2*, pages 1011–1014, San Francisco.

Galal, K. and Naimi, M. (2008). Effect of soil conditions on the response of reinforced concrete tall structures to near-fault earthquakes. *Struct. Des. Tall Spec. Build.*, 17(3):541–562.

Gandhi, S. R. and Selvam, S. (1997). Group effect on driven piles under lateral load. *ASCE*, 123(August):702–709.

Gazetas, G. (1991). Formulas and Charts for Impedances of Surface and Embedded Foundations. *J. Geotech. Eng.*, 117(9):1363–1381.

Gazetas, G. and Stokoe, K. H. (1991). Free Vibration of Embedded Foundations: Theory versus Experiment. *J. Geotech. Eng.*, 117(9):1382–1401.

Germanischer, L. and Hamburg, G. (2005). *Guideline for the certification of offshore wind turbines*. Edition, Germanischer Lloyd Industrial Services GmbH.

Givens, M. J., Stewart, J. P., Haselton, C. B., and Mazzoni, S. (2012). Assessment of Soil-Structure Interaction Modeling Strategies for Response History Analysis of Buildings. *Proc. 15th World Conf. Earthq. Eng.*, pages 1–10.

Global Wind Energy Council (2014). Global Wind Report Annual Market Update 2013. Technical report, GWEC.

Guin, J. and Banerjee, P. K. (1998). Coupled Soil-Pile-Structure Interaction Analysis under Seismic Excitation. *J. Struct. Eng.*, 124(4):434–444.

Haldar, S. and Babu, G. S. (2008). Effect of soil spatial variability on the response of laterally loaded pile in undrained clay. *Comput. Geotech.*, 35(4):537–547.

Haldar, S. and Sivakumar Babu, G. (2009). Design of laterally loaded piles in clays based on cone penetration test data: a reliability-based approach. *Géotechnique*, 59(7):593–607.

Han, Y. (2002). Seismic response of tall building considering soil-pile-structure interaction. *Earthq. Eng. Eng. Vib.*, 1(1):57–64.

Hansen, J. B. (1961). The Ultimate design of piles against transversal forces. *Conpenhagen*, Bulletin N(12):5–9.

Howe, R. (1955). A Numerical Method for Predicting the Behavior of Laterally Loaded Piling. Technical report, Shell Oil Company, Houston, TX.

Hsu, T.-W., Chen, Y.-j., and Wu, C.-y. (2001). Soil Friction Restraint of Oblique

Pipelines in Loose Sand. *J. Transp. Eng.*, 127(1):82–87.

IS 1893-1 (2016). *Criteria for Earthquake Resistant Design of Structures, Part 1: General Provisions and Buildings [CED 39: Earthquake Engineering]*. Number December. Bureau of Indian Standards, New Dehli, 6 edition.

IS 456 (2000). *Plain and Reinforced Concrete - Code of Practice*. Bureau of Indian Standards, New Dehli, 4 edition.

Ishihara, T. and Sarwar, M. W. (2008). Numerical and theoretical study on seismic response of wind turbines. *Eur. Wind Energy Conf. Exhib. 2008*, 5(March):2904–2908.

Jayantha, K., Asadul, H., and Kah, Y. L. (2010). Theoretical p-y Curve for Laterally Loaded Single Pile in Undrained Clay Using Bezier Curves. *J. Geotech. Geoenvironmental Eng. ASCE*, 136(1):265–268.

Karthigeyan, S., Ramakrishna, V. V., and Rajagopal, K. (2006). Influence of vertical load on the lateral response of piles in sand. *Comput. Geotech.*, 33(2):121–131.

Karthigeyan, S., Ramakrishna, V. V., and Rajagopal, K. (2007). Numerical Investigation of the Effect of Vertical Load on the Lateral Response of Piles. *J. Geotech. Geoenvironmental Eng. @ ASCE*, 133(5):512–521.

Katsanos, E., Thons, S., and Georgakis, C. (2016). Wind turbines and seismic hazard: a state-of-the-art review. *Wind Energy*, 19(11):2113–2133.

Kim, Y. and Jeong, S. (2011). Analysis of soil resistance on laterally loaded piles based on 3D soil-pile interaction. *Comput. Geotech.*, 38(2):248–257.

Kim, Y., Jeong, S., and Lee, S. (2011). Wedge Failure Analysis of Soil Resistance on Laterally Loaded Piles in Clay. *J. Geotech. Geoenvironmental Eng.*, 137(7):678–694.

Kok, S. and Bujang, B. (2008). Numerical Modeling of Laterally Loaded Piles. *Am. J. Appl. Sci.*, 5(10):1403–1408.

Kourkoulis, R., Gelagoti, F., Anastasopoulos, I., and Gazetas, G. (2011). Slope Stabilizing Piles and Pile-Groups: Parametric Study and Design Insights. *J. Geotech. Geoenvironmental Eng.*, 137(7):663–677.

Kramer, S. L. (1996). *Geotechnical earthquake engineering*. Pearson Education India.

Kranthikumar, A. and Jakka, R. S. (2020). Effect of Edge Distance on Lateral Capacity of Piles in Cohesionless Soil Slopes. *Indian Geotech. J.*, 50(6):925–934.

Kucukarslan, S., Banerjee, P. K., and Bildik, N. (2003). Inelastic analysis of pile soil structure interaction. *Eng. Struct.*, 25(9):1231–1239.

Majumder, M. and Ghosh, P. (2016). Intermittent geofoam in-filled trench for vibration screening considering soil non-linearity. *KSCE J. Civ. Eng.*, 20(6):2308–2318.

Makris, N. and Chang, S. P. (2000). Effect of viscous, viscoplastic and friction damping on the response of seismic isolated structures. *Earthq. Eng. Struct. Dyn.*, 29(1):85–107.

Matlock, H. (1970). Correlation for Design of Laterally Loaded Piles in Soft Clay. In *Proceeding Offshore Technol. Conf. Houst.* TX, Paper OTC 1204.

Matlock, H. and Reese, L. (1956). Non-dimensional solutions for laterally-loaded piles with soil modulus assumed proportional to depth. In *Proc. 8th Texas Conf. Soil Mech. Found. Eng.*, pages 1–41, Austin, Texas.

Matlock, H. and Reese, L. C. (1960). Generalized Solutions for Laterally Loaded Piles. *J. Soil Mech. Found. Div.*, 86(5):63–92.

Meyerhof, G. G., Mathur, S. K., and Valsangkar, A. J. (1981). Lateral Resistance and Deflection of Rigid Walls and Piles in Layered Soils. *Can. Geotech. J.*, 18(2):159–170.

Murphy, G., Doherty, P., Cadogan, D., and Gavin, K. (2016). Field experiments on instrumented winged monopiles. *Proc. Inst. Civ. Eng. Geotech. Eng.*, 169(3):227–239.

Muthukkumaran, K. (2014). Effect of slope and loading direction on laterally loaded piles in cohesionless soil. *Int. J. Geomech.*, 14(1):1–7.

Narasimha Rao, S., Ramakrishna, V., and Babu Rao, M. (1998). Influence of Rigidity on Laterally Loaded Pile Groups in. *J. Geotech. Geoenvironmental Eng.*, 124(6):542–549.

Nasr, A. M. (2014). Experimental and theoretical studies of laterally loaded finned piles in sand. *Can. Geotech. J.*, 51(4):381–393.

Naveen, B. and Denise Penelope, N. K. (2016). Comparison of Field Test

And Numerical Analysis for Laterally Loaded Piles. In *7th Int. Conf. from Sci. Comput. to Comput. Eng. 2016*, pages 117–124.

Naveen, B., Sitharam, T., and Vishruth, S. (2012). Numerical Simulations of Laterally Loaded Piles. In *Proc. Int. Conf. Gr. Improv. Gr. Control*.

Park, D. and Hashash, Y. M. (2004). Soil damping formulation in nonlinear time domain site response analysis. *J. Earthq. Eng.*, 8(2):249–274.

PEER (2022). PEER Ground Motion Database.

Peng, J., Clarke, B. G., and Rouainia, M. (2011). Increasing the Resistance of Piles Subject to Cyclic Lateral Loading. *J. Geotech. Geoenvironmental Eng.*, 137(10):977–982.

Peng, J. R. (2005). *Behaviour of Finned Piles in Sand under lateral loading*. PhD thesis, University of Newcastle upon Tyne.

Peng, J. R., Rouainia, M., and Clarke, B. G. (2010). Finite element analysis of laterally loaded fin piles. *Comput. Struct.*, 88(21-22):1239–1247.

Peng, J. R., Rouainia, M., Clarke, B. G., Allan, P., and Irvine, J. (2004). Lateral resistance of finned piles established from model tests. In *Proc. Int. Conf. Geotech. Eng.*, pages 565–571.

Phillips, R. and Valsangkar, A. A. (1987). *An experimental investigation of factorsaffecting penetration resistance in granular soils in centrifuge modelling*. PhD thesis, University of Cambridge Department of Engineering.

Poulos, H. (1971a). Behavior of Laterally Loaded Piles: 1-Single Piles. *J. Soil Mech. Found. ASCE*, 97(5):711–731.

Poulos, H. (1971b). Behavior of Laterally Loaded Piles: II-Pile Groups. *J. Soil Mech. Found. Eng. ASCE*, 97(5):733–751.

Poulos, H. G., Davis, E. H., and Others (1980). *Pile foundation analysis and design*, volume 397. Wiley New York.

Prakash, S. (1962). *Behavior of pile groups subjected to lateral loads*. University of Illinois at Urbana-Champaign.

Prasad, V. and Chari, T. R. (1999). Lateral Capacity of Model Rigid Piles in Cohesionless Soils. *Soils Found.*, 39(2):21–29.

Qin, C., Chian, S., and Wang, C. (2016). Kinematic analysis of pile behavior

for improvement of slope stability in fractured and saturated Hoek-Brown rock masses. *Int. J. Numer. Anal. Methods Geomech.*, 41(6):803–827.

Qin, C. and Chian, S. C. (2017). Kinematic analysis of seismic slope stability with stabilizing piles. In *Proc. 19th Int. Conf. Soil Mech. Geotech. Eng.*, volume 1, pages 2187–2190, Seoul.

Rahman, M. M. and Lo, S. (2014). Undrained behavior of sand-fines mixtures and their state parameter. *J. Geotech. Geoenvironmental Eng.*, 140(7):04014036.

Rathod, D., Muthukkumaran, K., and Sitharam, T. (2018). Effect of slope on p-y curves for laterally loaded piles in soft clay. *Geotech. Geol. Eng.*, 36:1509–1524.

Reese, L. C., COX, W. R., and Koop, F. D. (1974). Analysis of Laterally Loaded Piles in Sand. In *Proc. Offshore Technol. Conf. Houston, TX*, pages 473–483. Paper No. OTC 2080.

Reese, L. C. and Welch, R. C. (1975). Lateral Loading of Deep Foundations in Stiff Clay. *J. Geotech. Eng. Div. ASCE*, 101(No. GT 7):633–649.

Rollins, K. M. and Sparks, A. (2002). Lateral Resistance of Full-Scale Pile Cap with Gravel Backfill. *J. Geotech. Geoenvironmental Eng.*, 128(9):711–723.

Rudolph, C. and Grabe, J. (2013). Laterally loaded piles with wings - In situ testing with cyclic loading from varying directions. In *Proc. Int. Conf. Offshore Mech. Arct. Eng. - OMAE*, volume 6, pages OMAE2013–10026, V006T10A002; 7 pages, Nantes, France. American Society of Mechanical Engineers.

Sáez, E., Lopez-Caballero, F., and Modaressi-Farahmand-Razavi, A. (2013). Inelastic dynamic soil-structure interaction effects on moment-resisting frame buildings. *Eng. Struct.*, 51:166–177.

Sakr, M. A., Azzam, W. R., and Wahba, M. A. (2020). Model study on the performance of single-finned piles in clay under lateral load. *Arab. J. Geosci.*, 13(4):0–16.

Sallam, A., Azzam, W., and Nasr, A. (2023). Performance of fin pile subjected to torsional loads embedded in dry sand. *Proc. Inst. Civ. Eng. - Geotech. Eng.*, pages 1–12.

Santoni, R. L., Tingle, J. S., and Webster, S. L. (2001). Engineering Properties of Sand-Fibre Mixtures for Road Construction. *J. ofGeotechnical Geoenvironmental Eng.*, 127(March):258–268.

Sawant, V. A. and Shukla, S. K. (2012). Three-Dimensional Finite Element Analysis of Laterally Loaded Piles in Sloping Ground. *Indian Geotech. J.*, 42(4):278–286.

Scarfone, R., Morigi, M., and Conti, R. (2020). Assessment of dynamic soil-structure interaction effects for tall buildings: A 3D numerical approach. *Soil Dyn. Earthq. Eng.*, 128:105864.

Shamsher, P. and Sharma, H. D. (1990). *Pile Foundations in Engineering Practice*. A Wiley-Interscience Publication. John Wiley & Sons, Inc., New York.

Smith, M. (2009). *ABAQUS/Standard User's Manual, Version 6.9*. Dassault Systèmes Simulia Corp, United States.

SP 36 (Part1) (1987). *Compendium of Indian Standards on Soil Engineering: Part-1 LaboratoryTesting of Soils for civil Engineering Purposes [CED 43: Soil and Foundation Engineering] (Reaffirmed 2006)*. Bureau of Indian Standards (BIS), New Delhi, 110002.

Suits, L. D., Sheahan, T. C., Lee, J., Prezzi, M., and Salgado, R. (2011). Experimental Investigation of the Combined Load Response of Model Piles Driven in Sand. *Geotech. Test. J.*, 34(6):103269.

Tabatabaiefar, H. R. (2012). Determining Seismic Response of Mid-rise Building Frames Considering Dynamic Soil-Structure Interaction By. Technical Report December, University of Technology, Sydney.

Tabatabaiefar, H. R. and Clifton, T. (2016). Significance of Considering Soil-Structure Interaction Effects on Seismic Design of Unbraced Building Frames Resting on Soft Soils. *Aust. Geomech. J.*, 51:55–64.

Tomlinson, M. and Woodward, J. (2008). *Pile Design and Construction Practice*. E & FN Spoon Publishers, 5th editio edition.

Uncuoğlu, E. and Laman, M. (2011). Lateral resistance of a short rigid pile in a two-layer cohesionless soil. *Acta Geotech. Slov.*, 8(2):19–43.

Valamanesh, V. and Myers, A. T. (2014). Aerodynamic Damping and Seismic Response of Horizontal Axis Wind Turbine Towers. *J. Struct. Eng.*, 140(11):1–9.

Van Nguyen, Q., Fatahi, B., and Hokmabadi, A. S. (2017). Influence of Size and Load-Bearing Mechanism of Piles on Seismic Performance of Buildings Considering Soil–Pile–Structure Interaction. *Int. J. Geomech.*, 17(7):1–22.

Wolf, J. P. and Obernhuber, P. (1985). Non-linear soil-structure-interaction analysis using dynamic stiffness or flexibility of soil in the time domain. *Earthq. Eng. Struct. Dyn.*, 13(2):195–212.

Wolf, J. P. and Song, C. (2002). Some cornerstones of dynamic soil-structure interaction. *Eng. Struct.*, 24(1):13–28.

Wood, D. M. (2004). *Geotechnical Modelling*. Spon Press, London.

Xu, D., Xu, X., Li, W., and Fatahi, B. (2020). Field experiments on laterally loaded piles for an offshore wind farm. *Mar. Struct.*, 69(October 2019):102684.

Yaghobi, M. H., Hanaei, F., Fazel Mojtahedi, S. F., and Rezaee, M. (2019). Numerical finite element analysis of laterally loaded fin pile in sandy soil. *Innov. Infrastruct. Solut.*, 4(1).

Zhang, L., Silva, F., and Grismala, R. (2005). Ultimate Lateral Resistance to Piles in Cohesionless Soils. *J. Geotech. Geoenvironmental Eng.*, 131(1):78–83.

Zhang, X. and Far, H. (2022). Effects of dynamic soil-structure interaction on seismic behaviour of high-rise buildings. *Bull. Earthq. Eng.*, 20(7):3443–3467.

Zieliński, M., Fletcher, J., Ewen, M., Fulghum, N., Tunbridge, P., Jones, D., Lolla, A., Candlin, A., Worthington, B., Moore, C., Broadbent, H., Benham, H., Yang, M., and MacDonald, P. (2022). Ember's Global Electricity Review. Technical Report March, EMBER.

LIST OF PAPERS BASED ON THE THESIS

Journal Articles

1. **Bariker, P.**, and **Kolathayar, S.** (2022) Dynamic Soil Structure Interaction of a High-Rise Building Resting over a Finned Pile Mat. *Infrastructures*, **7**(10):142. https://doi.org/10.3390/infrastructures7100142

2. **Bariker, P.**, **Kolathayar, S.**, and **Chandrasekaran, S. S.** (2023) Lateral Resistance of Finned-piles in c - ϕ Soils: Experimental Investigations, and Numerical Studies. *Indian Geotechnical Journal.* https://doi.org/10.1007/s40098-023-00748-x

3. **Bariker, P.**, and **Kolathayar, S.** (2023) Model Tests and Numerical Modelling on Lateral Resistance of Novel Finned-Pile Groups. *Innovative Infrastructure Solutions.*, 8 (224). https://doi.org/10.1007/s41062-023-01187-6

4. **Bariker, P.**, **Kolathayar, S.**, and **Babu Narayan, K. S.** Seismic Response of Wind Turbine Resting on Innovative Finned Pile Foundations. *Soil Dynamics and Earthquake Engineering Journal.* (Under Review)

Book Chapters

1. **Bariker, P.**, **Kolathayar, S.** (2021) A Study on Trenching Techniques for Vibration Isolation: An Overview. In: Seismic Hazards and Risk. *Lecture Notes in Civil Engineering, vol 116.* Springer, Singapore. https://doi.org/10.1007/978-981-15-9976-7_26

2. **Bariker, P.**, **Kolathayar, S.** (2022) Appraisal of Innovative Finned-Pile Foundations to Resist Lateral Loads. In: Ground Characterization and Foundations. *Lecture Notes in Civil Engineering, vol 167.* Springer, Singapore. https://doi.org/10.1007/978-981-16-3383-6_61

International Conferences

1. **Bariker, P.**, **Kolathayar, S.** (2023) Performance of Bridge Pier Resting on Finned Pile Groups under Seismic Excitations. *21st Southeast Asian Geotechnical Conference, and 4th AGSSEA Conference*, *SEAGC-AGSSEA 2023*, Bangkok, Thailand.

CURRICULUM VITAE

PANKAJ BARIKER

DoB: December 23, 1993

Plot-D-5, Sector-52, Navanagar, Bagalkot, Karnataka, India-587103.

Email: pankajbariker@gmail.com

Contact No.: +91-8618157823

EDUCATIONAL QUALIFICATIONS

DOCTOR OF PHILOSOPHY (PH.D.), 2019-2023

Institution	:	National Institute of Technology Karnataka, Surathkal
University	:	National Institute of Technology Karnataka, Surathkal
Specialization	:	Geotechnical Enginnering, (Civil Engineering)
Grade	:	9.77/10

MASTER OF ENGINEERING (M.E.), 2017-2019

Institution	:	University Visvesvaraya College of Engineeting, Bengaluru
University	:	Bangalore University, Bangalore
Specialization	:	Geotechnical Enginnering, (Civil Engineering)
Grade	:	85.83% – Distinction

BACHELOR OF ENGINEERING (B.E.), 2012-2016

Institution	:	Basaveshwara Engineering College, Bagalkot
University	:	Visvesvaraya Technological University, Belagavi
Specialization	:	Civil Engineering
Grade	:	9.39/10 – First Class with Distinction

RESEARCH INTERESTS

Numerical Modeling in Geo-technical Engineering, Foundation Engineering, Slope Stability, Soil Reinforcement, Railway Geotechnics, Dynamic Analysis of Earthen Dams, Soil Stabilization, Basic Geo-mechanics.